Keratins as regulators of colonocyte mitochondria and intestinal barrier function

Taina Heikkilä

Master's Thesis

University of Turku
Faculty of Medicine
2.5.2020

Master's Degree of Biomedical Imaging
Light Microscopy Imaging

Credits: 45 ECTS

Supervisors:
1. Diana Toivola

2. Joel Nyström

Passed:

Grade:

The originality of this thesis has been checked in accordance with the University of Turku quality assurance system using the Turnitin OriginalityCheck service.

UNIVERSITY OF TURKU
Faculty of Medicine
Institute of Biomedicine

TAINA HEIKKILÄ:

Keratins as regulators of colonocyte mitochondria and intestinal barrier

Master's thesis, 82 pp., 3 Appendices
Light Microscope Imaging
May 2020

Keratins are part of a filamentous structures forming the cytoskeleton. Keratins provide structural support and are involved in several cell processes. Keratins are known to affect mitochondrial function in the liver but the role in mitochondrial function in the colon is less known. In previous studies K8 knockout ($K8^{-/-}$) in Caco-2 cells leaded to diminished mitochondrial respiration and decreased levels mitochondrial and caveolar calcium (Ca^{2+}) levels. In this study the involvement of K8 on mitochondrial function was further examined in $K8^{-/-}$ Caco-2 cells by microplate reader assays to determine the levels of mitochondrial membrane potential (MMP) and cardiolipin (CL), which are both needed for normal mitochondrial function. Mitochondrial distribution was studied by immunohistochemistry and mitochondrial motility by staining and live cell imaging. Caveolin proteins are involved in Ca^{2+} signaling and mitochondrial function. Therefore, distribution of caveolin-1 (Cav1) was studied by immunostaining. Intestinal barrier function is the ability of the epithelial cell layer of the intestinal wall to selectively pass substances across. The role of K8 in barrier function in Caco-2 cells was studied with a Cellzscope+ device. Loss of K8 in Caco-2 leads to decreased levels of MMP and CL, increased mobility of mitochondria and fragmented mitochondrial network as well to an aggregation of Cav1 protein, all which may affect to the energy metabolism in Caco-2 cells. Barrier formation was decreased and delayed in $K8^{-/-}$ compared $K8^{+/+}$ Caco-2 cells. In conclusion, this study further support findings on the role of keratins in regulation of mitochondrial morphology and function.

KEYWORDS: Keratin 8, Mitochondria, mitochondrial membrane potential, cardiolipin, caveolin-1, intestinal barrier function

Contents

Abbreviations

ADP = Adenosine diphosphate

ATP = Adenosine triphosphate

BSA = Bovine Serum Albumin

CI = Oxidative phosphorylation complex I

CII = Oxidative phosphorylation complex II

CIII = Oxidative phosphorylation complex III

CIV = Oxidative phosphorylation complex IV

Ca^{2+} = Calcium

CAC = Citric acid cycle

Cav1 = Caveolin-1

Cav2 = Caveolin-2

Cav3 = Caveolin-3

Ccl = Conductance/ capacitance

CD = Crohn's disease

CL = Cardiolipin

COOH = Carboxyl group

CRC = Colorectal cancer

CRISPR = Clustered regularly interspaced short palindromic repeats

CTCF = Corrected total cell fluorescence

Cu^{1+} = Cupric cation

Cu^{2+} = Cupric ion

DMEM = Dulbecco's Modified Eagle Medium

ETC = Electron transport chain

FBS = Fetal Bovine Serum

FCCP = Carbonyl cyanide 4-(trifluoromethoxy)phenylhydrazone

GFP = Green fluorescent protein

GI = Gastrointestinal tract

GLUT = Glucose transporter

HMGCS2 = 3-hydroxy-3-methylglutaryl-CoA synthase 2

IBD = Inflammatory bowel disease

IF = Intermediate filament

IntDen = Integrated density

K = Keratin

$K8^{+/+}$ = K8 wildtype

$K8^{-/-}$ = K8 knockout

L2000 = Lipofectamine 2000

MCT1 = Monocarboxylate transporter 1

MEF = Mouse embryonic fibroblast

MMP = Mitochondrial membrane potential

mRNA = Messenger RNA

NAO = Acridine Orange 10-nonyl bromide (Nonyl-Acridine Orange)

NDS = Normal donkey serum

NGS = Normal goat serum

NH = Amine group

NO = Nitric oxide

NP-40 = Nonidet P-40

PBS = Phosphate buffer saline

PFA= Paraformaldehyde

Q = Ubiquinone

RFP = Red fluorescent protein

RISC = RNA-induced silencing complex

ROS = Reactive oxygen species

RFU = Relative fluorescence units

siRNA = Small interfering RNA

TCA= Tricarboxylic acid cycle

TCHP = Trichoplein

TEER/TER = Trans-epithelial/endothelial electrical resistance

TJ = Tight junction

TMRE = Tetramethylrhodamine, ethyl ester

UC = Ulcerative colitis

OXPHOS = Oxidative phosphorylation

1. Introduction

1.1 The cytoskeleton

The cytoskeleton is a filamentous structure in the cytoplasm of eukaryotic cells responsible for maintaining the cell's shape, cell division and movements of the whole cell as well as its internal parts (Alberts et al., 2015; Wickstead and Gull 2011). The cytoskeleton keeps the shape and internal structures of the cell in a proper state while at the same time allowing cells to change and adapt to their environment and to the state of their life cycle (Alberts et al., 2015). This is possible since the cytoskeleton and its filaments are highly dynamic structures and are capable of fast reorganization as needed for example during cell division (Alberts et al. 2015).

Three types of filaments, microtubules, actin filaments and intermediate filaments (IFs), form the network of the cytoskeleton (Bershadsky and Vasiliev, 1988; Bittar and Khurana 2006; Alberts et al., 2015). Cytoskeletal filaments are assembled from tiny subunits (Alberts et al., 2015). Microtubules are composed of tubulin proteins and are needed for cell division in the form of the mitotic spindle, sensing or cell movement in the form of cilia as well as tracks for transporting intracellular cargoes (Albert et al.,2015). Actin filaments are formed by globular actin proteins (Alberts et al., 2015). The cell needs actin filaments for cell division, cell movement and to provide mechanical support (Pollard and Cooper, 2009). Actin filaments are part of a contractile apparatus, for example, during cell division actin filaments together with their associated protein, myosin, form a contractile ring forcing the cell to divide into two (Alberts et al., 2015). Intermediate filaments work mainly as structural support but are also important for many cell processes (Toivola et al., 2010; Margiotta and Bucci, 2016). IFs do not have a major role in cell movement as the other filaments do (Alberts et al., 2015). The diameter of IFs, which is around 10 nm, is between microtubules (24 nm) and actin filaments (7 nm) (Lodish et al., 2000).

1.1.1 Intermediate filaments

IFs are a heterogenous group of cytoskeletal filaments found almost in all metazoans (Hesse et al. 2011; Cooper and Sunderland, 2000). Expression of IFs is tissue and cell type specific (Strelkov and Herrmann, 2003; Toivola et al., 2010). IFs are more stable structures than other cytoskeletal filaments and are responsible for forming supportive skeleton of the cell and giving protection against mechanical stress (Toivola et al., 2010;

Alberts et al., 2015). IFs are also involved in the regulation of nuclear organization, cell signaling and cell cycle among others (Margiotta and Bucci, 2016). IFs form direct and indirect connections with several other cell structures, such as microtubules, cell junctions and the plasma membrane (Lodish et al., 2000). The importance of IFs for normal function of the human body is shown by IF mutations, since over 80 human diseases have been recognized to have connections to IF mutations (Sun et al. 2016)

1.1.2 Types of intermediate filaments

Other cytoskeletal filaments, actin and microtubules, are formed by only one type of proteins, while there are over 50 known IF proteins today (Cooper and Sunderland, 2000). These IF proteins are categorized into six types, mostly according to differences and similarities in their amino acid sequence (Table 1). (Cooper and Sunderland, 2000; Herrmann and Aebi, 2000; Lodish et al., 2000; Szeverenyi 2008; Kornreich et al., 2015; Leduc and Etienne-Manneville, 2015).

Keratins form the two first IF types: Type I acidic keratins and type II basic or neutral keratins. Keratins are most abundant in epithelial cells (Herrmann and Aebi, 2000; Lodish et al., 2000) and can be found in soft structures, e.g. in cells or hard structures e.g. horns or nails that are built from keratins after complex differentiation processes (Herrmann and Aebi, 2016). Type III IFs are formed by muscle cell-specific desmin and synemin found in skeletal muscle cells, vimentin IFs found in endothelial cells, fibroblasts and leukocytes, as well as some IFs expressed in peripheral neurons. (Cooper and Sunderland, 2000). Three different neurofilament IF proteins form the type IV IF protein group. Type IV neurofilaments are suggested to play important roles in supporting axons of motor neurons as well as in the development of central nervous system neurons. (Cooper and Sunderland, 2000). Type V IFs are nuclear lamins found in a nuclear envelope of all cell types (Cooper and Sunderland, 2000). Type VI IFs is formed by phakinin and filensin, which are found specifically from lens (Kornreich et al., 2015).

Table 1. Classification of intermediate filaments. IF proteins can be divided into 6 types. Type I-II are keratins, type III IFs consist of muscle cell and neuronal IFs, type IV IFs are mostly formed by neuronal IFs, type V is formed by nuclear lamins found from all cell type and type VI IFs consist of lens specific IF proteins.

Type	Protein	Location
I	Acidic keratins	Epithelial cells
II	Basic keratins	Epithelial cells
III	Vimentin Desmin Glial fibrillary acidic factor Peripherin Synemin	Mesencymal cells Muscle cells Astroglial cells Neurons Skeletal muscle cells
IV	Neurofilaments–L-M-H Internexin Nestin	Neurons Neurons CNS and muscle precursor cells
V	Nuclear Lamins	Universal (Nuclear membranes)
VI	Phakinin, Filensin	Lens

1.1.3 Structure of intermediate filaments

Despite being formed by a heterogenous group of proteins, all IFs share a similar structure with a central rod domain formed by a coiled-coil structure of two axially oriented and parallel α-helical chains. At both sides of this central domain are more variable non-helical amino-(N)-terminal head and carboxyl-(C)-terminal tail domains (Figure 1). (Geisler and Weber, 1982; Lodish et al., 2000; Parry et all., 2007; Herrmann and Aebi, 2016; Nafeey et al., 2016). The central domain contains three linker domains, called L1, L12 and L2, which divide the α-helix rod into four sub-helixes. These regions are called coil 1A, coil 1B, coil 2A and coil 2B (Figure 1). These coils form conserved areas of IFs since the length and number of amino acids are identical between different IFs on these sub-helices expect in coil 1B. (Herrmann et al., 2009) The head and the tail domains on the other hand exhibit highly variable sequences and sizes between different IFs. A typical IF contains 310 amino acids (Lees et al., 1988).

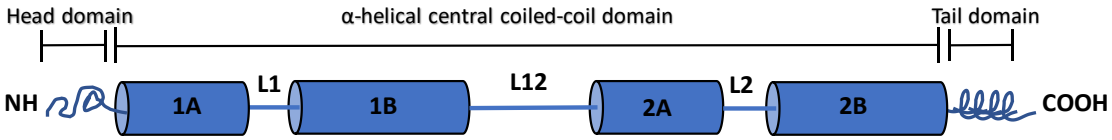

Figure 1. Structure of intermediate filaments. IFs are formed by α-helical central coiled-coil domain divided by three linkers, non-helical head amino-(N) terminal and tail carboxyl-(C)-terminal domains. Modified from: Childs, G. 2014. Intermediate Filaments [http://www.cytochemistry.net].

1.1.4 Assembly of intermediate filaments

While actin filaments and microtubules are hollow tubes, IFs organize themselves into stable structures resembling ropes. The assembly process of IFs starts with dimer formation: the central rod domains of two monomers fold around each other, leading to formation of coiled-coil dimers. Next dimers are joined to form antiparallel tetramers. These tetramers are capable of further assembling into protofilaments by joining to each other at the ends. Mature IFs are formed when several protofilaments are folded around each other (Figure 2). (Cooper and Sunderland, 2000) Single IF filaments can further organize themselves to larger IF bundles (Nafeey et al., 2016). In contrast to actin filaments and microtubules, which are polar, both ends of IFs are similar, and thus IFs are apolar with no minus or plus ends (Cooper and Sunderland, 2000).

IFs can be categorized into three assembly groups based on their polymerization with other IF monomers to form coiled-coil dimers. Group I and II keratins are featured by the need of a type I keratin to pair with a type II keratin to from a mature IF filament (assembly group 1). IF Group III and IV IFs are mostly homopolymeric IF proteins, although they can form heteropolymers within other members in their own group (assembly group 2). Group V nuclear lamins do not polymerize with other IF groups (assembly group 3). (Herrmann and Aebi, 2000). IFs may arrange themselves to form complex subcellular networks, which structures are somewhat dependent on the functional role of the IFs (Jacob et., 2018). For example, when keratin tetramers join laterally and these already laterally associated keratin tetramers further anneal longitudinally, keratin filaments grow forming eventually complex networks (Nafeey et al., 2016).

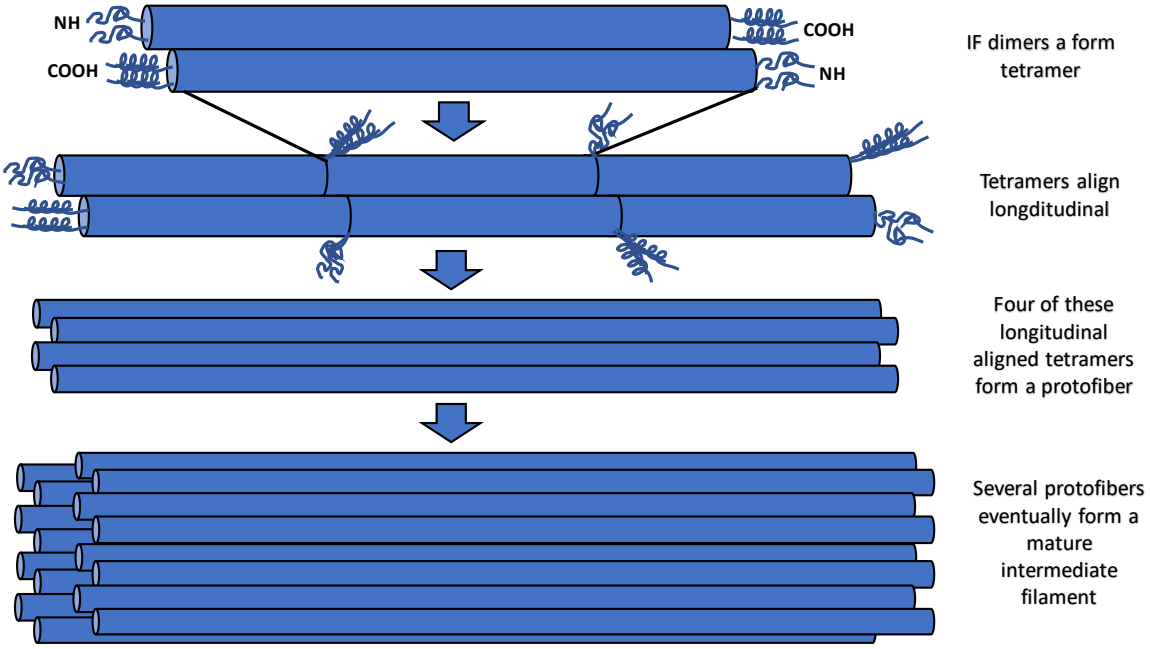

Figure 2. Assembly of intermediate filaments. Two IF monomers forms coiled-coil dimer. Two of these dimers are then joined to form tetramers. Several tetramers are then joined from end to end. Several tetramers eventually join, and form mature IF. Modified from: Childs, G. 2014. Intermediate Filaments [http://www.cytochemistry.net].

1.1.5 Keratins

Keratins, which form the biggest and most distinct subgroup of IFs, are found mostly in epithelial cells (Lodish et al., 2000; Schweizer et al., 2006). Keratin network extends from the plasma membrane to the edge of the nucleus (Fortier et al., 2013). 54 functional keratin genes have been found from the human genome, and these are divided into two types: 28 genes are type I keratins and 26 genes belong to type II keratins. Also 13 nonfunctional keratin genes exist in human genome. (Coulombe and Omary, 2002; Schweizer et al., 2006). Type I and type II keratins cannot form homodimers and instead make 1:1 obligatory heterodimers, which are then assembled to filaments in a similar way as other IFs. (Lodish et al., 2000). Expression of keratins and hetero-dimer pair formation is tissue-, cell type- and development stage-specific (Herrmann and Aebi, 2000; Lodish et al., 2000; Loschke et al., 2015). Some keratins are building blocks for appendages, such as hair or nails, and based on this type I and type II keratins can be further divided into type I and type II epithelial and hair keratins (Herrmann and Aebi, 2016). Type I keratins K1-K8 and type II keratins K9-K24 are classified as epithelial keratins (Schweizer et al., 2006). The formation of keratin networks is mostly regulated by post-translational

modifications, such as phosphorylation, sumoylation and acetylation, controlling keratin assembly, disassembly and function (Loschke et al., 2015)

In addition to the traditional and well-known function of providing mechanical support to cells, keratins have roles in signaling pathways, transportation, stress protection, cell migration and apoptosis, and they organize cellular organelles and affect protein targeting and synthesis (Kellner and Coulombe, 2009; Fortier et al., 2013; Kumar et al., 2015; Lähdeniemi et al., 2017). For example, keratins have been shown to regulate cell growth via mTOR signaling (Kellner and Coulombe, 2009) and keratins affect the localization or levels of glucose transporters (GLUT), ion transporters and monocarboxylate transporter 1 (MCT1) (Toivola et al., 2004; Vijayraj et al., 2009; Alam et al., 2013; Helenius et al., 2015; Asghar et al., 2016).

1.2 The intestine

The gastrointestinal (GI) tract is a hollow tube which goes from the mouth to the anus (Patton and Thibodeau, 2016). One way of dividing the GI tract is to separate it into two parts: the upper GI tract and the lower GI tract (Treuting et al., 2012; Treuting and Dintzis, 2012; Patton and Thibodeau, 2016). The lover digestive tract is made up of the small intestine, which can be divided into duodenum, jejunum and ileum, and large intestine (colon), which is formed by the caecum, colon and rectum (Rao and Wang, 2010; Treuting and Dintzis, 2012; Griffiths and Megan, 2015). The lower GI tract is responsible for digestion, absorption of nutrients, water and electrolytes and discarding waste (Steegenga et al., 2012; Patton and Thibodeau, 2016). The GI tract also functions in immune response (Ray and Wang, 2010).

1.2.1 The colon

The colon, the longest part of the large intestine, being around 1.5-meter-long in adult, is divided into four parts: the ascending, transverse, descending and sigmoid colon (Patton and Thibodeau, 2016). The ascending colon begins at the end of caecum, and is followed by the transverse colon, which is the largest part of the colon. After the transverse colon lies the descending colon. The descending colon is followed by the last part of the colon, the S-curved sigmoid colon which joins to the rectum. (Griffiths and Megan, 2015)

The wall of the colon is divided into four layers similar to the rest of GI tract; the mucosa, submucosa, muscularis and serosa (Rao and Wang, 2010; Treuting and Dintzis, 2012; Griffiths and Megan, 2015; Patton and Thibodeau, 2016). The innermost layer of the

colon, the mucosa, is formed by a layer of simple columnar epithelial cells, the lamina propria and the muscularis mucosae. Colon epithelium has transverse folds and tubular glands, also called as crypts, which increase its surface area. (Treuting and Dintzis, 2012; Steegenga et.,al 2012; Griffiths and Megan, 2015) Goblet cells, enteroendocrine cells, enterocytes and Paneth cells can be found from the mucosa of the colon (Treuting and Dintzis, 2012; Griffiths and Megan, 2015). Most of the absorption takes place at the mucosa where enterocytes absorb nutrients and goblet cells secrete mucus (Griffiths and Megan, 2015; Standring 2016). Submucosa is formed by blood vessels, connective tissue and the nerves and muscularis layer is formed by two layers of smooth muscle; the outer one is made of longitudinal muscle fibers and the inner one from circular muscle fibers, making it responsible of movements and contraction of the colon. The thin outermost layer of the colon, called serosa, is formed by simple squamous epithelial cells producing fluid to protect outside of the colon from irritation with its surroundings. (Griffiths and Megan, 2015; Standring, 2016)

The colon functions as a storage and fermentation place for undigested macronutrients and absorbs water. The colon is also a home for microorganisms, which are important for the immune system, produce vitamins and are responsible for above-mentioned fermentation. (Garret et al., 2010; Steegenga et al., 2012) The wall of the colon also works as a selective barrier that keeps indigestible compounds, which are turned to faeces, and harmful microorganisms on the luminal side, while making the absorption of nutrients, vitamins and water possible (Watson et al., 2005; Teshima et al., 2012 Standring, 2016).

1.2.2 Keratins and colon

Colon epithelial cells express type I keratins K18, K19 and K20 and type II keratins K7 and K8. The most abundant keratin is K8, while also K18 and K19 are common and found throughout the whole length of the colon crypt. In lesser amount K7, located in the base of the crypt and K20, located in the upper part of the crypt, can be found in the colon. (Figure 3) (Zhou et al., 2003). In the colon K8 forms heteropolymers with K18, K19 or K20 (Zhou et al., 2013) and mice lacking K8 lose protein expression of most other keratins as well (Baribault et al. 1994; Asghar et al., 2016).

Keratins seem to play several roles in the colon. The importance of keratins for normal colon function has been proven in mice by knocking out K8 ($K8^{-/-}$ mice) which leads to several problems. K8 knockout mice develop a colon inflammation phenotype (Baribault et al., 1994; Habtezion et al, 2005; Habtezion 2011), intestinal barrier function is

disrubted, and tumorigenesis is increased in colon cancer models (Misiorek et al., 2016). Absence of K8 leads to impaired energy metabolism in the colon (Helenius et al., 2015), colonic hyperplasia, diarrhea, reduced apoptosis, and the inflammation of the colon in these mice are similar to what is seen in inflammatory bowel diseases (IBD) (Baribault, et al., 1994; Habtezion et al., 2005). K8/K18 have been proven to affect differentiation of colon epithelia by affecting the signaling of Notch1 (Lähdeniemi et al., 2017). Some K8 mutations have also been found in a low number of inflammatory bowel diseases (IBD) patients (Owens et al., 2004) and some evidence suggest an association between K8 and IBD (Jong and Drenth, 2004), but the results are still controversial to some other studies (Büning et al., 2004; Tao et al., 2007).

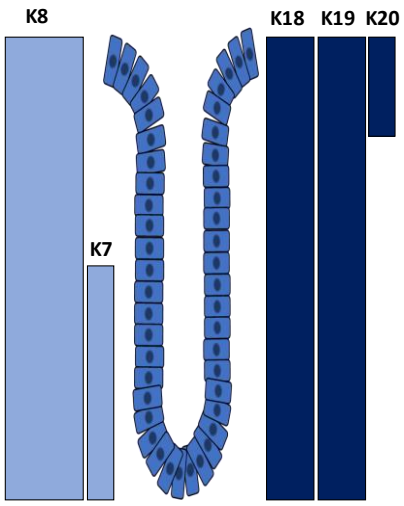

Figure 3. Keratin expression in the crypt of the colon. K8, K18 and K19 are the most common keratins expressed in the whole length of the colon crypts. Modified from: Zhou et al., 2003.

1.2.3 Colon diseases

Inflammatory bowel diseases (IBD) are a group of polygenic diseases affecting the colon and other parts of the GI tract (Jong and Drenth, 2004) and affect a huge number of people worldwide. The most common IBD diseases are ulcerative colitis (UC) and Crohn's disease (CD). CD can affect the whole GI tract but is mostly found in the colon and the ileum, while UC is only seen in the colon or in the rectum (Abraham and Cho, 2009; Mulder et al., 2014). UC is a mucosal inflammation with symptoms of abdominal pain and bloody diarrhea, while CD is a transmural inflammation with skip lesions (Mulder et al., 2014). Ulcerations of intestinal epithelia can be seen in both UC and CD. These ulcerations further disturb normal barrier function of the intestine (Zupancic et al., 2014). The prevalence of IBD has been high especially in industrial countries, but the incidence is going up also in developing countries (Malik, 2015). The estimated of number of people with IBD in Europe is 3.7 million and in North America 1.5 million and IBD healthcare costs are rising (van der Have et al., 2014). The prevalence of IBD in Finland has increased from 216 per 100 000 citizen in 1994 to 595 per 100 000 in 2008 (Jussila et al., 2013). The causes behind IBD are not clear, but it is an outcome of microbiological and

environmental factors, combined with genetical susceptibly (Jong and Drenth, 2004; Motte et al., 2003).

IBD also increases the risk of developing colorectal cancer (CRC) (Ullman and Itzkowitz, 2011). CRC is the third most diagnosed cancer, causing the third most of deaths from all cancer types (Rawla et al., 2019). What exactly causes CRC is not totally clear, but it is an outcome of genetic errors e.g. in genes affecting cell proliferation, apoptosis, differentiation and migration, and epigenetic changes caused by lifestyle choice such as diet and level of physical activity (Hirose et al., 2011; Watson and Collins 2011). Alterations in the gut microbiome is also one of the factors affecting the development of CRC (Datta et al., 2017). In K8 knockout mice models, the lack of K8 increases permeability of the intestine and leads to changes in gut microbiota, also K8 expression was lower in both human and mice cancer samples (Liu et al., 2017) and lack of K8 leaded also inducible CRC (Misiorek et al., 2016). It was suggested by Misiorek et al., 2016 that loss of K8 leads to increased levels of caspase-1 (due to activation of inflammasome). Caspase-1 increases IL-18 expression leading to increased levels of IL-22 via downregulation of IL-22 inhibitor. IL-22 activates STAT3 pathway leading to epithelial proliferation and defects in epithelial barrier. Therefore, it seems that keratins could work in preventing colon tumorigenesis by maintaining intestinal barrier, affecting inflammation and by having a role in keeping gut microbiota at a healthy state (Misiorek et al., 2016; Liu et al., 2017).

1.2.4 Barrier function

In addition to the digestive role of the GI tract, the luminal epithelium of the intestine also serves as a barrier between the intestine and rest of the body. Barrier function is the ability of the intestinal wall to selectively pass substances across it. The selective movement of molecules across the epithelial cell layer is achieved through a transcellular pathway by the help of transporters and channels or through endocytosis (Figure 4) (Teshima et al., 2012). Another way to go through the intestinal barrier is not by the help of channels or transporters but instead through tight junctions (TJs), which is defined as a paracellular pathway (Figure 4) (Teshima et al., 2012). The intestinal barrier makes absorption of only useful nutrients from the intestine possible and lets the immune system detect antigens, while at the same time preventing other harmful intraluminal, molecules from passing through the single-cell layer of epithelial cells of the intestinal wall, keeping the harmful

environment of the intestine separate from the rest of the body (Teshima et al., 2012, Watson et al., 2005).

Maintenance of the barrier function is essential for the proper function of the intestine (Peng et al., 2007) and one of the most important tasks of intestinal epithelial cells is to create this barrier (Ma et al., 2000). Defects in intestinal permeability has been associated with several disease conditions, such as in Crohn's disease, UC and colon cancer (Minkholm et al., 1994; Miki et al., 1998; Arnott et al., 2000).

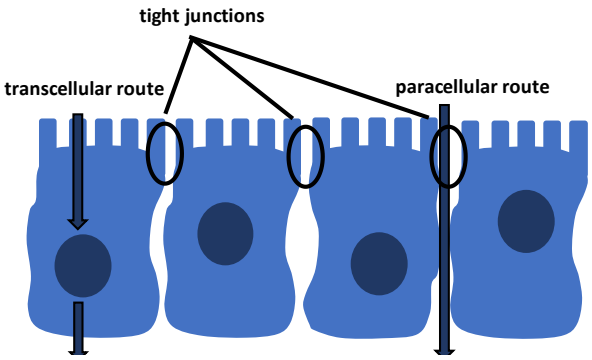

Figure 4. Intestinal barrier function. Intestinal barrier function is the ability of the intestine wall to selectively pass substances across. Molecules can cross the intestinal wall by two routes, through tight junctions via the paracellular route, or via channels and transporters or through endocytosis via transcellular route.

Several evidence show that keratins are needed for the maintenance of epithelial integrity (Liu et al., 2017). The lack of K8 in mice has been shown to lead impaired intestinal barrier formation (Wang et al., 2007; Misiorek et al., 2016). Certain human K8/K18 disease mutations have been shown to lead increased permeability of a monolayer of colorectal cancer cells via changes in the distribution of certain junction proteins on an *in vitro* colonocyte model (Zupancic et al., 2014). In keratinocytes keratins 5 and 14 have a role in the maintenance of TJs, which are needed to maintain the barrier function and mutations in these keratins leads to down-regulation of junction proteins (Liovic et al., 2009). K1 expression has been shown to be decreased in IBD patients and treatment of Caco-2 cells overexpressing K1, with IL-1β, substance diminishing barrier function, indicates that K1 hinders the effects of IL-1β, since Caco-2 cells maintained intact barrier despite the IL-1β treatment (Dong et al., 2017). Finally, it has also been shown that K8 is needed for maintaining placental barrier function (Jaquemar et al., 2003).

1.3 Mitochondria

Mitochondria are dynamic subcellular organelles whose shape can vary between different cell types and conditions (Youle and van der Bliek, 2012). Mitochondria are formed from two lipid membrane layers: the inner membrane, which forms folds called cristae, and the

smooth outer membrane layer (Nicholls and Ferguson, 2013). The inner membrane layer surrounds the mitochondrial matrix and contains enzyme complexes responsible for oxidative phosphorylation (OXPHOS) needed for energy metabolism and electron transport proteins, such as cytochrome c (Youle and van der Bliek, 2012). The outer membrane layer surrounds an intermediate space and the inner membrane (Youle and van der Bliek, 2012).

Mitochondria are main organelles responsible for production of energy in OXPHOS at the mitochondrial inner membrane (Jacobson et al., 2002; Jones, et al., 2017). In addition to energy production, mitochondria also have a role in apoptosis, in calcium (Ca^{2+}) signaling and production of reactive oxygen species (ROS) (Jacobson et al., 2002). Mitochondrial Ca^{2+} signaling controls the amount and the signaling of Ca^{2+} in a whole cell and works in protection against intracellular Ca^{2+} spikes which could harm the cell (Duchen et al., 2008; Schwarz and Leube, 2016).

1.3.1 Mitochondria and energy metabolism

Mitochondria are organelles responsible for production of energy in a cell in the form of the adenosine triphosphate (ATP) produced in the citric acid cycle (also known as tricarboxylic acid cycle or as Krebs cycle) and in an electron transport chain (ETC) in OXPHOS (Bratic and Trifunovic, 2010; Crowley et al., 2016; van der Bliek et al., 2017). Due to ATP production capacity mitochondria are often referred to as a powerhouse of the cell.

The citric acid cycle, containing eight enzymatic phases, takes place in the mitochondrial matrix. Acetyl CoA produced from carbohydrates, proteins and fats is taken into the citric acid cycle and oxidation of the molecule leads to formation of $FADH_2$ and NADH and several other compounds. $FADH_2$ and NADH work as electron donors in the ETC at the inner mitochondrial membrane. During OXPHOS electrons are moved from $FADH_2$ or NAHD through protein complexes to oxygen in ETC (Figure 5). The electrons move from high energy to a lower energy level releasing energy. NADH releases its electrons directly to oxidative phosphorylation complex I (CI) and $FADH_2$, being weaker electron donor, gives electrons to complex II (CII) instead of CI and less energy is produced this way. The electrons move from CI/CII to electron carrier ubiquinone (Q), which releases them to complex III (CIII). In turn, CIII transfers electrons further to the second electron carrier cytochrome c that passes them to complex IV (CIV), which finally transfers them to an oxygen, yielding H_2O (Figure 5). Part of the released energy is used to form a proton

gradient when oxidative phosphorylation complexes pump protons into the intermediate space. This proton gradient cause protons to move back into the matrix through ATP synthase, which uses this proton flow to generate ATP from adenosine diphosphate (ADP). ATP is further used as an energy source for cells. (Berg et al., 2002; van der Bliek et al., 2017).

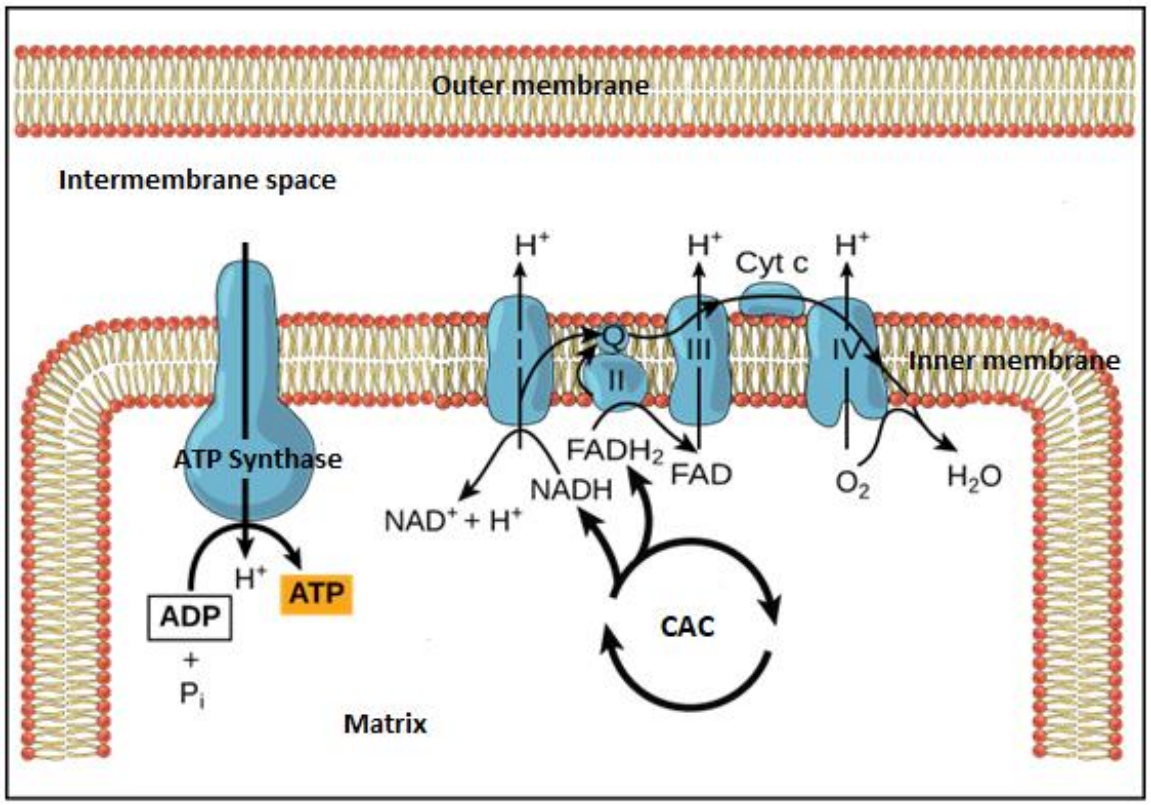

Figure 5. Oxidative phosphorylation (OXPHOS). Citric acid cycle (CAC) produce NADH and FADH which are used as electron donors in electron transport chain (ETC). During OXPHOS electrons are moved through protein complexes from $FADH_2$ or NAHD to the oxygen in ETC at the same time protons (H^+) are pumped into the mitochondrial intermembrane space forming proton gradient which is used by ATP synthase to generate ATP from ADP. ATP is the main energy source for the cell. Modified from: OpenStax.2016. Chapter 7 Cellular respiration. In: *Biology*. OpenStaxCnx Biology.

1.3.2 Mitochondrial membrane potential

During ATP production in OXPHOS, positively charged protons are actively transferred across the inner membrane into the intermembrane space of mitochondria by the work of proton pumps. This eventually leads to the formation of a negative charge inside the mitochondrial matrix and this proton gradient is harnessed to a production of ATP in OXPHOS. This internal negative charge is known as mitochondrial membrane potential (MMP). (Crowley et al., 2016) MMP is an essential force for transportation of charged

molecules, some of which are required for proper function of mitochondria (Zorova et al., 2018). Many mitochondrial processes, such as Ca^{2+} uptake and ATP production in OXPHOS, are dependent on MMP (Jones et al., 2017; Koopman et al., 2008). Mitochondrial organization is maintained by fission and fusion and in absence of normal membrane potential the balance of these two processes is disturbed leading to a fragmented mitochondrial network (Jones et al., 2017). Both optic atrophy-1 (OPA1) GTPase and mitofusins 1 and 2 responsible for fusion as well as dynamin-related protein I driving fission are affected by membrane potential (Jones et al., 2017). Since its crucial role for normal mitochondrial function, MMP is considered as a factor determining mitochondrial viability (Zorova et al., 2018)

1.3.3 Mitochondrial cardiolipin

Cardiolipin (CL) is a bisphosphatidyl glycerol lipid found mostly in the inner membrane of mitochondria, where 20% of lipids are CLs (Yan and Kang, 2012). CL is very hydrophobic and acidic as it is composed of a backbone of glycerol linking two phosphatidylglyceride groups into a dimeric structure of the CL, with four discrete alkyl groups (Jiang et al., 2000; Yan and Kang, 2012). CL is synthesized by mitochondria itself with the help of cardiolipin synthase and several other synthases, phosphatases and enzymes (Schlame and Haldar, 1993; Tamura et al., 2013). CL interacts with several mitochondrial proteins and it is needed for optimal function of many of these proteins, although the proteins do not require CL for normal function (Duncan et al., 2018; Schlame and Haldar, 1993). CL is essential for many important mitochondrial processes including apoptosis and OXPHOS (Yan and Kang, 2012; Yu et al., 2017). CL regulates synthesis and/ or ensures optimal activity of oxidative phosphorylation complex I (CI) (Yu et al., 2017), complex III (Lange et al., 2001), complex IV (Malkamäki and Sharma, 2019) and complex V (Acehan et al., 2011). CL interacts with the mitochondrial ADP/ATP carrier and since CL binds to a conserved residue on that carrier, which is common for all of mitochondrial carriers, it is proposed that CL could play a role in the function of all of mitochondrial carrier proteins (Duncan et al., 2018). CL also plays a role in cristae membrane integrity, which is an important factor for a formation of MMP (Ikon and Ryan, 2017). Elevated CL content has been associated with several pathologies e.g. Parkinson disease (Tyurina et al., 2013), Barth syndrome (Xu et al., 2016) and heart failure (Dolinsky et al., 2016).

1.3.4 Mitochondria and intermediate filaments

Several evidence suggest that mitochondria and the cytoskeletal filaments would have connections between each other (Kang, et al., 2008; Winter et al., 2008). It has been shown that some of IFs have a role in regulating mitochondria, for example the lack of or changes in vimentin has been shown to increase mitochondrial movement and fragmentation as well as disturbing anchoring of mitochondria to the cytoskeleton (Nekrasova et al., 2011). Binding of vimentin to mitochondria has also been shown to increase MMP, and phosphorylation of serine 55 of vimentin by RAC-1 seems to interrupt a connection between mitochondria and vimentin leading to decreased MMP and increased mitochondrial motility (Matveeva et al., 2015). Mitochondria have been shown to be connected to microtubules via axon-targeted syntaphilin docking protein in axons (Kang et al., 2008) and studies indicate that microtubules mediate mitochondrial movements (Morris and Hollenbeck, 1995). Also, one isoform of plectin, a cytolinker protein, works as a linker between IFs and mitochondria in mouse fibroblasts (Winter et al., 2008). During apoptosis vimentin IFs have been seen to bind CL and it is hypothesized that vimentin might affect the localization of CL (Manganelli et al., 2015). K8/K18 binds to trichoplein keratin filament-binding protein (TCHP) (Nishizawa et al., 2005). TCHP is further connected to the mitochondrial outer membrane (Cerqua et al., 2010).

In mouse β-cells the loss of K8 has been shown to lead to several alterations in mitochondria compared to wild type cells: mitochondria are smaller in size and more oval shaped. The mitochondrial network is more fragmented, mitochondrial transmembrane potential is lower, and mitochondria move more than normal. (Silvander et al., 2017). Loss of K8 in mouse hepatocytes caused similar effect: mitochondria were smaller and irregularly distributed (Tao et al., 2009). A more scattered mitochondria network has been shown to lead to decreased ATP production (Jeng et al., 2005). K6/K16 could also, control mitochondrial function, since loss of K16/K6 in skin keratinocytes have been shown to disturb mitochondrial respiration, MMP and cristae formation, as well as increased mitochondrial mobility (Steen et al., 2020). It has been shown that knockout of K8 from the mouse colon leads to decreased amount and activity of mitochondrial 3-hydroxy-3-methylglutaryl-CoA synthase 2 (HMGCS2). which is the rate-limiting enzyme in ketogenesis, and fewer mitochondrial cristae (Helenius et al., 2015). Recent studies also showed that loss of K8 in colorectal adenocarcinoma cells leads to diminished mitochondrial respiration, lower ATP production rate and decreased levels of OXPHOS

complexes (Nyström et al., unpublished data). Previous studies indicate that keratins may have a role in colon energy metabolism but requires further study.

1.4. Caveolae and caveolins

Caveolins are structural proteins of the caveolae (Figure 6) (Lin et al., 2004), which are vesicular invaginations of the cell membrane in several cell types (Kim et al., 2006; Chaudhary et al., 2014). Both have a role in a high number of cell processes, for example in Ca^{2+} signaling, cholesterol homeostasis, nitric oxide (NO) signaling, transcytosis and endocytosis (Thomsen et al., 2001; Parton and Simons, 2007).

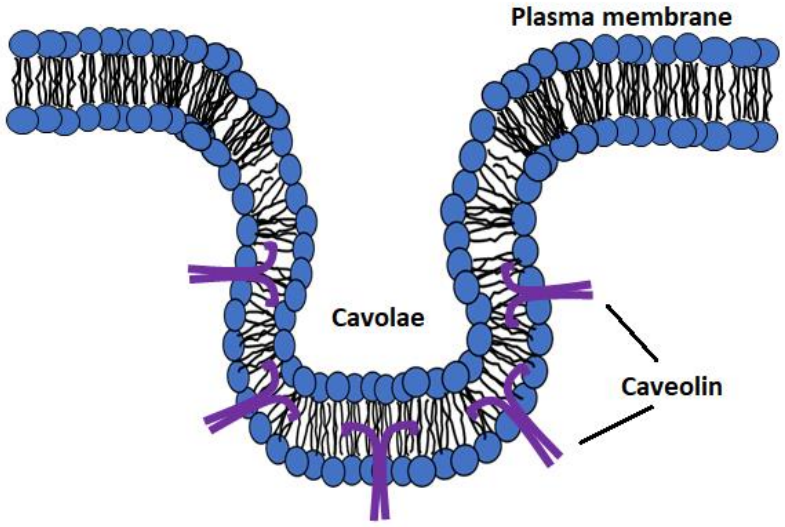

Figure 6. Caveolae and caveolins. Caveolae are invaginations of the cell membrane and caveolins are structural proteins of the caveolae. Caveolae functions in several important cell processes.

1.4.1 Caveolae

Caveolae are 50-100 nm invaginations of the cell membrane (Bauer et al., 2005) formed by caveolins, cavins and accessory proteins (Parton et al., 2018). Caveolae are flask-shaped lipid structures (Bauer et al., 2005; Kim et al., 2006) containing a high number of glycosphingolipids and cholesterol (Thomsen et al., 2001). It is proposed that caveolae are assembled in the Golgi apparatus and from there sent to the cell membrane in exocytic carriers (Berg et.al, 2009)

Caveolae are involved in many kinds of processes such as cell signaling, adhesion, lipid homeostasis, cell migration, transportation of cholesterol and endocytosis of several

compounds (Timme et al., 2000; Bauer et al., 2005; Grande-García et al., 2007; Mohan et al.,2015). Elevated expression of caveolae have been associated with several diseases, including several cancer types (Cohen et al., 2004) e.g. in prostate cancer (Timme et al., 2000), breast cancer (Bai et al., 2012) and colon cancer (Ha et al., 2012). Caveolae have been reported to be involved e.g. in endocytosis of cholera toxin in a certain cell types (Torgersen et al., 2001) and e.g. simian virus 40 uses caveolae for entry to the cells (Pelkmans et al., 2002). Lack of caveolae has been shown to damage NO signaling, a normal function of the cardiac system, reactiveness to insulin and cholesterol homeostasis (Bauer et al., 2005).

TJs are important for barrier function. It has been shown that endocytosis of some TJ components is caveolae-mediated. This caveolae-mediated endocytosis coexists with actin depolymerization leading to an impaired TJ proteins disturbing the formation of barrier function (Shen and Turner, 2006).

1.4.2 Caveolin-1

Caveolins are crucial components of caveolae. There are three different caveolin proteins in mammals: caveolin-1 (Cav1), caveolin-2 (Cav2) and caveolin-3 (Cav3). (Galbiati et al., 2001) There are five isoforms of these three caveolins and one or more of these isoforms are found in almost all tissue types (Liu et al., 2002). For example, Cav1 is abundant in endothelial cells (Gerbod-Giannone et al., 2019), fibroblast, smooth muscle cells, adipocytes and it can also be found in immune cells (Harris et al., 2002). Cav1 and Cav2 are usually expressed together as heterooligomers (Scheiffele et al., 1998) Formation of caveolae requires Cav1 in non-muscle cells (Yu et al., 2017). Since proteins can localize themselves into caveolae and are directly connected to caveolins, it has been proposed that caveolae would organize cell membrane signaling cascades and Cav1, together with its interacting proteins, could further adjust the signaling networks (Bauer et al., 2005).

Reduced levels of Cav1 mRNA and protein have been associated with human colon cancer (Bender et al., 2000). Cav1 appears to affect the development of cancer in two ways: as a tumor suppressing or as a tumor promoting factor, and whether it acts as a suppressor or promotor depends on cell type, cancer type and/or cancer phenotype (Ha and Chi, 2012). Cav1 expression is often increased in advanced colon tumors, which leads to changes in aerobic glycolysis. Tumor cells make more ATP and have higher glucose uptake, indicating that Cav1 may have a role in promoting tumor growth via higher

glucose uptake (Ha and Chi, 2012). The levels of Cav1 were decreased in the colon of mice with TNBS-induced colitis, suggesting that Cav1 could have a role in protection against inflammation in the colon. It was suggested that the role of Cav1 in anti-inflammatory response may be one factor behind the observed protective role in inflammation. (Weiss et al., 2015). For example, Cav1 have been seen to affect macrophages via Toll-like receptor 4 (Wang et al., 2009). Cav1 has also been shown to work in protection from advancement of the atherosclerosis via affecting to low density lipoprotein (LDL) endocytosis (Gerbod-Giannone et al., 2019). Lastly, increased levels of endothelial Cav1 in mice has been shown to hinder barrier function and NO synthesis (Bauer et al., 2005).

1.4.3 Caveolae/ caveolin-1 and intermediate filaments

Caveolin has been detected to be transported between caveolae in the plasma membrane and the Golgi apparatus in a microtubule dependent pathway (Conrad et al., 1995). Previously Cav1 has also been linked to the actin cytoskeleton via actin-crosslinker protein filamin (Stahlhut and Deurs, 2000). There is also evidence that caveolins/caveolae are connected to IFs and Cav1 has been shown to connect to IFs via tyrosine-14 in Cav1 (Santilman et al., 2007). It has been shown that Cav1 interacts with vimentin, indicating that vimentin IFs could have a role in regulating caveolae trafficking since in region with high amount of vimentin Cav1 vesicles move less and are less densely packed (Jiu, 2018). Caveolae have also been shown to be connected to keratin IFs in zebrafish notochord and it is suggested that IFs together with caveolae could work in maintaining the notochord as loss of Cav1 leads to an impaired structure of the notochord (Nixon et al., 2007). In Caco-2 cells lacking K8 decreased caveolar and mitochondrial Ca^{2+} levels have been reported (Nyström et al., unpublished data). Also, Cav3, which is essential for formation of caveolae in muscle cells, has been shown to be associated with desmin, a muscle-specific IF. It is hypothesized that Cav3 could connect and organize desmin to a network of IFs at the sarcolemma and have a role in the specialization of muscle cells (Mermelstein et al., 2006).

1.4.4 Caveolae/ caveolin-1 and mitochondria

Previous studies show that normal mitochondrial function is associated with Cav1; Cav1 null mouse embryonic fibroblast (MEF) cells exhibit altered mitochondrial function with higher MMP and glucose dependency. In addition to several other metabolic phenotypes seen in Cav1 null mouse, changes are also seen in mitochondria-dependent gene

expression. (Bosch et al., 2011; Asterholm et al., 2012). The loss of Cav1 in stromal cells has also been shown to lead to dysfunction of mitochondria (Pavlides et al., 2010). In stromal cells Cav1 deficiency increases NO synthesis. The increased amount of NO further leads to nitration of tyrosine at mitochondrial respiratory chain complexes causing mitochondrial dysfunction (Pavlides et al., 2010). Cav1 is also necessary for the function of some of enzymes needed for CL synthesis (Yu et al., 2017). Cav1 knockdown or knockout seems to cause decreased levels of CL which causes mitochondrial dysfunction via diminished activity of oxidative phosphorylation complex I and further leads to premature senescence in several different cell types via a p53-p21-dependent pathway, however the effect may be cell line and stressor dependent (Yu et al., 2017).

Caveolae have an important role in Ca^{2+} signaling (Parton & Pozo, 2013), and normal Ca^{2+} homeostasis is important for mitochondrial function (De Stefani & Rizzutom, 2016). Ca^{2+} uptake via mitochondrial Ca^{2+} uniporter (MCU) regulates mitochondrial ATP generation and dynamics (O-Uchi et al., 2013). Mitochondrial Ca^{2+} handling also in part controls Ca^{2+} signaling and amount of Ca^{2+} in other parts of a cell (Duchen et al., 2008).

Studies have also shown that caveolin can localize into mitochondria and affect ETC, fluidity of mitochondrial membranes and in a use of oxygen. Lack of Cav1 and Cav2 leads to impaired ATP synthesis. Caveolins could play a role in a decreased MMP in adaptation to stress as well as in Ca^{2+} homeostasis of the mitochondria. (Fridolfsson et al., 2012)

2. Aims and hypothesis

Several studied have shown that IFs and/or keratins affect mitochondria morphology and function (Nekrasova et al., 2011; Matveeva et al., 2015; Silvander et al., 2017; Winter et al., 2018). It has also been reported that $K8^{-/-}$ mouse colon epithelial cell mitochondria have reduced ketogenesis and fewer cristae (Helenius et al., 2015), and in that the loss of K8 in Caco-2 cells leads to diminished mitochondrial respiration and mitochondrial and caveolar Ca^{2+} signaling (unpublished data). Since both mitochondrial CL and MMP have a role in mitochondrial energy production, and $K8^{-/-}$ β-cells MMP is diminished, mitochondria mobility is increased and the mitochondrial network is fragmented (Silvander et al., 2017), it is hypothesized that the lack of K8 in Caco-2 cells cause changes in CL, MMP, the localization and mobility of mitochondria.

Since Cav1 has a role in Ca^{2+} signaling, CL synthesis (Yu et al., 2017) and mitochondrial function (Asterholm et al., 2012), changes in Cav1 upon knockout of keratins could be one factor behind diminished mitochondrial and caveolar Ca^{2+} signaling and mitochondrial respiration in Caco-2 cells (Nyström et al., unpublished data).

Lastly, keratins function in maintaining the intestinal barrier function (Zupancic et al., 2014; Wang et al., 2007) and the lack of K8 in mice has been shown to disturb barrier function (Misiorek et al., 2016). In this study it is hypothesized that the loss of K8 in Caco-2 cells disturbs barrier formation.

The major purposes of this study are to examine the role of K8 in mitochondrial function in Caco-2 cells, by determining mitochondrial CL and MMP levels and examining the distribution and movements of mitochondria as well as localization of Cav1. Also, the formation of the barrier function will be followed in Caco-2 cells with and without K8.

Aims of this study is to

1. Compare the appearance and localization of Cav1 between $K8^{+/+}$ and $K8^{-/-}$ Caco-2 cells

2. Analyze if loss of keratins in Caco-2 cells influences MMP.

3. Determine mitochondrial CL levels in absence of keratins in Caco-2 cells.

4. Study mitochondrial movement, appearance and localization after knockout of keratins in Caco-2 cells.

5. Analyze barrier function by measuring trans-epithelial/endothelial electrical resistance (TER) in Caco-2 cells with and without keratins.

3.Materials and methods

3.1 Cell Culture

3.1.1 CRISPR/Cas9 Caco-2 $K8^{+/+}$ and $K8^{-/-}$ cells

Caco-2 cells are a human epithelial cell line originally obtained from human colorectal adenocarcinoma (Lea, 2015). Caco-2 cells have been used to mimic the intestinal epithelial barrier and these cells can spontaneously form a monolayer of cells owning several features of common enterocyte cells (Lea, 2015). In CRISPR/Cas9 $K8^{-/-}$ Caco-2 cells the KRT8 gene has been knocked out using clustered regularly interspaced short palindromic repeats (CRISPR) and CRISPR-associated protein (Cas) genome edition technique, and a wild type control cell line was been generated from CRISPR/Cas9 - treated cells which still had the KRT8 gene (Misiorek et al., 2016).

3.1.2 Plating of the Caco-2 cells

$K8^{+/+}$ and $K8^{-/-}$ CRISPR Caco-2 cells were grown on 6-well cell culture plates (Cellstar®, Greiner Bio-One, Kremsmünster, Austria) in an 37 ºC incubator with 5 % CO_2 supply (Thermo Electron Corporation (today Thermo Fisher Scientific), Waltham, Massachusetts, United States). The cells were grown in Dulbecco's Modified Eagle Medium (DMEM, Sigma-Aldrich, St. Louis, Missouri, United States) containing 20 % Fetal Bovine Serum (FBS, Biowest, Nuaillé, France), with 100 µl/ml Streptomycin + 100 µl/ml Penicillin antibiotics (Sigma-Aldrich, St. Louis, Missouri, United States) and 2 mM L-glutamine (Biowest, Nuaillé, France).

$K8^{+/+}$ and $K8^{-/-}$ CRISPR Caco-2 cells were subcultured every time the cells reached 80-90 % confluency. $K8^{+/+}$ and $K8^{-/-}$ CRISPR Caco-2 cells were grown at the same time and divided at the same time points to keep passage number and conditions as similar as possible for both cell lines. However, since $K8^{+/+}$ Caco-2 cell growth was faster than for $K8^{-/-}$ cells, the cells were usually divided so that $K8^{+/+}$ were divided with lower split ratio than $K8^{-/-}$ cells.

CRISPR cells were divided around two or three times per week. All liquid substance used in cell culture were prewarmed (37 °C) before addition to live cells. To remove dead cells the cells were first washed with 1 ml phosphate buffer saline (PBS, Biowest, Nuaillé, France). After washing, the cells were detached from the well bottom by trypsinization

with 200 µl trypsin containing 0.25 % EDTA (Biowest, Nuaillé, France) at 37 ºC for 8-10 minutes. Trypsin causes cleavage of cell surface proteins by catalyzing the hydrolysis of peptide bonds, leading to detachment of adherent cells from the bottom of the well. When the cells were detached from the bottom, 800 µl of fresh medium was added to the wells and the cells were subcultured.

Caco-2 cells were grown on 10 cm dishes (Cellstar, Greiner Bio-One, Kremsmünster, Austria) in a 37 ºC incubator with 5 % CO_2 supply. The cells were grown in DMEM containing 10 % FBS, with 100 µl/ml Streptomycin + 100 µl/ml Penicillin antibiotics and 2 mM L-glutamine.

Caco-2 cells were divided around two or three times per week. To remove dead cells the cells were first washed two times with 8 ml phosphate buffer saline. After washing, the cells were detached from the well bottom by trypsinization with 2 ml trypsin containing 0.25% EDTA at 37 ºC for 8-10 minutes. When the cells were detached from the bottom 8 ml of DMEM was added to the dish and the cell suspension was moved to a 15 ml falcon tubes. The cells were centrifuged at 1000 rpm for 4 minutes after which the supernatant was discarded, and the pellet was resuspended in 10 ml of DMEM. Caco-2 cell were usually divided using a 1:4 split ratio onto a new 10 cm dish.

3.2 Transfection

Transfection is a method to introduce nuclei acids into a cell, and this can be achieved by using one of three different methods: chemical, biological or physical (Kim and Eberwine, 2010). In this thesis chemical transfection was applied by using lipofectamine 2000 (L2000) to deliver plasmid DNA or small interfering RNA (siRNA) into cells. Plasmid DNA used were Cav1 untagged- (kind gift from the Daniel Abankwa lab) and Cav1-GFP- and mito-RFP -plasmids (kind gift from the Kid Törnquist lab). Also, K8/K18 siRNA was introduced to the Caco-2 cells via L2000 based transfection.

3.2.1 siRNA transfection

Specific genes can be silenced by transfection of small interfering RNA (siRNA) into cells. Inside the cell this double-stranded siRNA forms, together with several proteins, RNA-induced silencing complexes (RISCs) leading to an unwinding of the double-strand structure of siRNA. Then this single-stranded siRNA binds to its complementary

messenger RNA (mRNA), activating mRNA cleavage which leads to a destruction of mRNA, silencing the gene encoding that mRNA. (Filipowicz et al., 2005).

L2000 based transfection of siRNAs was used to silence K8/K18 gene expression in Caco-2 cells. Mock- and scramble-transfected cells were used as negative controls. In scramble controls siRNA without any target on cells were used and in mock controls all other transfection reagents expect siRNA itself were added. (Strnad et al., 2016)

The transfection procedure was conducted three times to maximize the effectiveness of the K8/K18 silencing. Caco-2 cells were plated on 24-well plate (Cellstar®, Greiner Bio-One, Kremsmünster, Austria) according to the protocol in chapter 3.1.2. The cells were splitted so that the confluency would be around 20 %- 30 % the next day. On the next day the first transfection was conducted. L2000 (Invitrogen, Carlsbad, California, United States)-Opti-MEM (Gibco, Thermo Fisher scientific, Waltham, Massachusetts, United States) solution was prepared by mixing 1.5 µl L2000 with 25 µl 1x Opti-MEM for one 24-well plate well and, K8/K18 siRNA and K8/K18 scramble siRNA mixtures were made for each well by mixing 30 pmol of 100 µM K8 scramble and 30 pmol 100 µM K18 scramble siRNA to 25 µl of Opti-MEM or 30 pmol 100 µM K8 siRNA and 30 pmol 100 µM K18 siRNA to 25 µl Opti-MEM per well. Mock mixture contains only 25 µl of Opti-MEM per well. The L2000 and siRNA mixtures were then incubated 5 minutes in room temperature before mixing the siRNA-Opti-MEM mixture with the L2000-Opti-MEM mixture and the final mixtures were incubated for 20 minutes in room temperature. To remove dead cells and waste the cells were washed once with PBS and 0.5 ml of fresh media was added in each well. After incubation 50 µl of the siRNA- L2000, scramble siRNA- L2000 or mock mixtures were added per well, and the plate was gently swirled or tapped in order to mix. After 72 hours the transfected Caco-2 cells were subcultured onto a 12-well plate (Cellstar, Greiner Bio-One, Kremsmünster, Austria) and on the next day the second transfection was conducted in the same way as the first one, but with twice as much of all reagents. After 72 hours the cells were subcultured again onto 24-well plates containing12 mm coverslips (Fisher scientific, Hampton, New Hampshire, United States). On the next day the third siRNA transfection was done in the same way as the first one. In order to study caveolin-1, a number of mock, scramble siRNA- and siRNA-transfected cells were transfected with caveolin-1 -plasmid 48 hours after the last siRNA transfection (see chapter 3.2.2 for DNA transfection).

3.2.2 DNA transfection

$K8^{+/+}$ and $K8^{-/-}$ CRISPR Caco-2 cells were seeded in 12-well plates containing 12 mm microscope coverslips, according to the protocol mentioned in chapter 3.1.2, so that the confluency would be around 30 %-40 % the next day. The next day CRISPR Caco-2 cells or 48 hours from K8/K18 siRNA, mock- K8/K18 scramble siRNA- and K8/K18 siRNA-treated Caco2 cells (see chapter 3.2.1) were transfected with cav1-GFP or untagged Cav1 plasmid since Caco-2 cells do not express Cav1. Alternatively, CRISPR cells were transfected with mito-RFP to detect mitochondrial appearance and localization.

For transfection in 12-well plate L2000 -Opti-MEM solution was prepared by mixing 3.5 µl L2000 with 50 µl 1x Opti-MEM for one well , plasmid-Opti-MEM mixtures were made for each plasmid by mixing 1 µg of plasmid DNA with 50 µl Opti-MEM per well. L2000 and plasmid mixtures were then incubated 5 minutes in room temperature before mixing plasmid-Opti-MEM mixtures with L2000-Opti-MEM mixtures and incubated 20 minutes in room temperature. To remove dead cells and waste the cells were washed once with prewarmed PBS and 1 ml of fresh media was added in each well. After incubation, 100 µl of the plasmid- L2000 mixtures were added per well, and the plate was gently swirled or tapped in order to mix. DNA transfection in 24-well plates was done similarly but, with half of the amount of every substance used.

3.3 Immunostaining

Immunostaining is a method for detecting a specific protein in a tissue or in cells with the help of antibodies which identify only that specific target protein. Primary antibodies, which detect the protein(s) under investigation are first introduced to cells or tissue. Next secondary antibodies, conjugated with fluorophores, are used to detect the bound primary antibodies. (Maity et al., 2013)

For immunostaining of cells grown on coverslips in 12-well plates, the cells were washed 3 times with PBS (Medicago, Uppsala, Sweden) and fixed with 1 % paraformaldehyde (PFA, Sigma-Aldrich St. Louis, Missouri, United States) in for 15 minutes at room temperature. The coverslips were then washed 3 times with PBS for 5 minutes and transferred to a moisture chamber. The samples were first washed three times with 0.025% Triton-X (Sigma-Aldrich, St. Louis, Missouri, United States) in PBS for 5 minutes. Triton-X is a non-ionic surfactant which is used to permeabilizes cell membranes. Next 0.2% Nonidet P-40 (NP-40; Applichem, Darmstadt, Germany) in PBS was added for 5 minutes. NP-40 breaks lipid membranes making the cell more permeable

for staining. After NP-40 treatment the coverslips were again washed three times with 0.025% Triton-X for 5 minutes. Next, the samples were blocked with 2.5 % Bovine Serum Albumin (BSA, Sigma-Aldrich, St. Louis, Missouri, United States) for 20 minutes (buffer A) and then with 2.5 % BSA mixed with 1:50 normal donkey serum (NDS) and 1:50 normal goat serum (NGS) (buffer C) for 10 minutes. BSA is a non-reactive protein and used to block non-specific binding of the antibodies. NDS and NGS are further used to block un-specific binding of secondary antibodies which are produced in goat or donkey. After blocking the samples were incubated with primary antibody or antibodies diluted in buffer C overnight at 4 ºC (table 2).

On the next day the coverslips were washed three times 5 minutes with PBS before blocking for 10 minutes with buffer C. After blocking the samples were incubated with fluorescent secondary antibodies diluted in buffer C in the dark for 1 hour at room temperature (table 2). After incubation with the secondary antibody the samples were washed 5 min with PBS, followed by 5 min incubation with the nuclear stain DAPI (Invitrogen, Carlsbad California, United States) and/or DRAQ5 (Thermo Fisher Scientific, Waltham, Massachusetts, United States) diluted in PBS (table 2). If both DAPI and DRAQ5 were added to the same sample, DAPI was first added for 5 min, after which DRAQ5 was added for 5 min. The samples were washed with PBS one last time for 5 min and the coverslips mounted on top of a drop of Prolong Gold antifade (Thermo Fisher, Waltham Massachusetts, United States) on a microscope slide (Fisher Scientific, Hampton, New Hampshire, United States). Prolong Gold attaches the coverslips on the microscope slides and protects the samples from bleaching. The samples were kept 24 hours in dark at room temperature to let Prolong Gold to dry, before storage at 4 ºC in the dark, to protect the fluorescence antibodies from bleaching.

CRISPR/Cas9 Caco-2 $K8^{+/+}$ and $K8^{-/-}$ grown on 12 mm coverslips were washed once and incubated with 2.5 uM NAO to stain CL and 50 nM TMRE to detect mitochondria for 30 minutes in 37 °C in 5 % CO_2. After staining the samples were washed once with PBS and fixed with 1 % PFA for 15 minutes. Fixed samples were then washed 3 times with PBS and the coverslips were mounted using Prolong Gold as done previously.

Table 2. Used antibodies, plasmids and dyes. Plasmids, antibodies and dyes and their concentrations used in this study.

Target	Primary antibody or plasmid	Concentration	Secondary antibody or dye	Concentration	Excitation Wavelength (nm)
Caveolin-1 (untagged) Plasmid	**Caveolin-1** (Cell Signaling Technology, United States)	**1:400**	**Anti-rabbit Alexa Fluor 546** (Invitrogen, United States)	**1:200**	**546**
Caveolin-1-GFP-plasmid	**Cav1-GFP -plasmid**				**488**
Mitochondria	**TOM20** (Santa Cruz Biotehcnology, United States)	**1:300**	**Anti-Rabbit Alexa Fluor 488** (Invitrogen, United States)	**1:200**	**488**
			Anti-Rabbit Alexa Fluor 546 (Invitrogen, United States)		**546**
Mitochondrial membrane potential			**TMRE** (Abcam, United Kingdom)	**25-100 µM**	**549**
Cardiolipin			**NAO** (Sigma-Aldrich, United States)	**25-100 µM**	**495**
Mitochondria	**Mito-RFP -plasmid**				**555**
Nucleus			**DRAQ5** (Thermo fisher Scientific, United States)	**1:700-1:3000**	**647**
			DAPI (Invitrogen, United States)	**1:10 000**	**358-461**
Cell wall			**Phalloidin** (Molecular Probes Inc, United States)	**1:200**	**488 or 546**
Keratin 8	**K8** (Progen, Germany)	**1:300**	**Anti-Mouse Alexa Fluor 488** (Thermo fisher Scientific, United States)	**1:200**	**647**
			Anti-Mouse Alexa Fluor 546 (Thermo fisher Scientific, United States)		**546**
	Troma I (DSHB, Iowa)	**1:500**	**Anti-Rat Alexa Fluor 647** (Thermo fisher Scientific, United States)		**647**
			Anti-Rat Alexa Fluor 568 (Thermo fisher Scientific, United States)		**568**

3.3.1 Imaging of immunostained samples

Microscopy samples were imaged with a 3i CSU-W1 spinning disk microscope (3i Intelligent Imaging Innovations, Denver, Colorado, USA) or Leica TCS SP5 confocal microscope (Leica, Wetzlar, Germany) using 63x or 100x objectives.

3.4 Mitochondrial membrane potential measurement

MMP causes a negative charge around -180mV that can be detected with a positively charged tetramethylrhodamine ethyl ester (TMRE) dye. TMRE emits red fluorescence and the fluorescence intensity levels correlate with the level of MMP in the cells. (Crowley et al., 2016) MMP can be measured using TMRE since it is a lipophilic cation which is concentrated in mitochondria in proportion to MMP. TMRE can be used to measure MMP also since it does not to a high extent bind to the mitochondria themselves. TMRE inhibits OXPHOS to some extent (Scaduto et al., 1999).

3.4.1 Live cell imaging with TMRE

For live cell imaging of TMRE labelled cells, CRISPR $K8^{+/+}$ and $K8^{-/-}$ Caco-2 cells was plated on glass bottom microwell dishes (MatTek Corporation, Ashland MA USA) according the protocol mentioned in the chapter 3.1.2. On the next day the cells were washed two times with 37 ºC prewarmed Fluorobrite medium (Gibco, Thermo Fisher scientific, Waltham, Massachusetts, United States) containing 20 % FBS, with 100 µl/ml Streptomycin + 100 µl/ml Penicillin antibiotics and 2 mM L-glutamine. Fluorobrite is a DMEM based media designed for live cell imaging with lower background fluorescence than standard DMEM. After testing different concentrations (25 nM-200 nM) of TMRE (Abcam, Cambridge, United Kingdom) (Appendix C figure 7), 25 nM of TMRE was diluted in Fluorobrite media was added to the cells and incubated 20 minutes in a incubator (37 ºC, 5 % CO_2), since TMRE staining overall resulted in bright images and since TMRE can be slightly harmful to the cells (Scaduto et al., 1999) the lowest still working concentration was decided to be use. After incubation the TMRE solution was removed and changed to Fluorobrite media for imaging with a SP5 matrix confocal microscope (Leica, Wetzlar, Germany) with live cell imaging settings (37 ºC and 5 % CO_2).

3.4.2 Plate reader assay for TMRE

For plate reader TMRE measurements cells were plated in 96-well plates (Cellstar, Greiner Bio-One, Kremsmünster, Austria) following the basic protocol mentioned in chapter 3.1.2, except after trypsinization and addition of 800 µl DMEM in 6-well plate the cells were moved to a 15 ml falcon with 9 ml of DMEM. The cells were centrifuged at 1000 rpm for 4 minutes. The supernatant was discarded, and the pellet was resuspended into 3 ml of DMEM. The cell quantity was determine by pipeting 10 µl of the cell suspension into a Countess Cell Counting Chamber Slides (Invitrogen, Carlsbad, California, United States) and cells were counted using a Countess II Automated Cell Counter (Invitrogen, Carlsbad, California, United States). The cells were diluted with DMEM so that 60 000 cells per well could be pipetted into a 96-well plate. The cells were incubated overnight a 37 ºC incubator with 5 % CO_2 supply.

At first different cell amounts, TMRE concentrations and carbonyl cyanide 4-(trifluoromethoxy)phenylhydrazone (FCCP; Abcam, Cambridge, United Kingdom)

concentrations were tested to optimize the protocol (Appendix A). At first a too low cell amount (5 000 -15 000) were tested (Appendix A figure 3) and also on actual assay around 15 000 cells per well was first used. However, since a high number of cells got lost after TMRE treatment and washing and only very few cells remained at the well. The loss of cells can be due to TMRE being lightly harmful to the cells and since Caco-2 cells prefer growing in clusters and as such the too few cells on the well may cause them to be more prone to detach from the plate during the TMRE procedure. On later assays 50 000-65 000 cells per well was decided to use since there seemed to be more cells left in the wells after staining, while still not being too confluent, than with previously tested lower numbers of cells. The TMRE concentration from 150 nM to 1200 nM was tested, which all worked intensity being lowest at 150 nM and highest at 1200 nM as expected (Appendix A figure 1). However, it was decided to use 1000 nM TMRE for plate reader assay. FCCP works as a positive control in a TMRE assay since it depolarizes mitochondrial membrane potential by making the inner mitochondrial membrane permeable to protons, thus destroying the proton gradient of the inner mitochondrial membrane (Krhon et al., 1999; Kalbácová et al., 2003). FCCP concentrations from 10 µM to 50 µM were tested with 1000 nM TMRE staining (Appendix A figure 2). FCCP impaired MMP somewhat with all concentration and 50 µM was selected to be used based on several test.

On the next day the cells were washed two times with pre-warmed PBS. 50 µM of FCCP, diluted in Fluorobrite medium was added to control wells and incubated for 10 minutes in a 37 ºC incubator with 5 % CO_2 supply. 1000nM of TMRE diluted in Fluorobrite medium was added to the cells and incubated 20 minutes at the incubator. After incubation the TMRE solution was removed and the cells were washed once with PBS. Fluorobrite medium was added to the plate before TMRE measurement using a Hidex Sense microplate reader (Turku, Finland). The following measurement settings were used: 544 nm excitation with 20 nm bandwith and 616 nm emission with 8.5 nm bandwith, 15 flashes and bottom read mode.

Normalization of the results to the cell amount was tried, the cells were fixed with 1 % PFA 15 min, stained with DAPI and imaged with CellIQ (CM Technologies Oy, Tampere, Finland) but the washing steps after TMRE staining caused most of the cells to be washed away. Furthermore, live cells were stained with live cell nuclear dye Hoechst (Life Technologies, Carlsbad, California, United States) and imaged with an Eclipse Ti2-

E microscope (Nikon, Minato, Tokyo, Japan) with automatic 96-well 6x6 tile and z-stack settings but again many of the cells were washed off. There were also a lot of dead cells and cells were located on several levels, so that focusing on the cells did not work and hence all cells could not be imaged, since in every 96-well plate image some of the wells ended up being wrongly constructed from the smaller 6x6 tile images (Appendix B figure 7). Also, automatic imaging of 96-well with tile setting take several hours and in addition, the calculation of cell number from the images would also take a long time since the threshold should be set for every stack in Z-stack and the edges of wells should be excluded from every image. Finally, live cells were stained with PrestoBlue cell viability reagent (Invitrogen, Carlsbad, California, United States) which changes colour to red when in contact with the live cells. This colour change can be detected by absorbance- or fluorescence-based methods and used as indicator of cell viability and for cell quantification. In this study the PrestoBlue-stained cells were imaged with a Hidex microplate reader (Example of CL plate reader assay shown in appendix B figure 4), but when tested with different cell amounts, the results were not linear and thus the result of the PrestoBlue staining could not be trusted (Appendix B figure 5).

Since the normalization to the cell amount did not work, normalization against cell confluency was tried using an Incucyte S3 High Content microscope (Sartorius, Göttingen, Germany). Phase contrast imaging with the Incucyte microscope does not require any staining and the cells can be imaged right after TMRE measurement with a microplate reader (example of CL plate reader assay shown in appendix B figure 6). With the Incucyte microscope images of every well of the 96-well plate were automatically taken by using a 4x objective to take an image of the whole well or with a 10x objective to take a maximum of five images of a single well. However, the size of $K8^{-/-}$ and $K8^{+/+}$ CRISPR Caco-2 cells may differ and normalization to the confluency may not be the best method to use in this case.

3.5 Mitochondrial tracking by live cell imaging

Cells were grown on glass bottom microwell dishes, stained and washed similarly as were done in TMRE live cell imaging in chapter 3.4.1, expect mitochondrial were stained by incubation with 50 nM TMRE or 250 nM of Mitotracker deep red (Thermo Fisher Scientific, Waltham, Massachusetts, USA) for 30 minutes. Mitochondria were imaged using a Leica SP5 matrix confocal microscope using a 63x objective with live cell settings

(5% CO_2 and 37 °C). Cells were imaged every 10 s for 2 min to track the movements of mitochondria.

3.6 Cardiolipin measurement

10-N-nonyl-3,6-bis(dimethylamino)acridine (10-N-nonyl acridine orange, (NAO) is a fluorescent live cell dye which binds to CL in the inner membrane of the mitochondria independently of the membrane potential (Gallet et al., 1995; Mileykovskaya et al., 2001). When NAO binds to CL it causes the dye to form a dimer leading to a shift in excitation and emission wavelengths, from 496 and 525 nm to 450 and 640 nm (Petit et al., 1992; Gallet et al., 1995), which can then be detected with fluorescent- or absorbance-based methods. Positively charged NAO binds also to other negatively charged phospholipids (phosphatidylinositol and phosphatidylserine) but to a lot lesser extent than to CL (Gallet et al., 1995; Petit et al.,1992).

3.6.1 Live cell imaging with NAO

For live cell imaging CRISPR $K8^{+/+}$ and $K8^{-/-}$ Caco-2 cells were plated on glass bottom microwell dishes according to the protocol in chapter 3.1.2. On the next day, the cells were washed two times with prewarmed Fluorobrite media. Based on commonly used concentrations of NAO for live cell imaging (Jacobson et al., 2002; Gohil et al., 2005), concentrations of 25 nM or 50 nM (Appendix C figure 9) of NAO (Sigma Aldrich, St. Louis, Missouri, United States) diluted in Fluorobrite was tested by adding dye to the cells and incubated 20 minutes in 37 ºC. After incubation the NAO solution was removed and changed to a Fluorobrite and the cells were imaged using a Leica SP5 matrix confocal microscope with live cell imaging settings under 37ºC and 5% CO_2 with excitation wavelength 495 nm and emission wavelength at 519 nm using 63x objective. Live cell imaging of NAO was not continued after testing with 2 concentrations due to extensive bleaching.

3.6.2 Plate reader assay for NAO

For plate reader measurement of NAO CRISPR cells were plated in 96-well plates as done in chapter 3.4.2. The next day, the cells were washed two times with PBS. 2.5 µM of NAO diluted in fluorobrite was added to the cells and incubated for 20 minutes in 37 ºC incubator with 5% CO_2 supply. After incubation the NAO solution was removed, and

the cells were washed once with PBS. Fluorobrite media was added to the plate before NAO measurement with a Hidex Sense microplate reader. The following measurement settings were used: 485 nm excitation with 10 nm bandwidth and 535 nm emission with 20 nm bandwith,15 flashes and bottom read mode.

For NAO plate reader a similar test with cell amount were conducted as TMRE plate reader chapter 3.4.2, with first assays done with too low cell amount and later assays the same 60 000 cells, was used for NAO plate reader assay, since NAO and TMRE assay were conducted around same time. Different dye concentrations were tested to optimize the protocol. NAO concentrations between 0.5 µM- 5 µM were tested (Appendix A figure 1). Since common concentration of NAO used for plate reader in literature is 2.5 µM (Widlansky et al., 2010), NAO in too high concentrations is toxic to cells impairing mitochondrial respiration (Maftah et al., 1990), and the test with 2.5 µM gave a good signal, it is used in the NAO plate reader assays in this study.

Normalization of the plate reader results was done as in case of TMRE microplate reader as explained in the chapter 3.4.2. (Appendix B). In addition to normalization against cell amount or confluence, also normalization of plate reader results by protein assay was tested (Appendix B figure 3), following protein assay protocol in chapter 3.7. But since a lot of cells were lost during NAO staining and following washing steps, and the total protein amount might be changed upon the loss of keratins and then the amount of the proteins between the $K8^{+/+}$ and $K8^{-/-}$ cells can be different, the protein assay is not a trustworthy method for normalization of plate reader results.

3.7 Protein assay

For protein assay analysis, lysates of CRISPR/Cas9 $K8^{+/+}$ and $K8^{-/-}$ cells were first done. After washing cells with cold PBS, cold homogenization buffer containing 1x complete protease inhibitor cocktail (Roche, Switzerland) and 2% phenylmethylsulfonyl fluoride (PMSF) to inhibit protein degradation was added and the cells were scraped from the wells. After boiling the samples for 5 minutes in 95 °C, the samples were mechanized syringe shedding 8 times with 27G needle. Protein assay was done using Pierce™ BCA Protein Assay Kit (Thermo Scientific, Waltham, MA, USA). The assay was conducted according manufactures microplate procedure protocol, with some modifications. The protein assay kit uses the bicinchoninic acid (BCA) assay method to quantify total protein

with colorimetric detection. Proteins in the samples cause the reduction of cupric ion (Cu^{2+}) to cupric cation (Cu^{1+}) in an alkaline medium and the kit uses this feature by detecting Cu^{1+} by BCA. Blank sample containing homogenization buffer only and actual samples were diluted 1:10 with distilled water. 25 µL of each BSA made protein standard (50 µg/ml, 100 µg/ml, 250 µg/ml, 500 µg/ml, 750 µg/ml and 1000 µg/ml), blank and samples were pipetted in duplicates into a 96-well microplate. 200 µL of working reagent containing 50 parts of buffer A and 1 part of buffer B were pipetted in the wells. The plate was tapped gently to mix and incubated at 37 ℃ for 30 minutes in the dark. After this the plate was further incubated in room temperature for 10 minutes in the dark before absorbance of 560 nm was measured with a spectrophotometer (Wallac Victor^{2TM}, Perkin Elmer Waltham, Massachusetts, USA). Total protein was calculated in Excel as in the Pierce™ BCA Protein Assay Kit protocol. A standard curve was created from the average of blank-corrected 560 nm measurements for each BSA standard vs. its concentration. A standard curve was then used to determine the protein concentrations of the samples.

3.8 Barrier function measurement

A CellZscope+ device (Nanoanalytics, Münster Germany) was used to determine the impedance of the cell layers capable of forming barrier, and will give values for ohmic resistance (TER, transepithelial / -endothelial resistance) and capacitance (Ccl) of the cell layer. The TER values correlate with the permeability and integrity of cell layers. Ccl value measures confluency of the cell layer (Srinivasan et al., 2015) Cells are grown on semipermeable filter inserts. Two electrodes are used to get readings of electrical current; one electrode is placed into the apical compartment inside the inserts and the other is located on the basolateral side in the lower compartment, so that the cell layer is located between the two electrodes (Image 7).

Caco-2, CRISPR/Cas9 Caco2 $K8^{+/+}$ and $K8^{-/-}$ cells were counted as done in chapter 3.4.2 and plated on 6.5 mm polystyrene Transwell Permeable Support inserts (COSTAR, Corning Incorporated, Kennebunk ME USA) 10 000 (experiment 1) or 30 000 (experiment 2) cells was counted per insert. Reference (control) inserts contained no cells. The cells were incubated two days at 37 ºC, 5% CO_2 incubator before starting the barrier function measurements with the Cellzscope+ device. The measurements took three to four weeks and 3/4 of the media was changed every two days and a complete media change was done once a week.

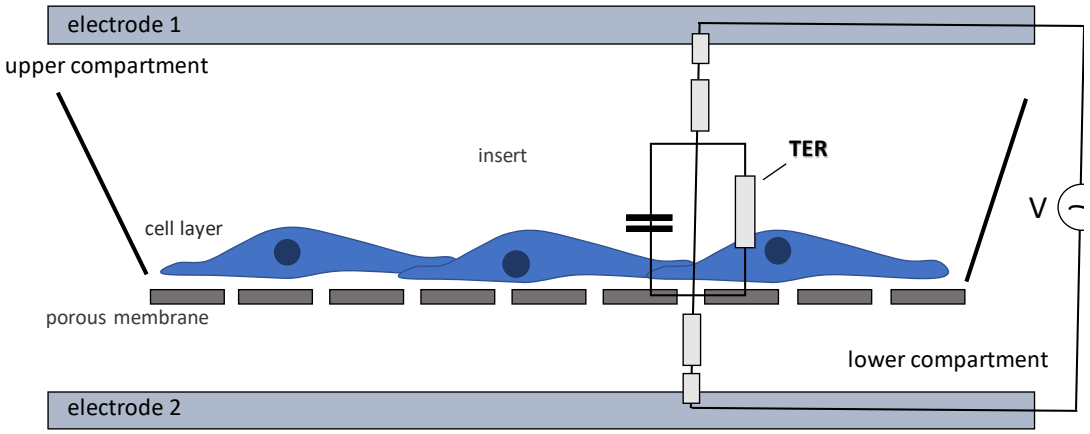

Figure 7. The CellZscope+ device and TER measurement. Two electrodes, measuring electrical resistance, are placed so that the cell layer grown on semipermeable insert is located between them.

When the barrier was formed Caco-2 cells were transfected once with K8/K18 siRNA similar way as done in the chapter 3.2.1. Also, two types of controls without knockout of K8 were done; three inserts of the negative control scramble and three inserts of mock controls, also three inserts were left without transfection.

For L2000 Opti-MEM solution was prepared by mixing 0.7 µl L2000 with 12.5 µl Opti-MEM for one insert. K8/K18 siRNA and K8/K18 scramble siRNA mixtures were made for each by mixing 10 pmol/ insert of 100 µM K8 scramble and 100 µM K18 scramble siRNA to Opti-MEM or 10 pmol/insert 100 µM K8 siRNA 100 µM K18 siRNA Opti-MEM. L2000, scramble and siRNA mixtures were then incubated 5 minutes in room temperature before mixing siRNA-Opti-MEM and scramble mixtures with L200+Opti-MEM mixtures and incubated 20 minutes in room temperature. After incubation 25 µl of the siRNA, scramble or mock mixtures were pipetted to the inserts.

In the second experiment only a scramble siRNA control was used as negative control for siRNA treatment. In the second experiment the transfection was done with higher siRNA concentration: 20 pmol of scrambled siRNA per insert and 20 pmol K8/K18 siRNA per insert since 10 pmol did not seem to be enough to knock out K8/K18 as was done previously. However, transfection still did not cause any difference in barrier function measurements.

3.9 Quantification and statistics

3.9.1 Quantification of MMP from live cell imaging

The corrected total cell fluorescence (CTCF), or in this case more correct term to use would be the corrected total mitochondrial fluorescence, was measured from TMRE live cell imaging microscope images. CTCF measurements were conducted by using Image J software (Reuden et al., 2017) by first drawing an area of interest (ROI) around 10 mitochondria in one cell in the image (Figure 8) while two or three background ROIs without mitochondria were drawn. Image J then calculates the area mean fluorescence and integrated density for the ROIs. CTCF was then determined in Excel by calculating the average area of mitochondria multiplied with the mean fluorescence of background readings and the resulting value was then subtracted from the average of integrated density of all 10 mitochondria. The significance of result was determined by Student's t-test.

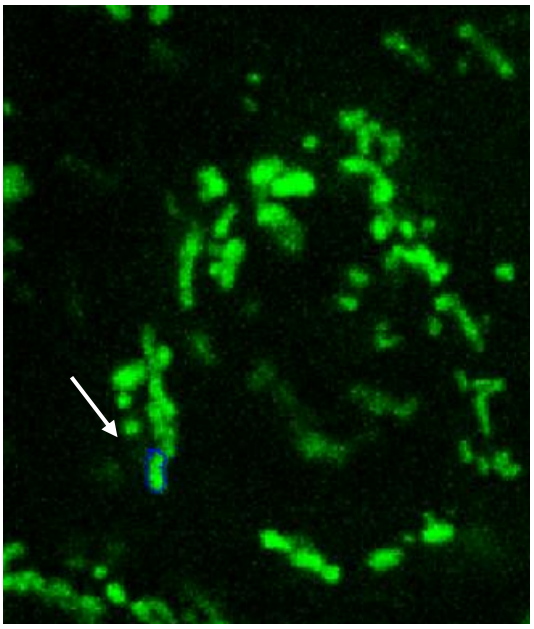

Results

File Edit Font Results

	Area	Mean	IntDen	RawIntDen
1	0.161	128.222	20.601	1154
2	0.339	111.947	37.971	2127
3	0.678	100.026	67.855	3801
4	0.750	82.810	62.089	3478
5	0.428	132.125	56.609	3171
6	2.713	104.086	282.436	15821
7	0.464	115.577	53.645	3005
8	0.500	140.179	70.069	3925.000
9	0.553	101.839	56.359	3157.000
10	0.768	104.047	79.870	4474.000

CTCF = Integrated Density - (Area of mitochondria x Mean fluorescence of background)

Figure 8. Mitochondrial membrane potential measurement from live cell imaging. CTCF was calculated for MMP live cell imaging experiment. By using Image J software, ROI was drawn around 10 mitochondria per image and two to three background ROIs. Then area, mean fluorescence and integrated density (IntDen) were measured for every ROI by the software. After this the CTCF was calculated in Excel by calculating first average of mitochondria areas times mean fluorescence of background readings. The result was subtracted from the average of the IntDen of the 10 mitochondria. The image is zoomed for drawing ROI. Arrow + blue circle= ROI area around mitochondria. Green= TMRE. CTCF= Corrected total cell fluorescence.

3.9.2 Quantification and statistics of plate reader experiments

Plate reader results represents the average of at least 16 wells per genotype from which the average of 8 blank wells (only cells in Fluorobrite media) per genotype has been subtracted, to reduce any possible interference from the background readings. The plate reader assay was repeated at least 3 times and two-tailed Student T-test was used to measure statistical difference between the genotypes. T-test results were considered significant if p-values were *$p<0.05$, **$p<0.01$ and ***$p<0.001$.

3.9.3. Mitochondrial tracking

Mitochondria clusters movements were followed using manual tracking plugin Fiji software (Schindelin et al., 2012). 10-15 mitochondria cluster per image were tracked and in total 92-208 mitochondria cluster per genotype were tracked. Fiji then calculates the velocity of every mitochondria cluster at every time point. The average velocity of every mitochondrial cluster track was calculated in Excel and the significance of the results was determined by student T-test. T-test results were considered significant if P-values were *$p<0.05$, **$p<0.01$ and ***$p<0.001$

4. Results

4.1 Caco-2 cells have more, larger caveolin-1 aggregates and less, smaller caveolin-1 dots in cells without keratins

Previously done microarray indicated that cavin-1 and Cav1 mRNA levels were decreased in $K8^{-/-}$ mice colonic epithelial cells (unpublished data). Previous studies has also been shown that mitochondrial and caveolar Ca^{2+} signaling and mitochondrial respiration are diminished in $K8^{-/-}$ Caco-2 cells (Nyström et al., unpublished data) and since Cav1 has a role in Ca^{2+} signaling, CL synthesis (Yu et al., 2017) and mitochondrial function (Asterholm et al., 2012), changes in Cav1 upon knockout of K8 could be one factor behind these changes.

The possible influence of keratins on the Cav1 distribution was studied by transfection of Cav1 into CRISPR/Cas9 $K8^{+/+}$ and $K8^{-/-}$ Caco-2 cells followed by immunostaining and microscopy. Immunostaining revealed that there were more large aggregates of Cav1 and less smaller Cav1 dots in $K8^{-/-}$ compared to $K8^{+/+}$ cells and this could be seen with both Cav1 -GFP (Figure 9A) and untagged Cav1 (Figure 9B) plasmid constructs. K8 staining confirmed that $K8^{-/-}$ cells lack keratin filaments, even though some K8 dots remained, while $K8^{+/+}$ cells have an intact K8 filament network (not shown).

Immunostaining of Caco-2 cells treated with K8/K18 siRNA and transfected with untagged Cav1 plasmid showed that there were cells lacking K8 completely, while in some cells the transfection was not effective, and they still had keratin filaments (Figure 10). All mock-treated control Caco-2 cells had K8 filaments as expected (Figure 10). Also, K8/K18 siRNA-treated Caco-2 cells showed similar effect on Cav1 protein as CRISPR/Cas9 $K8^{-/-}$ cells, having more aggregation of larger Cav1 particles in areas lacking K8 filaments, than mock treated Caco-2 cells (Figure 10).

Staining of F-actin with phalloidin to detect cell membranes for distinguishing individual cells for quantification, showed that in some cases the membranes of individual cells could clearly seen, but in other cases the staining of membranes was messy, independent of siRNA. Therefore F-acting staining could not be used to separate cells from each other in these cases for quantification (not shown).

In summary the loss of K8 in Caco-2 cells lead to the aggregation of Cav1 compared to the cells with normal K8 network.

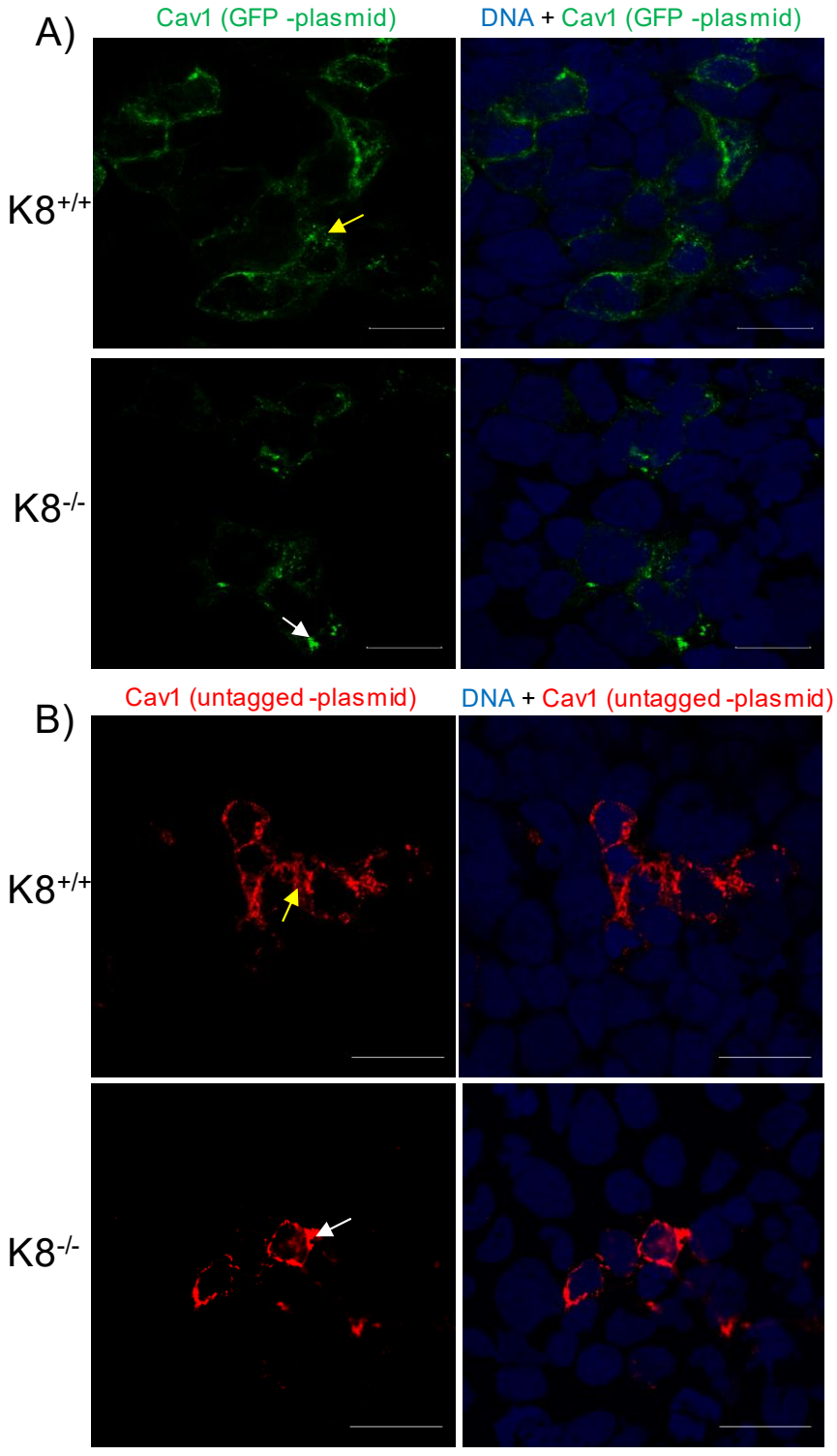

Figure 9. CRISPR/Cas9 Caco-2 K8$^{-/-}$ cells have larger Cav1 aggregates and less small Cav1 speckles. Cav1 localization was analysed in the CRISPR/Cas9 Caco2 K8$^{+/+}$ and K8$^{-/-}$ cells by transfecting the cells with a) Cav1 GFP- (green colour) or b) untagged Cav1-plasmids and immunostained for nucleus (blue colour) and in the case of untagged Cav1 for Cav1 (red colour). K8$^{-/-}$ cells (white arrows) have larger Cav1 aggregates compared to K8$^{+/+}$ cells (yellow arrows). Scale bar =25 µm.

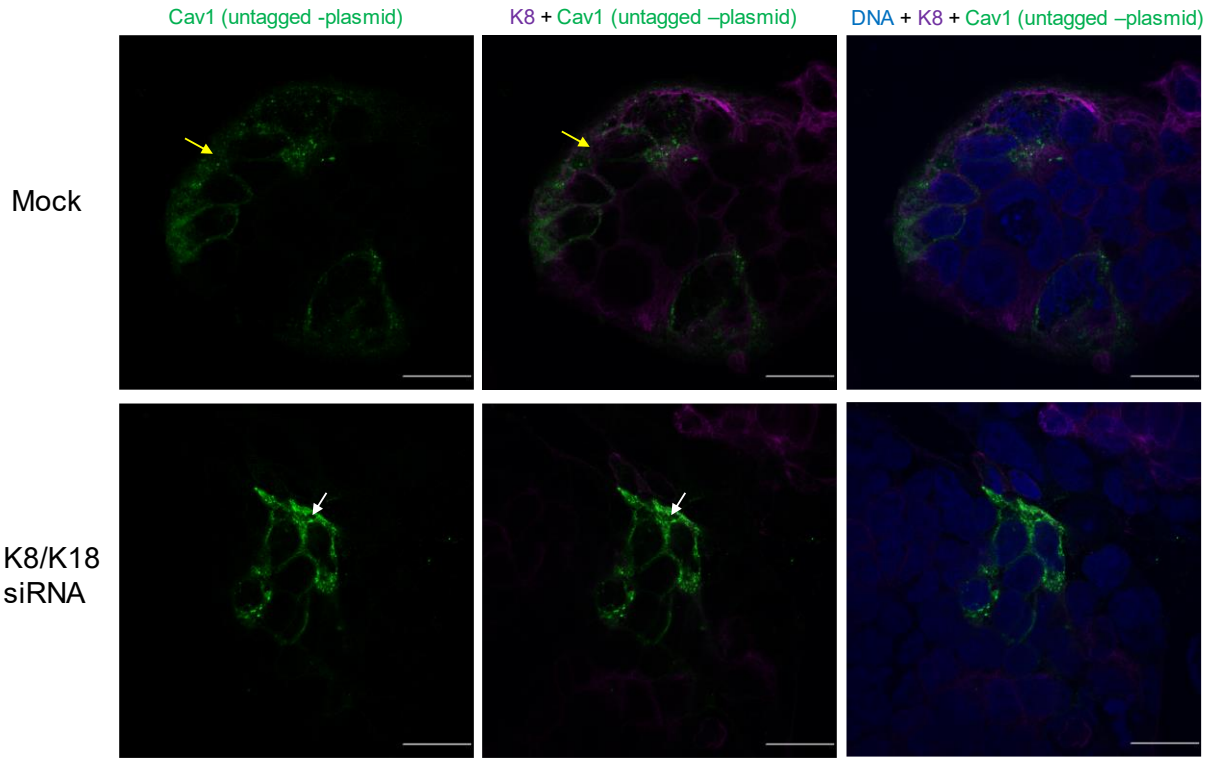

Figure 10. In Caco-2 cells transfected K8/K18 siRNA to downregulated K8 leads to the aggregation of the Cav1 and decreased amount of small Cav1 speckles. To study Cav1 localization in Caco-2 cells, the cells were mock-transfected or transfected with K8/K18 siRNA, after which the cells were transfected with Cav1 plasmid and immunostained for Cav1 (green), nucleus (blue colour) and K8 (magenta). Mock treated Caco-2 cells have smaller Cav1 speckles (yellow arrow) compared to K8/K18 siRNA treated cells lacking K8 (white arrow). Scale bar = 25 µm.

4.2 Mitochondrial membrane potential is lower in the absence of K8 in Caco-2 cells

Since in previous studies keratins have been shown to affect mitochondrial function and energy metabolism in e.g. colon epithelial and β-cells (Helenius et al., 2015; Silvander et al., 2017) and in Caco-2 cells (Nyström et al., unpublished), the effect of keratins on mitochondrial membrane potential (MMP) was measured in CRISPR/Cas9 Caco2 $K8^{+/+}$ and $K8^{-/-}$ cells using TMRE.

At first labelling CRISPR/Cas9 Caco-2 cells with TMRE and live cell imaging with confocal microscopy was conducted.Even though, in several images from live cell imaging it seemed that TMRE intensity indicating MMP levels would be decreased in CRISPR/Cas9 Caco-2 $K8^{-/-}$ cells compared to $K8^{+/+}$ cells (Figure 11A), quantification of the images showed that $K8^{+/+}$ cells (Figure 11B, black bar) compared to $K8^{-/-}$ cells (Figure 11B white bar) have no difference in MMP levels, even though in $K8^{-/-}$ cells may be lightly but insignificantly decrease overall, taking in account all the images and tested

concentrations of TMRE (Appendix C figure 8). However, since live cell imaging could not be done exactly at the same time for both genotypes and due to possible differences in bleaching of the dye between the genotypes the results of live cell imaging are not fully reliable. Also, TMRE staining with fixed samples imaged with confocal microscope were tested, but the staining did not seem to work (not shown).

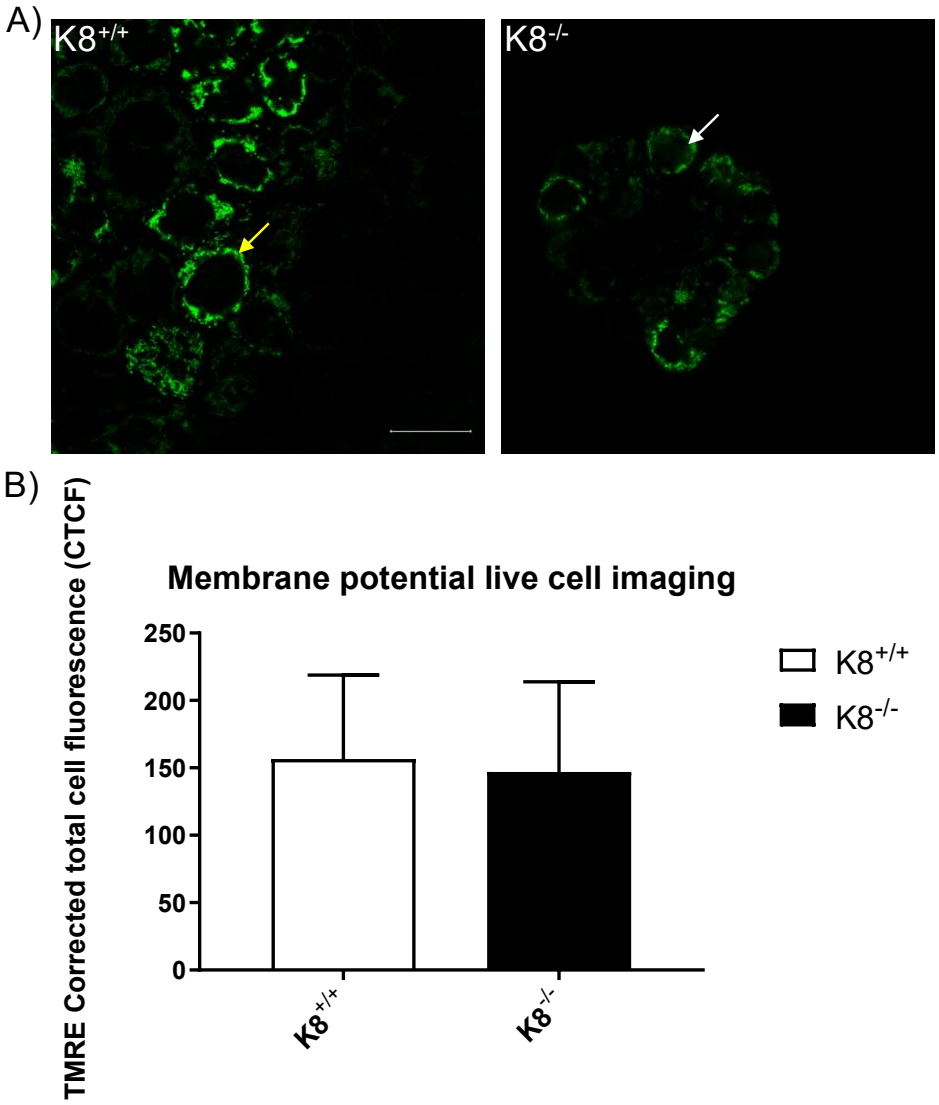

Figure 11. According to live cell microscopy MMP had a trend of light decrease in CRISPR K8$^{-/-}$ Caco-2 cells. A) CRISPR/Cas9 K8$^{+/+}$ and K8$^{-/-}$ cells were labelled with 25 nM TMRE to detect mitochondria (green colour) and live cell imaging with confocal microscope was conducted. Intensity of TMRE seemed to be decreased on some of the CRISPR/Cas9 K8$^{-/-}$ Caco-2 cells (white arrow) compared to K8$^{+/+}$ cells (yellow arrow). B) Quantification of TMRE intensity from live cell images. There are no significant difference in MMP levels between CRISPR/Cas9 Caco-2 K8$^{-/-}$ cells (black bar) compared to K8$^{+/+}$ cells (white bar), even though MMP may have a trend to be lightly lower in K8$^{-/-}$cells. However, bleaching of the dye make the result untrustworthy. Results are average of 25 images per genotype, with 10 mitochondria per image. Scale bar = 25 µm. Data is presented as mean plus/minus standard deviation.

Plate reader assay with TMRE showed that in the $K8^{-/-}$ cells MMP decreased compared to $K8^{+/+}$ cells (Figure 12). Also, TMRE fluorescence intensity levels were lower in positive control samples treated with FCCP (Figure 12), as expected. Normalization of the plate reader results to the number of cells by live cell or fixed cell nuclear staining or to confluency by Incucyte S3 High Content microscope imaging (Appendix B) was attempted but was unsuccessful, since a lot of cells were lost after TMRE staining and/or the washing and fixation steps after it. Analyzed by eye most of the plate reader assays more of $K8^{-/-}$ cells seemed to be lost compare to $K8^{+/+}$ cells during the plate reader assay (Appendix B figure 6 and 7), which makes plate reader assay results unreliable without normalization.

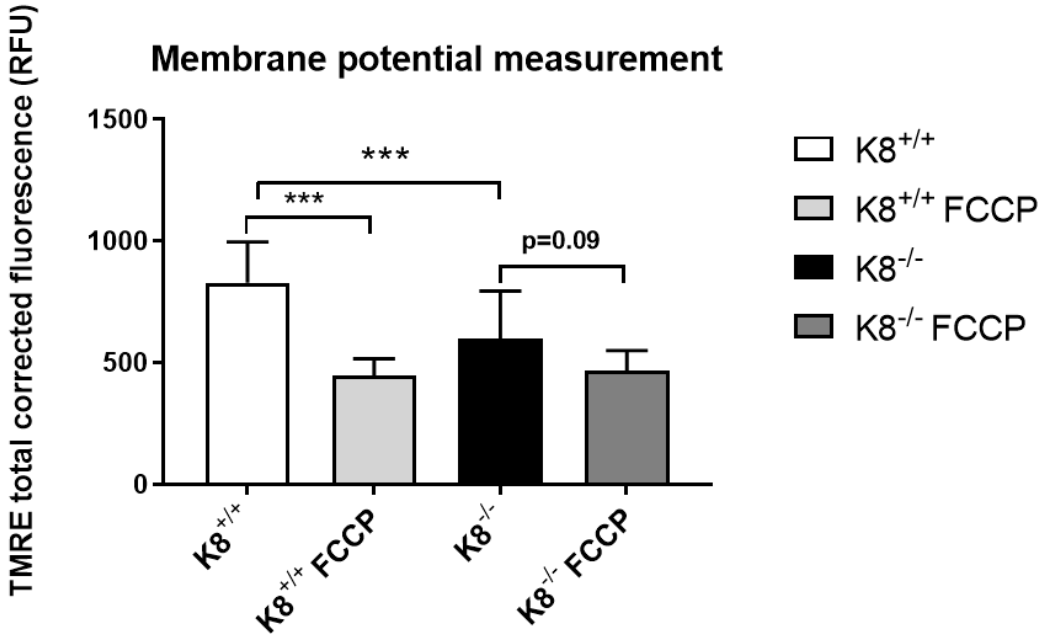

Figure 12. MMP is decreased in CRISPR/Cas9 $K8^{-/-}$ Caco-2 cells compared $K8^{+/+}$ Caco-2 cells in plate reader assay. CRISPR/Cas9 $K8^{+/+}$ (white bar) and $K8^{-/-}$ (black bar) Caco-2 cells were stained with TMRE and a plate reader assay was conducted. 8 blank wells with cells only (no TMRE dye) per genotype have been subtracted from the results and all wells were normalized to one reference well intensity. Results are the average of 29 wells per genotype from one plate reader experiment. RFU = relative fluorescence units. dark grey bar = CRISPR/Cas9 Caco-2 $K8^{+/+}$ TMRE intensity with FCCP. Light grey bar = CRISPR/Cas9 Caco-2 $K8^{-/-}$ TMRE intensity with FCCP. P-value was determined with student-t test. ***p<0.001. Data is presented as mean plus/minus standard deviation.

4.3 Lack of K8 in CRISPR/Cas9 Caco-2 cells lead to decreased levels of cardiolipin

To further study mitochondrial function and the diminished respiration phenotype in absence of keratins in previous studies (Nyström et al., unpublished), the CL levels in CRISPR/Cas9 $K8^{+/+}$ and $K8^{-/-}$ Caco-2 cells were studied using the fluorescent CL-marker NAO in a plate reader setting. The fluorescence intensity of NAO, revealing the levels of CL, was significantly higher in CRISPR/Cas9 Caco2 $K8^{+/+}$ cells compared to $K8^{-/-}$ cells (Figure 13). Normalization of plate reader results to the number of cells, protein amount or to confluency was attempted, but it was unsuccessful due to loss of cells in washing steps after NAO staining (Appendix B). Live cell imaging by confocal microscopy was also tested with NAO-stained CRISPR/Cas9 Caco2 cells (Appendix C figure 9), but due to extensive and quick bleaching of the fluorescence dye live cell imaging was not continued. Also, NAO staining with fixed samples imaged with confocal microscope was tested, but staining was unsuccessful (not shown).

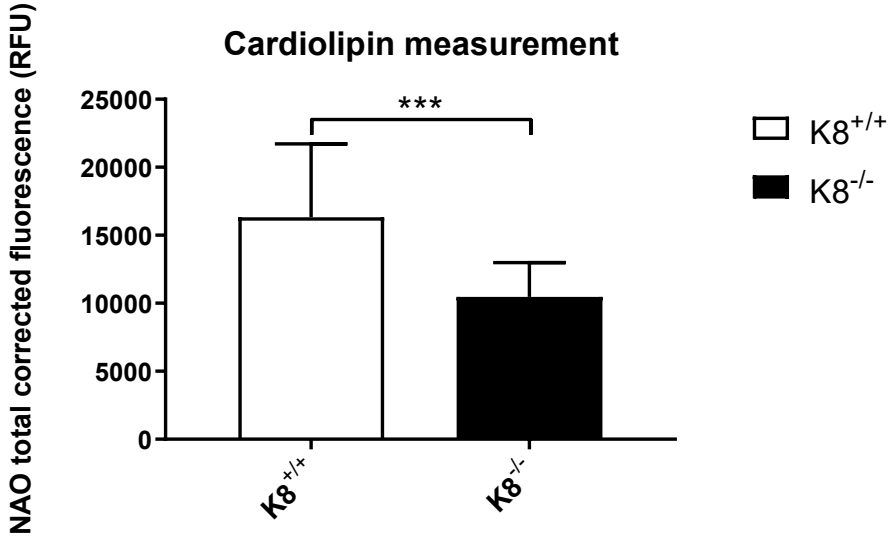

Figure 13. Mitochondrial cardiolipin levels are decreased in $K8^{-/-}$ CRISPR/Cas9 Caco-2 cells compared to $K8^{+/+}$ CRISPR/cas9 Caco-2 cells. CRISPR/Cas9 Caco-2 $K8^{+/+}$ (white bar) and $K8^{-/-}$ (black bar) cells were labelled with NAO to detect CL and a plate reader assay was conducted to detect the intensity levels of the NAO. The average of blank wells with cells only (no NAO dye) have been subtracted from the results and all wells are normalized to one reference well intensity. Results are the average of 16 wells per genotype from one plate reader experiment. n=16. P-value was determined with student t-test. ***$p<0.001$, data is presented as mean plus/minus standard deviation. RFU = relative fluorescence units.

4.4 Mitochondria are more dispersed in CRISPR K8$^{-/-}$ Caco-2 cells

According to previous studies IFs may affect mitochondrial localization and distribution (Nekrasova et al., 2011; Silvander et al., 2017; Steen et al., 2020). To analyze if the same is true also in Caco-2 cells lacking K8, mitochondria distribution and localization were studied by transfection with a mitochondrial marker, mito-RFP, and/or immunostaining. Immunostaining of mitochondria with TOM20 showed that the mitochondrial network could be more fragmented in CRISPR/Cas9 K8$^{-/-}$ Caco-2 cells compared to K8$^{+/+}$ cells (Figure 14), even if the cells in these settings have very small cytoplasmic volume and the mitochondrial patterns are hard to evaluate and quantify. The distribution of the mitochondrial network could be seen more clearly in mito-RFP transfected cells (Figure 14B), but cells were highly heterogenous regarding mitochondrial appearance. However, according to the TOM20 staining the mitochondrial network seemed to be less organized in K8$^{-/-}$ cells compared to K8$^{+/+}$ cells, where TOM20 staining made a clear pattern around the cells near the cell membrane following K8 staining. This pattern was less clear or missing from many of the K8$^{-/-}$ cells (Figure 14 A, white arrows).

In case of K8/K18 siRNA treated or mock treated Caco-2 cells, a slightly similar but milder effect on the re-distribution of mitochondria was seen in Caco-2 cells which lack K8 as in CRISPR/Cas9 K8$^{-/-}$ cells (Figure 15).

In conclusion, in Caco-2 cells lacking K8 filaments exhibit a more dispersed mitochondrial network

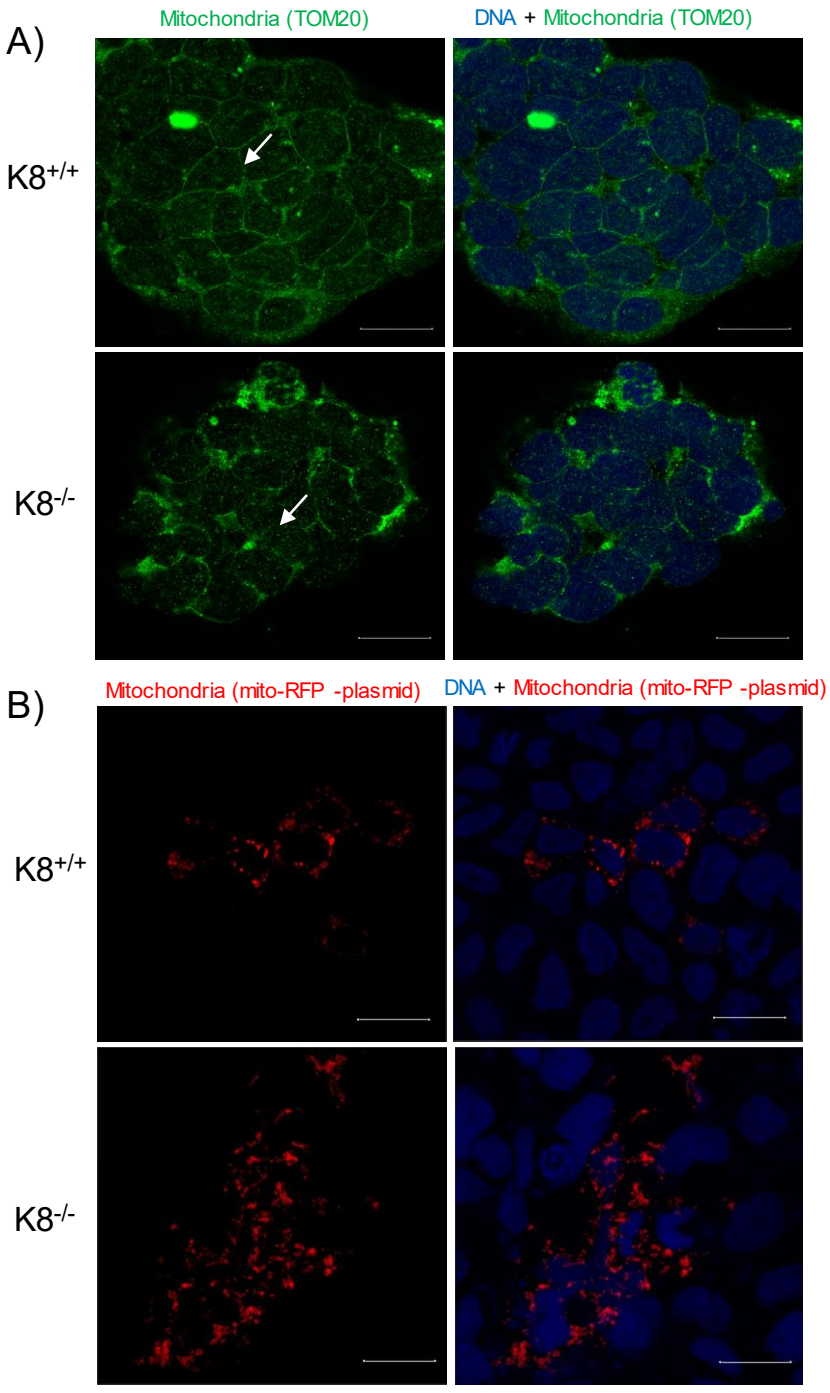

Figure 14. Loss of K8 in CRISPR/Cas9 Caco-2 leads to dispersed mitochondrial network. To study mitochondria localization as a function of K8, CRISPR/Cas9 Caco2 $K8^{-/-}$ and $K8^{+/+}$ cells were A) fixed and immunostained with TOM20 antibody to detect mitochondria (green colour) or B) transfected with mito-RFP (red colour) and fixed. Images are maximum z-projection of the cell monolayer. Blue = nuclei (DRAQ5). Scale bar = 25 µm. Arrows = example of the cell where mitochondria staining made a clear pattern around the cells near the cell membrane in $K8^{+/+}$ cells, but not in $K8^{-/-}$ cells.

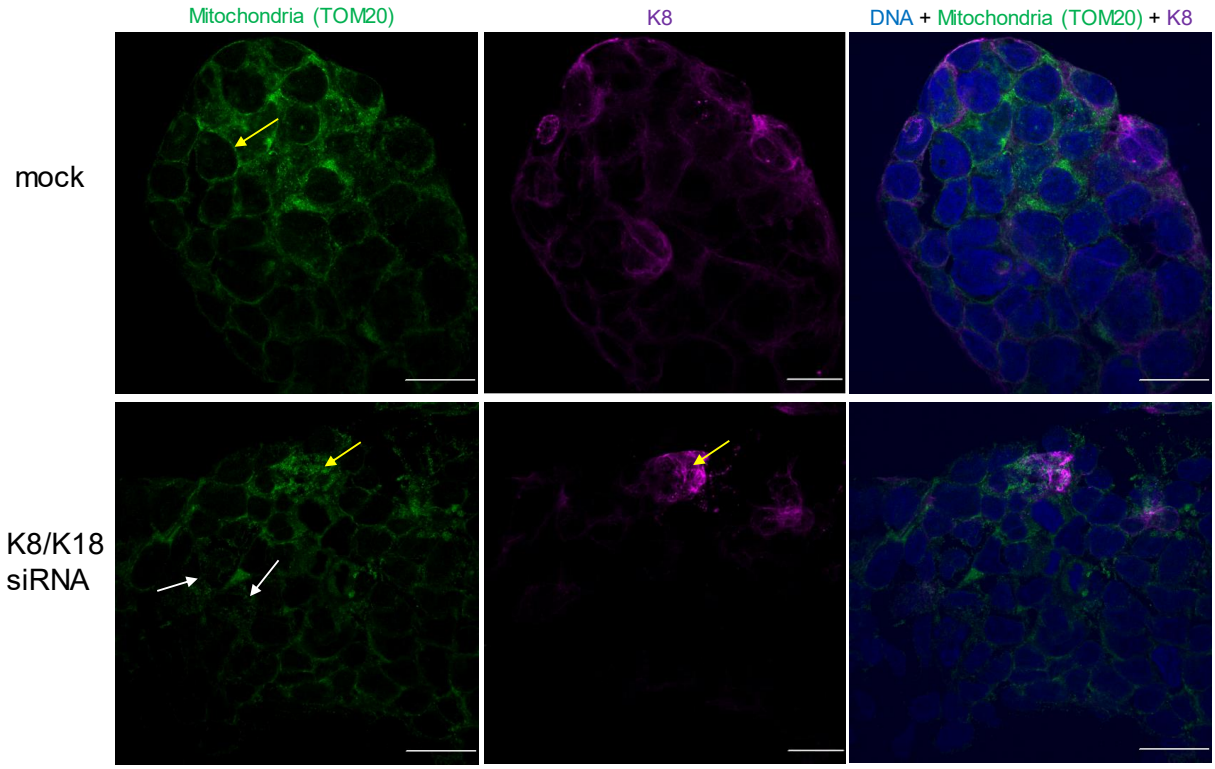

Figure 15. In Caco-2 cells treated with K8/K18 siRNA to downregulated K8 mitochondria are more dispersed. To study localization of mitochondria Caco-2 cells were mock-transfected or transfected with with K8/K18 siRNA and immunostained for mitochondria (green colour), K8 (magenta colour) and for DNA (blue colour). With TOM20 staining, cells in which K8 still remained (yellow arrows), mitochondria made more clear pattern around the cells near the cell membrane following K8 staining, even though similar pattern could still be seen in cells lacking K8 (white arrows) it was less clear and missing from some cells. Scale bar = 25 µm.

4.5 Mitochondrial mobility is increased upon the loss of K8 in Caco-2 cells

In previous studies mitochondrial mobility have been reported to be increased upon the loss of keratins (Silvander et al., 2017; Steen et al., 2020). To examine the role of K8 in mitochondrial movements in Caco-2 cells, CRISPR/Cas9 $K8^{+/+}$ and $K8^{-/-}$ Caco-2 cells were labelled with Mitotracker Deep Red or TMRE and imaged over time. Individual mitochondria clusters were tracked with the Fiji manual tracking plugin. Analysis of mitochondrial mobility showed that mitochondria moved significantly faster in CRISPR/Cas9 $K8^{-/-}$ Caco-2 cells compared to $K8^{+/+}$ cells as seen with both dyes (Figure 16).

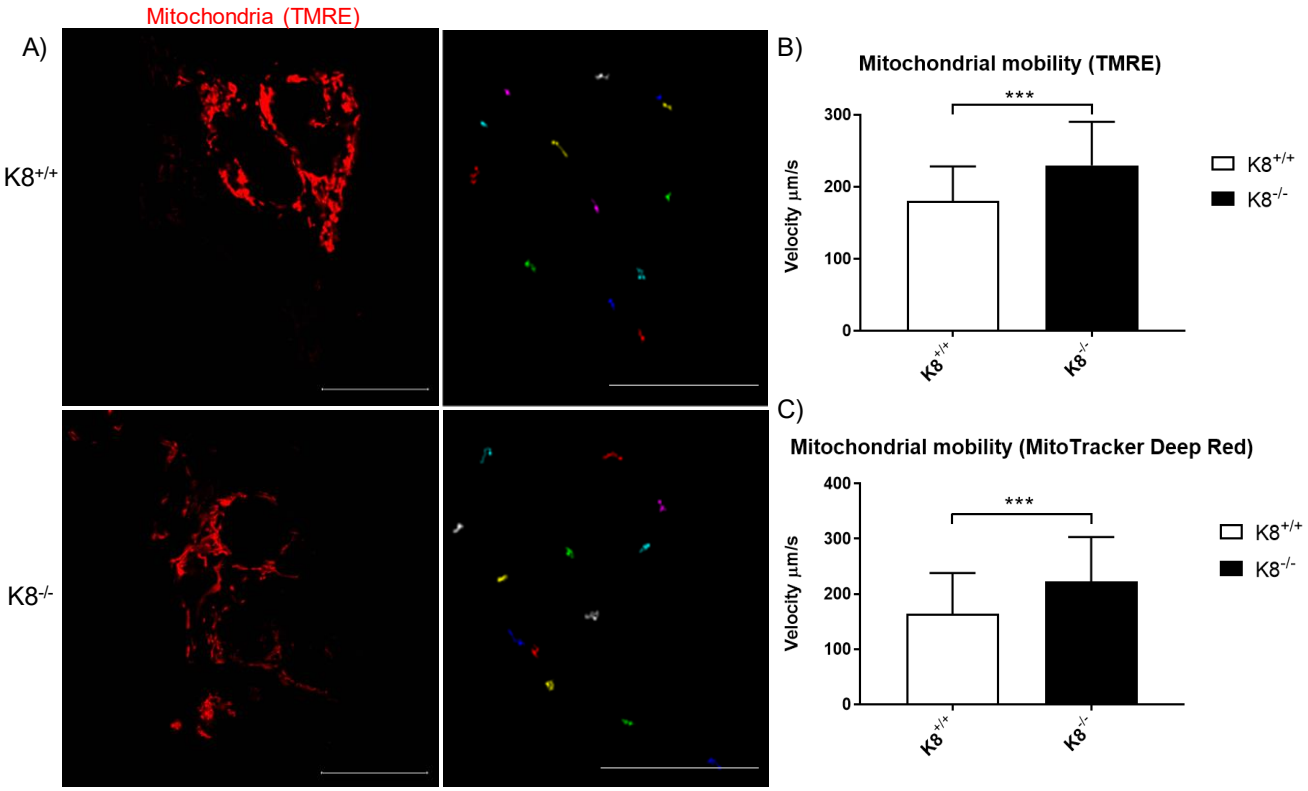

Figure 16. Mitochondria movement analysis. Mitochondria were labelled with MitoTracker deep red or TMRE and tracked by confocal microscopy. A) Example of mitochondrial tracking with TMRE (red colour) in CRISPR/Cas9 K8$^{+/+}$ and K8$^{-/-}$ Caco-2 cells. In zoomed images mitochondria cluster time lapse tracks marked in different colors. B) Velocity of mitochondria stained with TMRE. C) Velocity of mitochondria stained with Mitotracker Deep Red. Results are average of 208 mitochondria for Mitotracker deep red and 100 mitochondria for TMRE. Student t-test were used to determine p-value. *** $p<0.001$. Scale bar = 25 µm. Data is presented as mean plus/minus standard deviation.

4.6 Intestinal barrier formation is disturbed in CRISPR K8 $^{-/-}$ Caco-2 cells

Previously, in K8$^{-/-}$ mice intestinal barrier function has been shown to be disrupted (Wang et al., 2007; Misiorek et al., 2016) and several other studies indicate that keratins function in maintaining and/or formation of barriers (Liovic et al., 2009; Zupancic et al., 2014). CRISPR/Cas9 Caco-2 K8$^{+/+}$ and K8$^{-/-}$ cell monolayers were followed with a Cellzscope+ device, to investigate if similar distribution of the barrier formation can be seen in Caco-2 cells lacking keratins as has been seen in previous studies.

For this, two pilot experiments were performed. In the first experiment done with lower cell amounts and older (higher passage) CRISPR/Cas9 Caco-2 K8$^{-/-}$ cultures, cells formed only a very mild increase in TER after around 250-450 hours of the experiment (Figure 17 A1) even though the cells reached confluency already at 130 hours (Figure 17

B1). However, $K8^{-/-}$ cells lost this confluency after 400 hours. Importantly, CRISPR/Cas9 Caco-2 $K8^{+/+}$ TER values reached higher values earlier than $K8^{-/-}$ cells, TER being at a maximum value already at around 250 hours from the start of the experiment, but with very high variation between inserts (Figure 17 B1). $K8^{+/+}$ cells reached confluency also earlier than $K8^{-/-}$ and remained confluent. In the second experiment, with a higher amount of younger (lower passage) cells, in the CRISPR/Cas9 Caco-2 $K8^{-/-}$ cells barrier was formed starting from 100 hours (Figure 17 A2 blue line), but the formation of the barrier was delayed compared to $K8^{+/+}$ cells where the formation of the barrier started already at around 70 hours (Figure 17 A2, violet line), the reason behind delayed barrier formation in $K8^{-/-}$ is probably due to delay in reaching confluency compared to $K8^{+/+}$ cells (Figure 17 B2). However, in $K8^{+/+}$ cells it took shorter time period to achieve higher TER values and it took longer time to TER values to decrease after cells start to loose confluency than in $K8^{-/-}$ cells. $K8^{-/-}$ cells took longer time to achieve lower TER values and also lost TER in shorter time period after losing confluency (Figure 17 B1 and B2) than $K8^{+/+}$ cells.

Barrier function experiment were conducted also for Caco-2 cells, which were transfected with K8/K18 siRNA after TER values had risen (barrier had formed) and cell layer reached confluency. However, siRNA transfection did not seem to have any effect on TER levels and barrier function in Caco-2 cells before and after K8/K18 siRNA transfection (not shown) resembled CRISPR/Cas9 $K8^{+/+}$ Caco-2 cells.

Barrier function experiments revealed that the lack of K8 in Caco-2 cells could disturb the formation of the barrier function.

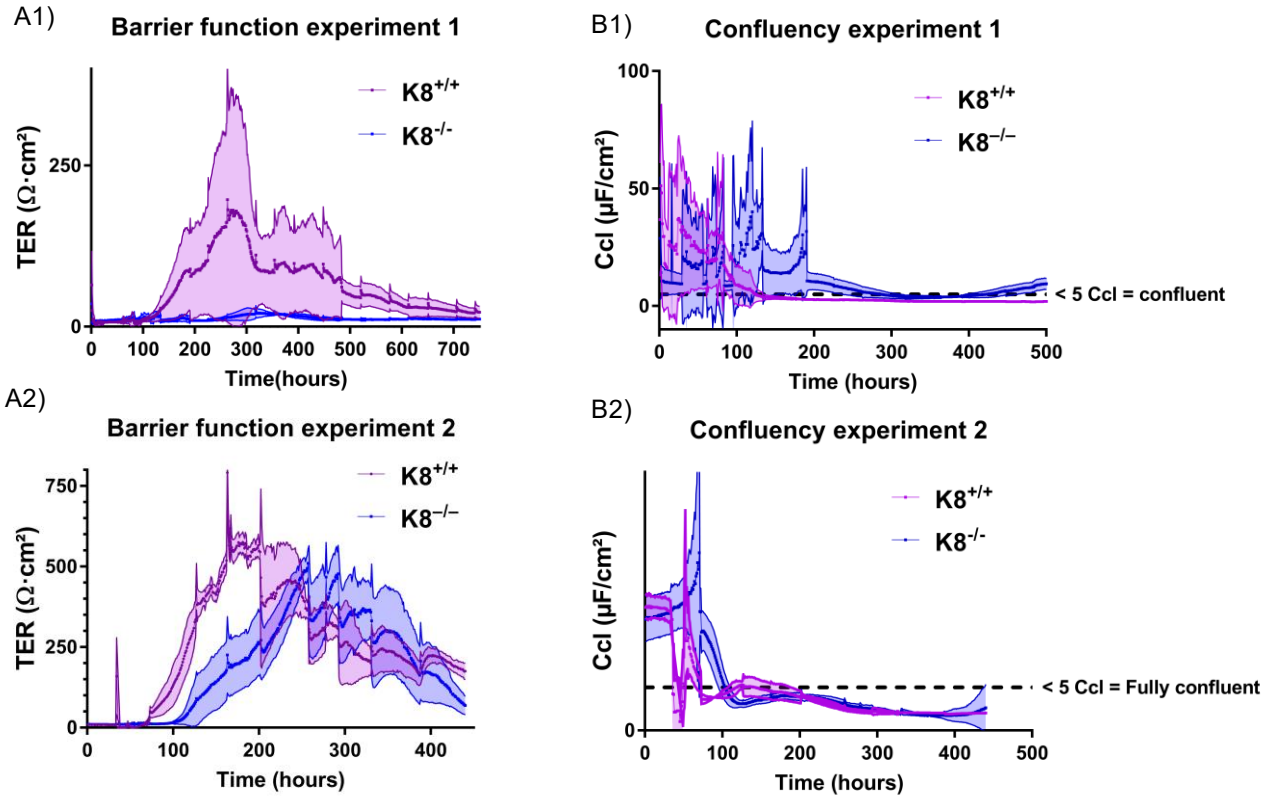

Figure 17. Loss of K8 in CRISPR/cas9 Caco-2 disturbs barrier formation. CRISPR/Cas9 Caco-2 $K8^{+/+}$ and $K8^{-/-}$ cells were seeded on insert and A) barrier function (TER, transepithelial resistance) and B) confluency (conductance, Ccl) were measured by the Cellzscope+ device in two different experiments. Cell layer is confluent when Ccl value is less than 5. Cellzscope+ measures automatically long-term measurements of transepithelial /transendothelial resistance of cell layers under physiological conditions. Results are average of 4 $K8^{+/+}$ cell inserts and 6 $K8^{-/-}$ cell inserts. Magenta = CRISPR/Cas9 Caco-2 $K8^{+/+}$. Blue = CRISPR/Cas9 Caco-2 $K8^{-/-}$.

5. Discussion

5.1 Keratins have a role in mitochondrial function in Caco-2 cells

Several studies have linked IFs to the mitochondrial morphology and function (Nekrasova et al., 2011; Matveeva et al., 2015; Silvander et al., 2017; Winter et al., 2018; Steen et al., 2020). Furthermore, the loss of K8 in mouse colon leads to diminished energy metabolism, as $K8^{-/-}$ mice colonocytes have a lower rate of ketogenesis in mitochondria and decreased levels of rate-limiting ketogenesis enzyme HMGCS2. Also, mitochondria in $K8^{-/-}$ mouse colon had fewer and more diffuse cristae. (Helenius et al., 2015). The lack of K8 in Caco-2 cells has also been seen to lead decreased mitochondrial and caveolar Ca^{2+} signalling and decreased mitochondrial respiration (Nyström et al., unpublished data). In this study the *in vitro* Caco-2 cell model was used to further characterize and determine possible causes behind the diminished energy metabolism phenotype in $K8^{-/-}$ Caco-2 cell.

In mouse β-cells the loss of K8 has been reported to lead to alterations in mitochondrial appearance and localization, and to decrease MMP (Silvander et al., 2017). Since, the MMP and the mitochondria-specific lipid CL, have crucial roles in energy production in mitochondria by affecting OXPHOS, changes in them could be behind the K8 knockout energy metabolism phenotype. First live cell imaging with confocal microscope was done to measure CL and MMP levels, but the results were untrustworthy, since $K8^{-/-}$ and $K8^{+/+}$ Caco-2 cells could not be imaged exactly at the same time and due to high bleaching of the dyes the levels of bleaching might differ between the genotypes.

According to this thesis, both MMP and CL levels could be decreased in CRISPR/Cas9 Caco-2 $K8^{-/-}$ cells compared to $K8^{+/+}$ cells, but since normalization to the number of cells or confluency of cells did not succeed, the decreased levels of MMP and CL seen can be due to different amounts of cells between the genotypes, rather than a true difference between the intensity levels of the dyes. The results of normalization tests showed that after TMRE or NAO staining some of the cells were washed away. However, plate reader assay shown in this study the number of cells seemed to be somewhat similar between the genotypes. In most cases more $K8^{-/-}$ cells seemed to detach than $K8^{+/+}$ cells after staining and following washing (Appendix B figures B6 and B7), which makes the result of plate reader assay questionable without normalization, as the same number of cells were plated per genotype. Since keratins filaments work in protection of the cell against stress, the $K8^{-/-}$ cell might be more prone to harmful effect of NAO and TMRE dyes and

as such die and detach from the plate. Also, lack of K8 filaments may lead to diminished mechanical support and decrease in hemidesmosomes, which could further affect the cell viability and/or make them prone to detach from the plate. After several tests with different cell amounts and washing protocols, some of the plate reader assays were done in such a way that a more similar number of cells per genotype were left to the wells after plate reader assay. However, even if an equal amount of cells would remain after the assay, normalization to confluence could be problematic as cells may be of different sizes between the two genotypes and, in fact, by eye $K8^{-/-}$ cells appear to be slightly smaller in size than $K8^{+/+}$ cells. Also, normalization to protein assay has similar kind problems since the total protein amount between genotypes may differ. To overcome the problem of losing cells after treatment, a reagent like Cell-Tak tissue adhesive could be used to adhere cells to the bottom of the plate harder and faster. Gluing cells to the bottom of wells could make normalization unnecessary as plating cells and doing the plate reader assay could be done at the same day and the cells would not have time to proliferate and in theory there should be the same amount of cells during the plate reader assay as when plated.

In addition, staining CL with NAO may not be the most reliable way to study the levels of CL, since binding of NAO to CL *in vivo* can be unspecific (Gohil et al., 2005). NAO, in high concentrations, is also toxic to cells, leading to impaired mitochondrial respiration (Maftah et al., 1990). In the future CL levels in Caco-2 cells could be analysed by thin layer chromatography (Gohil et al., 2005) to confirm that CL levels are diminished in $K8^{-/-}$ Caco-2 cells compared to $K8^{+/+}$ cells.

If the decreased levels of CL and MMP seen without normalization were the true situation, and since both MMP and CL are crucial for normal function of mitochondria and for OXPHOS (Koopman et al. 2008; Yan and Kang, 2012; Jones, et al., 2017; Zorova et al., 2018) these changes could disturb mitochondrial function and ATP production, possibly leading to diminished energy metabolism. Such diminished energy metabolism phenotype has also been seen in $K8^{-/-}$ Caco-2 cells (Nyström et al., unpublished data). The levels of mitochondrial protein prohibitin are also seen to be diminished in Caco-2 cells lacking K8 (Nyström et al., unpublished data). One way in which prohibitin affects mitochondrial function is by controlling CL development (Richter-Dennerlein et al., 2014), and therefore the decreased CL levels may have been caused by decreased prohibitin levels. Changes in CL levels also affect mitochondrial appearance, since CL has a role in maintaining the integrity of mitochondrial cristae membranes (Ikon and Ryan, 2017). Lack of K8 in mice β-cells and colonocytes changed the appearance of

mitochondrial cristae (Misiorek et al., 2016; Silvander et al., 2017) and CL could be one factor causing this change. To confirm if lack of K8 influences the structure of mitochondria, transmission electron microscopy could be conducted in the future to study mitochondria appearance in detail in $K8^{-/-}$ and $K8^{+/+}$ Caco-2 cells. MMP is generated via proton pumps during OXPHOS (Crowley et al., 2016) and as such faults in OXPHOS, which has previously been seen in $K8^{-/-}$ Caco-2 cells with diminished mitochondrial respiration and decreased levels of the OXPHOS complexes (Nyström et al., unpublished data), may lead to disruptions in the generation of MMP. CL regulates the activity and/or synthesis of several of the OXPHOS complexes (Lange et al., 2001; Yu et al., 2017; Acehan et al, 2011; Malkamäki and Sharma, 2019). The lack of CL has been shown to diminish activity of the ADP/ATP carrier and CIV leading to reduced import of protons, which further disturbs MMP (Jiang et al., 2000), and as such the decreased CL levels could be one factor behind the lower levels of some of the OXPHOS complexes in $K8^{-/-}$ Caco-2 cells (Nyström et al., unpublished data). Reduced levels of OXPHOS complexes may also disturb generation of proton gradient possibly affecting to the formation of MMP.

The distribution of mitochondria was studied in Caco-2 cells by immunostaining. The immunostaining was conducted in two ways for Caco-2 cells: with mitochondria specific staining with TOM20 antibody or by transfection of mito-RFP -plasmid. Mitochondrial movement in Caco-2 cells were followed by staining with TMRE or Mitotracker deep red and live cell imaged taking images every 10 second for 2 min. Mitochondrial motility experiments with both used dyes showed that mitochondria moved significantly faster in $K8^{-/-}$ Caco-2 cells compared to $K8^{+/+}$ Caco-2 cells. Although, mitochondrial network was highly heterogeneous and no clear difference was seen between $K8^{-/-}$ Caco-2 cells compared to $K8^{+/+}$ cells in TOM20 staining, in overall it seemed that the mitochondrial network could be more fragmented in the Caco-2 $K8^{-/-}$ cells compared to $K8^{+/+}$ cells. The mitochondrial network seemed to be less organized in $K8^{-/-}$ cells compared to $K8^{+/+}$ cells, where TOM20 staining made a clear pattern around the cells accumulating near to the cell membrane, which was missing from many of the $K8^{-/-}$ cells. Also, by the eye, in $K8^{+/+}$ cells TOM20 staining seemed to follow keratin staining, which could indicate that keratins could be co-localizes with or bind to mitochondria. However, same kind mitochondrial organization, was seen also in some of the $K8^{-/-}$ cells, although with lesser amount than in $K8^{+/+}$ cells. The RFP tagged plasmid transfected mitochondria were more clearly distributed in several of $K8^{-/-}$ Caco-2 cells compared to $K8^{+/+}$ cells.

In previous studies in mice β-cells the loss of K8 leaded to fragmented mitochondrial network and increased mitochondrial mobility (Silvander et al., 2017). Also, loss of K16/K6 in skin keratinocytes disturb mitochondrial respiration and cristae formation, as well as increased mitochondrial mobility (Steen et al., 20 20). The rate of ATP production is lower when mitochondria are dispersed (Jeng et al., 2011) and as such a fragmented mitochondrial network leading to lower production of ATP could also partly explain the diminished mitochondrial respiration and ATP production seen in Caco-2 cells (Nyström et al., unpublished data). Also, elevated mitochondrial movements might affect energy metabolism since mitochondria accumulate to areas with high energy demands (Morris and Hollenbeck 1995). MMP drives also Ca^{2+} uptake into mitochondria and Ca^{2+} increase has been shown to lead decrease in mitochondrial movement and inhibition of mitochondrial movement increases Ca^{2+} uptake into mitochondria. (Yi et al., 2004). Ca^{2+} control of mitochondrial movement provides means to arrange ATP production and Ca^{2+} buffering of the mitochondria into areas where those are needed (Yi et al.,2004). As such keratins may affect to the Ca^{2+} homeostasis via Cav1 and MMP leading to the changes on mitochondrial movement or vice versa keratins may stabilize mitochondria further affecting Ca^{2+}-signalling and further energy production.

Apolar keratins and other IFs might affect mitochondria by anchoring them so that mitochondrial movements are decreased, and they are kept in place, while polar microtubules and actin filaments have been shown to function in mediating mitochondrial movements (Morris and Hollenbeck 1995). Changes in linker proteins connecting mitochondria to keratins upon the loss of K8, might be one reason behind the disturbed mitochondrial localization and movement in $K8^{-/-}$ Caco-2 cells. For example, the levels of plectin, a cytolinker protein, which has been shown to connect IFs to mitochondria (Winter et al., 2008), were decreased in hepatocytes lacking K8 (Galarneau et al., 2007). Rac1 has been shown to regulate mitochondrial motility via PAK1 kinase and phosphorylation mutations of vimentin IFs have been proposed to affect PAK1 and as such lead to an increase in mitochondrial motility (Matveeva et al., 2015). Decrease on Mitofusin 2 (MFN2) has been shown to lead fragmentation of mitochondrial network and diminished levels of OXPHOS complexes with lower levels of MMP and ATP generation (Bach et al., 2003; Pich et al., 2005). K8/K18 have been reported to bind to trichoplein keratin filament-binding protein (TCHP) (Nishizawa et all., 2005), which is connected to the mitochondrial outer membrane (Cerqua et al., 2010), as such TCHP or some other protein linking mitochondria and keratins together may work in anchoring mitochondria

in place via keratins. Interestingly, MFN2 and TCHP are decreased in Caco-2 cells upon the loss of K8 (Nyström et al., unpublished data) and loss of these proteins, connecting keratins to mitochondria, might lead to a changes in mitochondrial function, movement and distribution in $K8^{-/-}$ Caco-2 cells seen in this study. Previously the loss of K6 in keratinocytes have been reported to lead increase in ROS levels. However, it was not known if increased ROS levels where a result of dysfunction of mitochondria or if already elevated ROS levels caused the reported alterations on mitochondria. (Steen et al., 2020) ROS levels were not studied in this thesis. In conclusion, to confirm the changes in mitochondrial distribution seen in this study, additional immunostaining with a good cell membrane marker, followed by quantification of mitochondrial distribution from a high number of images should be conducted.

In summary, it seems that in Caco-2 cells lacking of K8 might exhibit disturbed mitochondrial function as seen by diminished levels of MMP and CL, distribution of the mitochondrial network and increased mitochondrial movement, all of which can contribute to the impaired respiration in mitochondria in $K8^{-/-}$ Caco-2 cells (unpublished data). This suggest that K8 could modify mitochondrial mobility and distribution, probably via anchoring mitochondria on place, which further affect on mitochondrial respiration and Ca^{2+} signalling.

5.2 The distribution of caveolin-1 is affected by keratins

Cav1 is required for the formation of the caveolae and is important for several cell processes and in addition to many other functions, they have a role to play in normal mitochondrial function and energy metabolism (Asterholm et al., 2012). Caveolae in the cell membranes have been reported to be located close to mitochondria and as such these could be connected and caveolins could function in adaptation to stress by adjustin mitochondrial function and morphology (Fridolfsson et al., 2012). Interestingly in this study mitochondrial TOM20 staining indicated that in $K8^{+/+}$ cells mitochondria would be packed close to the cell membrane, when in several $K8^{-/-}$ Caco-2 cells mitochondria did not exhibit this kind of clustering on cell membranes. Cav1 is needed for CL biosynthesis and Cav1 deficiency have been associated with higher MMP (Bosch et al., 2011), and via increased NO levels to disturbed function of OXPHOS complexes (Pavlides et al., 2010). Caveolae participate in the regulation of mitochondrial Ca^{2+} signalling which in turn affects the function of mitochondrial ATP production and dynamics (O-Uchi et al., 2013).

IFs have previously been linked to caveolae/caveolins (Nixon et al., 2007; Jiu, 2018). IFs have been shown to be connected to Cav1 via tyrosine-14 in Cav1 (Santilman et al., 2007) and Cav1 also interacts with vimentin (Jiu, 2018). In recent studies it was seen that loss of K8 in Caco-2 cells leaded to decreased levels of mitochondrial and caveolar Ca^{2+} signaling and decreased mitochondrial respiration in Caco-2 cells (Nystrrön et al., unpublished data). Since caveolae/Cav1 affects Ca^{2+}signalling and Cav1 has a role in mitochondrial function, it was studied if the distribution of Cav1 in Caco-2 cells would be changed upon the loss of K8, by immunostaining.

In this study it is shown that there are fewer small Cav1 speckles and more large Cav1 aggregates in $K8^{-/-}$ Caco-2 cells compared to $K8^{+/+}$ cells. Based on this K8 could affect the distribution of Cav1 and since Cav1 is crucial component of caveolae vesicles it could interrupt many important cell processes such as the previously seen changes in Ca^{2+} signalling and mitochondrial respiration in Caco-2 cells (Nyström et al., unpublished data). Since Cav1 is needed by some of the CL synthesis enzymes (Liu et al., 2017), the above-mentioned changes in Cav1 distribution could partly explain the decreased CL levels in $K8^{-/-}$ Caco-2 cells. Diminished caveolar Ca^{2+} signalling seen in $K8^{-/-}$ Caco-2 cells (Nyström et al., unpublished data) could be affected by the Cav1 localization. Further down-stream, a possible Cav1-mediated decrease in CL could have negative consequences for MMP and OXPHOS, as discussed above. It is, however, important to remember that Cav1 does not naturally occur in Caco-2 cells and in this study Cav1 had to be transfected into the cells. As such these results of Cav1 in Caco-2 cells do not reflect entirely natural situation, however the experiments of Cav1 in Caco-2 cells could be used as a model to study the function of Cav1 in the colon. However, to confirm that the distribution of Cav1 upon the loss of K8 is the true situation quantification and statistical tests should be conducted for a high number of images with proper cells membrane marker to separate individual cells.

In summary K8 seems to affect the distribution of Cav1 protein in Caco-2 cells, which likely negatively affects several important cell processes including caveolar Ca^{2+}-signalling and mitochondrial function which all have been seen to be changed in $K8^{-/-}$ Caco-2 cells.

5.3 Keratins affect the formation of the intestinal barrier

Intestinal barrier function is the ability of the intestinal wall to selectively pass substances across and defects in this barrier has been associated with several disease conditions for

example IBD (Arnott et al., 2000). Keratins have a role in maintaining intestinal barrier (Liu et al., 2017; Wang et al., 2007) and it has previously been seen that in $K8^{-/-}$ mouse colon the intestinal barrier is disrupted (Misiorek et al., 2016). In this study it was investigated whether the intestinal barrier is also disrupted in $K8^{-/-}$ Caco-2 cells compared to $K8^{+/+}$ Caco-2 cells. Intestinal barrier function measurement was conducted twice with CellZscope+ devise.

In the first experiment using a low number of older cells ($K8^{+/+}$ cells passage 29 and $K8^{-/-}$ cells passage 27) per insert a proper barrier was not formed in $K8^{-/-}$ cells. In the second experiment using a high number of younger cells ($K8^{+/+}$ cells passage 16 and $K8^{-/-}$ cells passage 14) per insert, formation of the barrier in $K8^{-/-}$ cells was delayed and lower compared to K8 wild type cells. However, to statistically confirm the results the barrier function experiment should be repeated with both cell settings.

K8/K18 siRNA treatment were conducted to silence K8 from Caco-2 cells after the cells had reached confluency and formed barrier. However, there were no difference on the results after K8/K18 siRNA and Caco-2 cells resembled CRISPR/Cas9 $K8^{+/+}$ cells before and after the siRNA treatment (not shown). Probably the transfection was not effective since siRNA transfection was done only once, when usually it is repeated three times to ensure effectiveness of transfection. Also, too confluent inserts might result in lower transfection rate and as such K8/K18 siRNA transfection may not result in complete knockout of K8 in this case or maybe knocking out K8 after formation of the barrier was not enough to disturb the barrier anymore.

These results indicate that K8 could have a role in maintaining barrier function also in Caco-2 cells as previously seen in mice (Misiorek et al., 2016). Based on this study it would also seem that high passage $K8^{-/-}$ Caco-2 cells are not capable of forming a barrier (Figure 17 A1). In other hand low passage $K8^{-/-}$ Caco-2 cells did form a barrier but it took longer time to reach lower levels of TER in $K8^{-/-}$ cells and in these cells TER declined faster than in $K8^{+/+}$ cells (Figure 17 A2) after the cells start to lose confluency (Figure 17 B2). The TER value reached higher levels in younger cells in both genotypes (Figure 17 A2) than older ones (Figure 17 A1). $K8^{+/+}$ Caco-2 cells formed barrier in both experiments. Based on this it could be hypothesized that the passages number of the Caco-2 cells could affect on how well the cells achieve barrier function without K8. It would seem that younger cells could form barrier despite the lack of K8 when older cells could not. Younger Caco-2 cells could also have stronger barrier than older ones. However, the

results may be affected by the fact that younger cells were plated in a higher number than older ones and the experiment was also done only once per cell passage number.

K8 might maintain the intestinal barrier by affecting the normal function of TJs via junction proteins as seen following loss of K5 and K14 in keratinocytes which led to disturbed barrier function via abnormal function of TJs caused by the loss of junction proteins (Liovic et al.,2009). In addition, mutation of K18 has been shown to cause mislocalization of TJ proteins (Zupancic et al., 2014). TJs may be affected via signaling pathways where keratins have been proven to be involved. For example, K16 has been shown to affect the ERK1/2 pathway in psoriatic patients (Chen et al., 2019), while ERK1/2 controls TJ protein distribution (Kim and Breton, 2016). Protein kinase C (PKC) controls the development of TJs and is needed for the formation of polarity in epithelial cells (Lu et al., 2015), and in mice PKC-α was regulated by keratins via Rack1 (Kröger et al., 2013). The changes in Cav1 in this study could also affect the normal function of TJs since caveolae are involved in the endocytosis of some components involved TJ formation (Shen and Turner, 2006). However, Toivola et al., 2004, did not detected abnormalities in TJs in $K8^{-/-}$ mice, but several membrane proteins involved in ion transportation were mistargeted leading to elevated electrolyte transportation. In $K8^{-/-}$ mice interleukin-18 (IL-18) levels was increased and it was hypothesized that increased levels of IL-18 lead to high IL-22 levels through the restrained levels of IL-22 inhibitor (Misiorek et al., 2016). High levels of IL-22 further cause activation of STAT3-signaling cascade leading to the diminished barrier function phenotype seen in these mice. Finally, keratins are connected to hemidesmosomes and desmosomes between the cells, and distribution of these may also affect barrier of cell layers (Fortier et al., 2013; Lähdeniemi et al., 2017).

The diminish barrier function in $K8^{-/-}$ Caco-2 cells seen in this study, further supports previous findings indicating that K8 is needed on for the formation and/or maintenance of the intestinal barrier (Liovic et al., 2009; Misiorek et al., 2016; Liu et al., 2017). Caco-2 cell system could be used as an alternative to study the intestinal barrier as well as that alterations in keratins could partly have a role in diseases resulting from the distributed intestinal barrier.

6. Conclusions

According to this study the lack of K8 in Caco-2 cells leads to 1) caveolin-1 aggregation, 2) a disturbed mitochondrial network and increased mitochondrial mobility, 3) diminished levels of mitochondrial cardiolipin and mitochondrial membrane potential and 4) defects in the formation of barrier function (Figure 18). Changes in caveolin-1 may disturb biosynthesis of cardiolipin in mitochondria and the formation of barrier function via possible caveolin-1-mediated changes in endocytosis of tight junction components. Changes in mitochondria and caveolin-1 seen in this study could also be a reason behind the previously seen decrease in mitochondrial and caveolar of Ca^{2+} signalling in Caco-2 cells lacking K8 (unpublished data). Normal levels and function of caveolin-1, cardiolipin and mitochondrial membrane potential are needed for normal energy production in mitochondria and changes in these parameters may be part of the reasons behind the previously seen diminished energy metabolism $K8^{-/-}$ Caco-2 cells. However, since the unsuccessful normalization or quantification for the results, the changes seen may not be actual true situation.

In summary, this study shows that K8 may have a role in normal energy metabolism in Caco-2 cells via regulation of mitochondrial function. K8 functions also in the formation of barrier in the Caco-2 cell barrier model. It could also be concluded that Caco-2 cell system could be used as alternative/another model to study effects of the keratin knockout on different parameters in the colon, including barrier defects. Finally, further studies are needed to find out the exact molecular mechanisms for how keratins are able to regulate the above-mentioned processes.

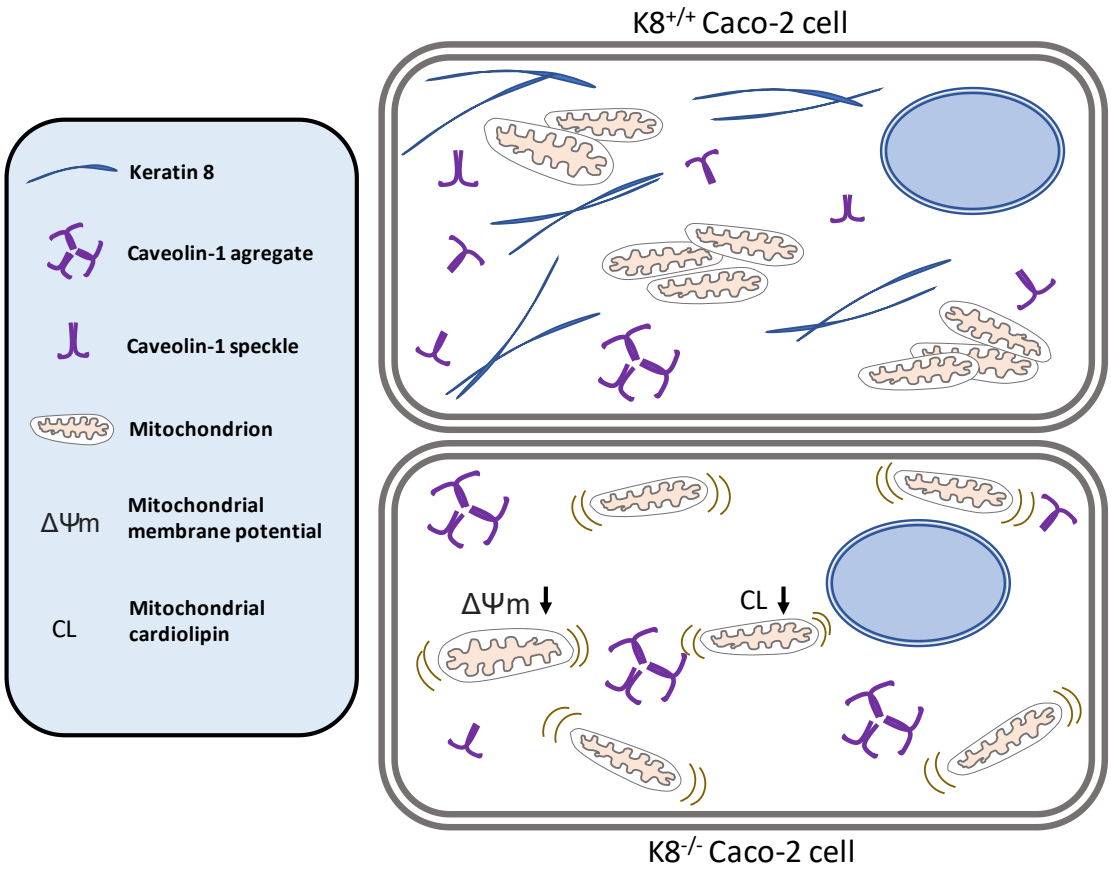

Figure 18. Summary of the effects of K8 loss in Caco-2 cells. In K8$^{-/-}$ cells there are more larger caveolin-1 aggregates and less smaller caveolin-1 speckles. Loss of K8 also causes lower mitochondrial membrane potential and mitochondrial cardiolipin levels. The mitochondrial network is more fragmented and mitochondrial mobility is higher. Loss of K8 in Caco-2 cells also disturbs the barrier function formation.

7. Acknowledgements

This thesis was done in the Toivola epithelial biology laboratory. I would like to thank Diana Toivola for the opportunity to conduct my master thesis work in her supportive lab with interesting research topics.

I would also like to thank Joel Nyström for the great mentoring during the lab work and writing of the thesis. I also would like to express my gratitude to all Toivola lab members for help during lab work and for creating a nice and easy-going work environment.

References

Abraham, C., Cho, JH. 2009. Inflammatory Bowel Disease. *The New England Journal of Medicine.* 361:2066-2078.

Acehan, D., Malhotra, A., Xu Y., Ren, M., Stokes, D.L., Schlame, M. 2011. Cardiolipin affects the supramolecular organization of ATP synthase in mitochondria. *Biophys. J.* 100:2184–2192.

Albert, B., Johnson, A., Lewis, J., Morgan, D., Raff, M., Roberts, K., Walter, P. 2015. Chapter 16 The Cytoskeleton. In: Molecular biology of cell. Pp.889-962.*Garland Science*.

Alam, C., Silvander, J., Daniel, E., Tao, G., Kvarnstrom, S., Alam, P., Omary, M., Hanninen, A., Toivola, D. 2013. K8 modulates β-cell stress responses and normoglycaemia. *Journal of Cell Science.* 126:5635-5644.

Arnott, I.D., Kingstone, K., Ghosh, S. 2000. Abnormal intestinal permeability predicts relapse in inactive Crohn disease. *Scandinavian Journal of Gastroenterology.* 35:1163-1169.

Asghar, M.N., Priyamvada, S., Nyström, J.H., Anbazhagan A.N., Dudeja P.K, Toivola D.M. 2016. K8 knockdown leads to loss of the chloride transporter DRA in the colon. *Am. J. Physiol. Gastrointest. Liver. Physiol.* 310: G1147-54.

Asterholm, I.W., Mundy, D.I., Weng, J., Anderson, R.G.W., Scherer, P.E. 2012. Altered Mitochondrial Function and Metabolic Inflexibility Associated with Loss of Caveolin-1. *Cell Metabolism.* 15:171-185.

Bach, D., Pich, S., Soriano, F.X., Vega, N., Baumgartner, B., Oriola, J., Daugaard, J.R., Lloberas, J., Camps, M., Zierath, J.R., et al. 2003. Mitofusin-2 determines mitochondrial network architecture and mitochondrial metabolism. A novel regulatory mechanism altered in obesity. *J. Biol. Chem.* 278:17190-7.

Bai, L., Deng, X., Li, Q., Wang, M., An, W., Deli, A., Gao, Z., Xie, Y., Dai, Y., Cong, Y.S. 2012. Down-regulation of the cavin family proteins in breast cancer. *J. Cell. Biochem.* 113:322-328.

Baribault, H., Penner, J., Iozzo, R.V., Wilson-Heiner, M. 1994. Colorectal hyperplasia and inflammation in K8-deficient FVB/N mice. *Genes & Development.* 8: 2964-2973.

Bauer, P.M., Yu, J., Chen, Y., Hickey, R., Bernatchez, P.N., Looft-Wilson, R., Huang, Y., Giordano, F., Stan, R.V., Sessa, W.C. 2005. *Proc. Natl. Acad. Sci. USA.* 102:204-209.

Bittar, E.E., and Khuruna, S. 2006. Advances in Molecular and Cell Biology Volume 37 Aspects of the Cytoskeleton. Elsvier. 350 pp.

Bender, F.C., Reymond, M.A., Bro, C., Quest, A.F. 2000. Caveolin-1 Levels Are Down-Regulated in Human Colon Tumors, and Ectopic Expression of Caveolin-1 in Colon Carcinoma Cell Lines Reduces Cell Tumorigenicity. *Cancer Research.* 60:5870-5878.

Berg, J.M., Tymoczko, J.L., Stryer, L. 2002. Chapter 18 Oxidative phosphorylation. In: *Biochemistry*. New York. W H Freeman.

Berg, K.D., Tamas, R.M., Riemann, A., Niels-Christiansen, L.L., Hansen, G.H., Michael Danielsen, E. 2009. Caveolae in fibroblast-like synoviocytes: static structures associated with vimentin-based intermediate filaments. *Histochem. Cell. Biol.* 131:103-14.

Bershadsky, A.D., Vasiliev, J.M. 1988. Cytoskeleton. *Plenum Press*.

Bosch, M., Marí, M., Herms, A., Fernández, A., Fajardo, A., Kassan, A., Giralt, A., Colell, A., Balgoma, D., Barbero, E., et al. 2011. Caveolin-1 deficiency causes cholesterol-dependent mitochondrial dysfunction and apoptotic susceptibility. *Current Biology.* 21:681-686.

Bratic, I., Trifunovic, A. 2010. Mitochondrial energy metabolism and ageing. *Biochimica et Biophysica Acta (BBA)- Bioenergetics.* 1797:961-967.

Büning, C., Halangk, J., Dignass, A., Ockenga, J., Deindl, P., Nickel, R., Genschel, J., Landt, O., Lochs, H., Schmidt, H., Witt, H. 2004. K8 Y54H and G62C mutations are not associated with inflammatory bowel disease. *Digestive and Liver Diseases.* 36:388-391.

Cerqua, C., Anesti, V., Pyakurel, A., Liu, D., Naon, D., Wiche, G., Baffa, R., Dimmer, K.S., Scorrano, L. 2010. Trichoplein/mitostatin regulates endoplasmic reticulum-mitochondria juxtaposition. *EMBO Rep.*11:854-60.

Chaudhary, N., Guillermo, A.G., Howes, M.T., Lo, H.P., McMahon, K., Rae, J.A., Schieber, N.L., Hill, M.N., Gaus, J., Yap, A.S., Parton, R.G. 2014. Endocytic Crosstalk: Cavins, Caveolins, and Caveolae Regulate Clathrin-Independent Endocytosis. *PLoS Biology.* 12: e1001832.

Chen, J.G., Fan, H.Y., Wang, T., Lin, L.Y., Cai, T.G. 2019. Silencing KRT16 inhibits keratinocyte proliferation and VEGF secretion in psoriasis via inhibition of ERK signaling pathway. *Kaohsiung. J. Med. Sci.* 352:84–296.

Cohen, A.W., Hnasko, R., Schubert, W., Lisanti, M.P. 2004. Role of caveolae and caveolins in health and disease. *Physiol. Rev.* 844:1341–1379.

Conrad, P.A., Smart, E.J., Ying, Y.S., Anderson, R.G., Bloom, G.S. 1995. Caveolin cycles between plasma membrane caveolae and the Golgi complex by microtubule-dependent and microtubule-independent steps. *J. Cell. Biol.* 131: 1421-33.

Cooper, G.M., Sunderland, M.A. 2000. Chapter 11. The Cytoskeleton and Cell Movement; Intermediate filament. In: *The cell: A molecular approach* (edited by Sunderland MA). Sinauer Associates.

Coulumbe, P.A., Omary, M.B. 2002. 'Hard' and 'soft' principles defining the structure, function and regulation of keratin intermediate filaments. *Current Opinion in Cell Biology.* 14:110–122.

Crowley, L.C., Christensen, M.E., Waterhouse, N.J. 2016. Measuring Mitochondrial Transmembrane Potential by TMRE Staining. *Cold Spring Harbour Protocols.* 12.

Datta, S., Chowdhury, S., Roy, H.K. 2017. Metabolism, microbiome and colorectal cancer. *Aging (Albany NY).* 9:1086–1087.

De Stefani, D., Rizzuto, R., Pozzan, T. 2016. Enjoy the Trip: Calcium in Mitochondria Back and Forth. *Annu. Rev. Biochem.* 85:161-92.

Duchen, M.R., Verkhratsky, A., Muallem, S. 2008. Mitochondria and calcium in health and disease. *Cell. Calcium.* 44:1-5.

Duncan, A.L., Ruprecht, J.J., Kunji, E.R.S., Robinson, A.J. 2018. Cardiolipin dynamics and binding to conserved residues in the mitochondrial ADP/ATP carrier. *Biochim. Biophys. Acta Biomembr.* 1860:1035-1045.

Dolinsky, V.W., Cole, L.K., Sparanga, G.C., Hatch, G.M. 2016. Cardiac mitochondrial energy metabolism in heart failure: Role of cardiolipin and sirtuins. *Biochimica et Biophysica Acta.* 1861:1544-1554.

Dong, X., Liu, Z., Lan, D., Niu, J., Miao, J., Yang, G., Zhang, F., Sun, Y., Wang, K., Miao, Y. 2017. Critical role of Keratin 1 in maintaining epithelial barrier and correlation of its down-regulation with the progression of inflammatory bowel disease. *Gene.* 608:13–19.

Filipowicz, W., Jaskiewicz, L., Kolb, F.A., Pillai, R.S. 2005. Post-transcriptional gene silencing by siRNAs and miRNAs. *Curr. Opin. Struct. Biol*. 15:331-41.

Fortier, A.M., Asselin, E., Cadrin, M. 2013. K8 and 18 loss in epithelial cancer cells increases collective cell migration and cisplatin sensitivity through claudin1 up-regulation. *J. Biol. Chem.* 288:11555–11571.

Fridolfsson, H.N., Kawaraguchi, Y., Ali, S.S., Panneerselvam, M., Niesman, I.R., Finley, J.C., Kellerhals, S.E., Migita, M.Y., Okada, H., et al. 2012. Mitochondria-localized caveolin in adaptation to cellular stress and injury. *FASEB J.* 26:4637–4649.

Galarneau, L., Loranger, A., Gilbert, S., Marceau, N. 2007 Keratins modulate hepatic cell adhesion, size and G1/S transition. *Exp. Cell. Res.* 313:179–194.

Galbiati, F., Engelman, J., Volonte, D., Zhang, X.L., Minetti, C., Li, M., Hou, H., Kneitz, B., Edelmann, W., Lisanti, M.P. 2001. Caveolin-3 Null Mice Show a Loss of Caveolae, Changes in the Microdomain Distribution of the Dystrophin-Glycoprotein Complex, and T-tubule Abnormalities. *The Journal of Biological Chemistry*. 276:21425-21433.

Gallet, P.F., Maftah, A., Petit, J.M., Denis-Gay, M., Julien, R. 1995. Direct cardiolipin assay in yeast using the red fluorescence emission of 10-N-nonyl acridine orange. *Eur. J. Biochem.* 2281:113-9.

Garrett, W.S., Gordon, J.I., Glimcher, L.H. 2010. Homeostasis and inflammation in the intestine. *Cell.* 140:859-870.

Geisler, N., Weber, K. 1982. The amino acid sequence of chicken muscle desmin provides a common structural model for intermediate filament proteins. *EMBO J.* 1:1649-1656.

Gerbod-Giannone, M.C., Dallet, L., Naudin, G., Sahin, A., Decossas, M., Poussard, S., Lambert, O. 2019. Involvement of caveolin-1 and CD36 in native LDL endocytosis by endothelial cells. *Biochim. Biophys. Acta. Gen. Subj.* 1863:830-838.

Gohil, V.M., Gvozdenovic-Jeremic, J., Schlame, M., Greenberg, M.L. 2005. Binding of 10-N-nonyl acridine orange to cardiolipin-deficient yeast cells: Implications for assay of cardiolipin. *Analytical Biochemistry.* 343:350–352.

Grande-García, A., Echarri, A., de Rooij, J., Alderson, N.B., Waterman-Storer, C.M., Valdivielso, J.M., del Pozo, M.A. 2006. Caveolin-1 regulates cell polarization and directional migration through Src kinase and Rho GTPases. *J. Cell. Biol.* 177:683-694.

Griffiths, M. 2015. Chapter 4: The small intestine and Chapter 5: The Large Intestine. In: *Crash Course Gastrointestinal System* (edited by Horton-Szar D). pp.51-98. Mosby Elsevier.

Ha, T.K., Chi, S.G. 2012. CAV1/caveolin 1 enhances aerobic glycolysis in colon cancer cells via activation of SLC2A3/GLUT3 transcription. *Autophagy.* 8:1684-5.

Habtazion, A., Toivola, D.M., Butcher, E.C., Omary, B. 2005. Keratin-8-deficient mice develop chronic spontaneousTh2 colitis amenable to antibiotic treatment. *Journal of Cell Science.* 118:1971-1980.

Habtezion, A., Toivola, D.M., Asghar, M.N., Kronmal, G.S., Brooks, J.D., Butcher, E.C., Omary, M.B. 2011. Absence of K8 confers a paradoxical microflora-dependent resistance to apoptosis in the colon. *Proc. Natl. Acad. Sci. USA.* 108:1445-50.

Harris, J., Werling, D., Hope, J.C., Taylor, G., Howard, C.J. 2002. Caveolae and caveolin in immune cells: distribution and functions. *Trends Immunol.* 23:158-164.

Helenius, T.O., Misiorek, J.O., Nyström, J.H., Fortelius, L.E., Habtezion, A., Liao, J., Asghar, M.N., Zhang, H., Azhar, S., Omary, B.M. 2015. K8 absence down-regulates colonocyte HMGCS2 and modulates colonic ketogenesis and energy metabolism. *Molecular Biology of the Cell.* 26: 2298-2310.

Herrmann, H., Aebi, U. 2000. Intermediate filaments and their associates: multi-talented structural elements specifying cytoarchitecture and cytodynamics. *Current Opinion in Cell Biology.* 12:79–90.

Herrmann, H., Strelkov, S.V., Burkhard, P., Aebi, U. 2009. Intermediate filaments: primary determinants of cell architecture and plasticity. *J. Clin. Invest.* 119:1772-1783.

Herrmann, H., Aebi, U. 2016. Intermediate Filaments: Structure and Assembly. *Cold Spring Harbor Perspectives in Biology.* 8: a018242.

Hesse, M., Magin, T.M., Weber, K. 2011. Genes for intermediate filament proteins and the draft sequence of the human genome: novel keratin genes and a surprisingly high number of pseudogenes related to keratin genes 8 and 18. *Journal of Cell Science.* 114:2569-2575.

Hirose, H., Ishii, H., Mimori, K., Tanaka, F., Takemasa, I., Mizushima, T., Ikeda, M., Yamamoto, H., Sekimoto, M., Doki, Y., et al. 2011. The Significance of PITX2 Overexpression in Human Colorectal Cancer. *Annals of Surgical Oncology.* 18: 3005-3012.

Ikon, N., Ryan, R.O. 2017. Cardiolipin and mitochondrial cristae organization. *Biochim. Biophys. Acta. Biomembr.* 1859:1156-1163.

Jacob, J.T., Coulombe, P.A., Kwan, R., Omary, M.B. 2018. Types I and II Keratin Intermediate Filaments. *Cold Spring Harb. Perspect. Biol.* 10: a018275.

Jacobson, J., Duchen, M.R., Heales, S.J.R. 2002. Intracellular distribution of the fluorescent dye nonyl acridine orange responds to the mitochondrial membrane potential: implications for assays of cardiolipin and mitochondrial mass. *Journal of Neurochemistry.* 82:224–233.

Jaquemar, D., Kupriyanov, S., Wankell, M., Avis, J., Benirschke, K., Baribault, H., Oshima, R.G. 2003. K8 protection of placental barrier function. *J. Cell. Biol.* 161:749-56.

Jheng, H.F., Tsai, P.J., Guo, S.M., Kuo, L.H., Chang, C.S., Su, I.J., Chang, C.R., Tsai, Y.S. 2011. Mitochondrial Fission Contributes to Mitochondrial Dysfunction and Insulin Resistance in Skeletal Muscle. *Mol. Cell. Biol.* 32:309-319.

Jiang, F., Ryan, M.T., Schlame, M., Zhao, M., Gu, Zhiming., Klingenberg, M., Pfanner, N., Greenberg, M.L. 2000. Absence of Cardiolipin in the crd1 Null Mutant Results in Decreased Mitochondrial Membrane Potential and Reduced Mitochondrial Function. *The Journal of Biological Chemistry.* 275: 22387–22394.

Jiu, Y. 2018. Vimentin intermediate filaments function as a physical barrier during intracellular trafficking of caveolin-1. *Biochemical and Biophysical Research Communications.* 507:161-167.

Jong, D.J., Drenth, J.P. 2004. Absence of an association of the IBD2 locus gene K8 and inflammatory bowel disease in a large genetic association study. *Digestive and Liver Disease.* 36:380-383.

Jones, E., Gaytan, N., Garcia, I., Herrera, A., Ramos, M., Agarwala, D., Rana, M., Innis-Whitehouse, W., Schuenzel, E., Gilkerson, R. 2017. A threshold of transmembrane potential is required for mitochondrial dynamic balance mediated by DRP1 and OMA1. *Cellular and Molecular Life Sciences.* 74:1347-1363.

Jussila, A., Virta, L.J., Salomaa, V., Mäki, J., Jula, A., Färkkilä, M.A. 2013. High and increasing prevalence of inflammatory bowel disease in Finland with a clear North-South difference. *The Journal of Crohn's and Colitis.* 7:256-2562.

Kalbácová, M., Vrbacký, M., Drahota, Z., Melkova, Z. 2003. Comparison of the Effect of Mitochondrial Inhibitors on Mitochondrial Membrane Potential in Two Different Cell Lines Using Flow Cytometry and Spectrofluorometry. *Cytometry Part A.* 52A:110–116.

Kang, J.S., Tian, J.H., Pan, P.Y., Zald, P., Li, C., Deng, C., Sheng, Z.H. 2008. Docking of axonal mitochondria by syntaphilin controls their mobility and affects short-term facilitation. *Cell.* 132:137-48.

Kellner, J.C., Coulombe, P.A. 2009. Keratins and protein synthesis: the plot thickens. *J. Cell. Biol.* 187:157-159.

Kim, B., Breton, S. 2016. The MAPK/ERK-Signaling Pathway Regulates the Expression and Distribution of Tight Junction Proteins in the Mouse Proximal Epididymis. *Biol. Reprod.* 94:22.

Kim, T.K., Eberwine, J.H. 2010. Mammalian cell transfection: the present and the future. *Anal. Bioanal. Chem.* 397:3173-8.

Kim, H., Kim, K., Lee, R. 2006. Expression of caveolin-1 is correlated with Akt-1 in colorectal cancer tissues. *Experimental and Molecular Pathology.* 80:165–170.

Koopman, W., Distemaier, F., Esseling, J., Willems, P. 2008. Computer-assisted live cell analysis of mitochondrial membrane potential, morphology and calcium handling. *Methods.* 46:304-311.

Kornreich, M., Avinery, R., Malka-Gibor, E., Laser-Azogui, A., Beck, R. 2015. Order and disorder in intermediate filament proteins. *FEBS Lett.* 14:2464-76.

Krohn, A.J., Wahlbrink, T., Prehn, J.H. 1999. Mitochondrial Depolarization Is Not Required for Neuronal Apoptosis. *The Journal of Neuroscience.* 19:7394-7404.

Kröger, C., Loschke, F., Schwarz, N., Windoffer, R., Leube, R.E., Magin, T.M. 2013. Keratins control intercellular adhesion involving PKC-α-mediated desmoplakin phosphorylation. *J. Cell. Biol.* 201:681–692.

Kumar, V., Bouameur, J.E., Bär, J., Rice, R.H., Hornig-Do, HT., Roop, D.R., Schwarz, N., Brodesser, S., Thiering, S., Leube RE, et al. 2015. A keratin scaffold regulates epidermal barrier formation, mitochondrial lipid composition, and activity. *The Journal of Cell Biology.* 211:1057-1075.

Lange, C., Nett, J.H., Trumpower, B.L., Hunte, C. 2001. Specific roles of protein-phospholipid interactions in the yeast cytochrome bc1 complex structure. *EMBO J.* 20:6591-600.

Lin, S., Yeh, J., Chen, W.T., Chen, H., Chen, S., Chang, J. 2004. Promoter CpG Methylation of Caveolin-1 in Sporadic Colorectal Cancer. *Anticancer Research.* 24: 1645-1650.

Liovic, M., D'Alessandro, M., Tomic-Canic, M., Bolshakov, V.N., Coats, S.E., Lane, E.B. 2009. Severe keratin 5 and 14 mutations induce down-regulation of junction proteins in keratinocytes. *Experimental Cell Research.* 315:2993-30003.

Liu, C., Liu, E.D., Meng, Y.X., Dong, X.M., Bi, Y.L., Wu, H.W., Jin, Y.C., Zhao, K., Li, J.J., Yu, M., et al. 2017. K8 reduces colonic permeability and maintains gut microbiota homeostasis, protecting against colitis and colitis-associated tumorigenesis. *Oncotarget.* 27; 8:96774-96790.

Liu, P., Rudick, M., Anderson, R.G. 2002. Multiple functions of caveolin-1. *J. Biol. Chem.* 277:41295-41298.

Lea, T. 2015. Caco-2 Cell Line. In: *The Impact of Food Bioactives on Health* (edited by Verhoeckx K, et al.), pp 103-111. Springer, Cham.

Leduc, C., Etienne-Manneville, S. 2015. Intermediate filaments in cell migration and invasion: the unusual suspects. *Curr. Opin. Cell. Biol.* 32:102-112.

Lees, J.F., Shneidman, P.S., Skuntz, S.F., Carden, M.J., Lazzarini, R.A. 1988. The structure and organization of the human heavy neurofilament subunit (NF-H) and the gene encoding it. *EMBO J.* 7:1947-55.

Lodish, H., Berk, A., Zipursky, S.L. 2000. Section 19.6. Intermediate Filaments. In: *Molecular Cell Biology*. *W. H. Freeman New York*.

Loschke, F., Seltmann, K., Bouameur, J.E., Magin, T.M. 2015. Regulation of keratin network organization. *Current Opinion on Cell Biology.* 32:56-64.

Lu, R., Dalgalan, D., Mandell, E.K., Parker, S.S., Ghosh, S., Wilson, J.M. 2015. PKCι interacts with Rab14 and modulates epithelial barrier function through regulation of claudin-2 levels. *Mol Biol Cell. 268*:1523–1531.

Lähdeniemi, I., Misiorek, J., Antila, C., Landor, S., Bergström, L., Sahlgren, C., Toivola, D. 2017. Keratins regulate colonic epithelial cell differentiation through the Notch1 signalling pathway. *Cell Death and Differentiation.* 24:984-996.

Ma, T.Y., Tran, D., Hoa, N., Nguyen, D., Merryfield, M., Tarnawski, A. 2000. Mechanism of extracellular calcium regulation of intestinal epithelial tight junction permeability: role of cytoskeletal involvement. *Microscopy Research & Technique.* 51:156-168.

Maftah, A., Petit, J.M., Julien, R. 1990. Specific interaction of the new fluorescent dye 10-N-nonyl acridine orange with inner mitochondrial membrane. A lipid-mediated inhibition of oxidative phosphorylation. *FEBS Lett.* 260:236-40.

Malik, T. 2015. Inflammatory Bowel Disease: Historical Perspective, Epidemiology, and Risk Factors. *Surgical Clinics of North America.* 95:1105-22.

Malkamäki, A., Sharma, V. 2019. Atomistic insights into cardiolipin binding sites of cytochrome c oxidase. *Biochim. Biophys. Acta. Bioenerg.* 1860:224-232.

Manganelli, V., Capozzi, A., Recalchi, S., Signore, M., Mattei, V., Garofalo, T., Misasi, R., Degli Esposti, M., Sorice, M. 2015. Altered Traffic of Cardiolipin during Apoptosis: Exposure on the Cell Surface as a Trigger for "Antiphospholipid Antibodies". *J. Immunol. Res.* 2015:847985.

Margiotta, A., Bucci, C. 2016. Role of Intermediate Filaments in Vesicular Traffic. *Cells.* 5:20.

Matveeva, E.A., Venkova, L.S., Chernoivanenko, I.S., Minin, A.A. 2015. Vimentin is involved in regulation of mitochondrial motility and membrane potential by Rac1. *Biology Open.* 4:1290-1297.

Mermelstein, C.S., Martins, E.R., Portilho, D.M., Costa, M.L. 2006. Association between the muscle-specific proteins desmin and caveolin-3 in muscle cells. *Cell Tissue Res.* 327:343-351.

Miki, K., Moore, D.J., Butler, R.N., Southcott, E., Couper, R.T., Davidson, G.P. 1998. The sugar permeability test reflects disease activity in children and adolescents with inflammatory bowel disease. *The Journal of Pediatrics.* 133:740-754.

Mileykovskaya, E., Dowhan, W., Birke, R.L., Zheng, D., Lutterodt, L., Haines, T.H. 2001. Cardiolipin binds nonyl acridine orange by aggregating the dye at exposed hydrophobic domains on bilayer surfaces. *FEBS Letters.* 507:187-190.

Misiorek, J.O., Lähdeniemi, I.A.K., Nyström, J.H., Paramonov, V.M., Gullmets, J.A., Saarento, H., Rivero-Müller, A., Husoy, T., Taimen, P., Toivola, D.M. 2016. K8-deletion induced colitis predisposes to murine colorectal cancer enforced by the inflammasome and IL-22 pathway. *Carcinogenesis.* 37:777-786.

Mohan, J., Morén, B., Larsson, E., Holst, M.R., Lundmark, R. 2015. Cavin3 interacts with cavin1 and caveolin1 to increase surface dynamics of caveolae. *Journal of Cell Science.* 128:979–991.

Morris, R.L., Hollenbeck, P.J. 1995. Axonal transport of mitochondria along microtubules and F-actin in living vertebrate neurons. *J. Cell. Biol.* 131:1315-26.

Motte, C.A., Hascall, V.C., Drazba, J., Bandyopadhyay, S.K., Strong, S.A. 2003. Mononuclear leukocytes bind to specific hyaluronan structures on colon mucosal smooth muscle cells treated with polyinosinic acid:polycytidylic acid: inter-alpha-trypsin inhibitor is crucial to structure and function. *American Journal of Pathology.* 163:121–133.

Munkholm, P., Landgholz, E., Hollander, D., Thornberg, K., Orholm, M., Katz, K.D., Binder, V. 1994. Intestinal permeability in patients with Crohn's disease and ulcerative colitis and their first degree relatives. *Gut.* 35:68-72.

Mulder, D.J., Noble, A.J., Justinich, C.J., Duffin, J.M. 2014. A tale of two diseases: the history of inflammatory bowel disease. *Journal of Crohn's and Colitis.* 8:341-348.

Nafeey, S., Martin, I., Felder, T., Walther, P., Felder, E. 2016. Branching of keratin intermediate filaments. *Journal of Structural Biology.* 194:415-422.

Nekrasova, O.E., Mendez, M.G., Chernoivanenko, I.S., Tyurin-Kuzmin, P., Kuczmarski, E.R., Gelfand, V.I., Goldman, R.D., Minin, A.A. 2011. Vimentin intermediate filaments modulate the motility of mitochondria. *Molecular Biology of the Cell.* 22: 2282-2289.

Nicholls, D., and Ferguson, S. 2013. Bioenergetics Ch 10-12. Pp 303-386. Elsevier.

Nishizawa, M., Izawa, I., Inoko, A., Hayashi, Y., Nagata, K., Yokoyama, T., Usukura, J., Inagaki, M. 2005. Identification of trichoplein, a novel keratin filament-binding protein. *J. Cell. Sci*. 118:1081-1090.

Nixon, S.J., Carter, A., Wegner, J., Ferguson, C., Floetenmeyer, M., Riches, J., Key, B., Westerfield, M., Parton, R.G. 2007. Caveolin-1 is required for lateral line neuromast and notochord development. *J. Cell. Sci.* 120:2151-61.

O-Uchi, J., Jhun, B.S., Hurst, S., Bisetto, S., Gross, P., Chen, M., Kettlewell, S., Park, J., Oyamada, H., Smith, G.L., et al. 2013. Overexpression of ryanodine receptor type 1 enhances mitochondrial fragmentation and Ca^{2+}-induced ATP production in cardiac H9c2 myoblasts. *Am. J. Physiol. Heart. Circ. Physiol.* 305:H1736-751.

Owens, D.W., Wilson, N.J., Hill, A.J., Rugg, E.L., Porter, R.M., Hutcheson, A.M., Quinlan, R.A., van Heel, D., Parkes, M., Jewell, D.P., et al. 2004. Human K8 mutations that disturb filament assembly observed in inflammatory bowel disease patients. *Journal of Cell Science.* 117:1989-1999.

Parry, D.A., Strelkov, S.V., Burkhard, P., Aebi, U., Herrmann, H. 2007. Towards a molecular description of intermediate filament structure and assembly. *Exp. Cell. Res.* 313:2204-2216.

Parton, R.G., del Pozo, M.A. 2013. Caveolae as plasma membrane sensors, protectors and organizers. *Nat. Rev. Mol. Cell. Biol.* 14:98-112.

Parton, R.G. and Simons, K. 2007. The multiple faces of caveolae. *Nature Reviews.* 8:185-194.

Parton, R.G., Tillu, V.A., Collins, B.M. 2018. Caveolae. *Curr. Biol.* 28: R402-R405.

Patton, E.T. and Thibodeau G.A. 2016. Chapters 38 Upper Digestive Tract, Chapter 39 Lowe Digestive Tract. In: *Anatomy and physiology*. p 860-887. Elsevier.

Pavlides, S., Tsirigos, A., Vera, I., Flomenberg, N., Frank, P.G., Casimiro, M.C., Wang, C., Fortina, P., Addya, S., Pestell R.G., et al. 2010. Loss of stromal caveolin-1 leads to oxidative stress, mimics

hypoxia and drives inflammation in the tumor microenvironment, conferring the "reverse Warburg effect": a transcriptional informatics analysis with validation. *Cell Cycle.* 9:2201-2219.

Pelkmans, L., Püntener, D., Helenius, A. 2002. Local actin polymerization and dynamin recruitment in SV40-induced internalization of caveolae. *Science.* 296:535-9.

Peng, L., He, Z., Chen, W., Holzman, I.R., Lin, J. 2007. Effects of Butyrate on Intestinal Barrier Function in a Caco-2 Cell Monolayer Model of Intestinal Barrier. *Pediatric research.* 61: 37–41.

Petit, J.M., Maftah, A., Ratinaud, M.H., Julien, R. 1992. 10N-nonyl acridine orange interacts with cardiolipin and allows the quantification of this phospholipid in isolated mitochondria. *Eur. J. Biochem.* 209:267-73.

Pich, S., Bach, D., Briones, P., Liesa, M., Camps, M., Testar, X., Palacín, M., Zorzano, A. 2005. The Charcot-Marie-Tooth type 2A gene product, Mfn2, up-regulates fuel oxidation through expression of OXPHOS system. *Hum. Mol. Genet.* 14:1405-1415.

Pollar, T.D. and Cooper JA. 2009. Actin, a Central Player in Cell Shape and Movement. *Science.* 326:1208-1212.

Rao, J.N., and Wang, J.Y. 2010. Intestinal Architecture and Development. In: *Regulation of Gastrointestinal Mucosal Growth* (edited by San Rafael, CA). Morgan & Claypool Life Sciences.

Rawla, P., Sunkara, T., Barsouk, A. 2019. Epidemiology of colorectal cancer: incidence, mortality, survival, and risk factors. *Prz. Gastroenterol.* 14; 2:89–103.

Rueden, C.T., Schindelin, J., Hiner, M.C. 2017. ImageJ2: ImageJ for the next generation of scientific image data. *BMC Bioinformatics.* 18:529.

Richter-Dennerlein, R., Korwitz, A., Haag, M., Tatsuta, T., Dargazanli, S., Baker, M., Decker, T., Lamkemeyer, T., Rugarli, E.I., Langer, T. 2014. DNAJC19, a mitochondrial cochaperone associated with cardiomyopathy, forms a complex with prohibitins to regulate cardiolipin remodeling. *Cell Metab.* 20:158-71.

Scaduto, R.C. Jr., and Grotyohann, L.W. 1999. Measurement of mitochondrial membrane potential using fluorescent rhodamine derivatives. *Biophys. J.* 76: 469–77.

Scheiffele, P., Verkade, P., Fra, A.M., Virta, H., Simons, K., Ikonen, E. 1998. Caveolin-1 and -2 in the exocytic pathway of MDCK cells. *J. Cell Biol.* 140:795-806.

Schindelin, J., Arganda-Carreras, I., Frise, E. 2012. Fiji: an open-source platform for biological-image analysis. *Nature methods.* 9:676-682.

Schlame, M., Haldar, D. 1993. Cardiolipin Is Synthesized on the Matrix Side of the Inner Membrane in Rat Liver Mitochondria. *The Journal of Biological Chemistry*. 268:74-79.

Schwarz, N., and Leube, R.E. 2016. Intermediate Filaments as Organizers of Cellular Space: How They Affect Mitochondrial Structure and Function. *Cells.* 5;5(3).

Schweizer, J., Bowden, P., Coulombe, P., Langbein, L., Lane, E.B., Magin, T.M., Maltais, L., Omary, M.B., Parry, D., Rogers, M.A., Wright, M.W. 2006. New consensus nomenclature for mammalian keratins. *The Journal of Cell Biology.* 174: 169–174.

Santilman, V., Baran, J., Anand-Apte, B., Evans, R.M., Parat, M.O. 2007. Caveolin-1 polarization in transmigrating endothelial cells requires binding to intermediate filaments. *Angiogenesis.* 10:297-305.

Shen, L., Turner, J.R. 2006. Role of Epithelial Cells in Initiation and Propagation of Intestinal Inflammation. Eliminating the static: tight junction dynamics exposed. *Am. J. Physiol. Gastrointest. Liver Physiol.* 290: G577–G582.

Silvander, J.S.G., Kvanström, S.M., Kumari-Ileiva, A., Shrestha, A., Alam, C.M., Toivola, D.M. 2017. Keratins regulate β-cell mitochondrial morphology, motility, and homeostasis. *The FASEB Journal.* 30:4578-4587.

Sun, J., Groppi, V.E., Gui, H., Chen, L., Xie, Q., Liu, L., Omary, M.B. 2016. High-Throughput Screening for Drugs that Modulate Intermediate Filament Proteins. *Methods Enzymol.* 568:163-185.

Srinivasan, B., Kolli, A.R., Esch, M.B., Abaci, H.E., Shuler, M.L., Hickman, J.J. 2015. TEER measurement techniques for in vitro barrier model systems. *Journal of Laboratory Automation.* 20:107-126.

Stahlhut, M., and van Deurs, B. 2000.Identification of Filamin as a Novel Ligand for Caveolin-1: Evidence for the Organization of Caveolin-1–associated Membrane Domains by the Actin Cytoskeleton. *Mol. Biol. Cell.* 11:325-37.

Standring, S. 2016. Chapter 65: Small intestine and Chapter 66: Large Intestine. In: *Gray's Anatomy*. pp 1123-1159. Elsevier.

Steegenga, W.T., de Wit, N.J., Boekschoten, M.V., IJssennagger, N., Lute, C., Keshtkar, S., Bromhaar, M.M.G., Kampman, E., de Groot, L.C., Muller, M. 2012. Structural, functional and molecular analysis of the effects of aging in the small intestine and colon of C57BL/6J mice. *BMC Med. Genomics.* 5:38.

Steen, K., Chen, D., Wang, F., Majumdar, R., Chen, S., Kumar, S., Lombard, D.B., Weigert, R., Zieman, A.G., Parent, C.A., Coulombe, P.A. 2020. A role for keratins in supporting mitochondrial organization and function in skin keratinocytes. *Mol. Biol. Cell.* mbcE19100565.

Strand. P., Guldiken, N., Helenius, T.O., Misiorek, J.O., Nyström, J.H., Lähdeniemi, I.A.K., Silvander, J.S.G., Kuscuoglu, D., Toivola, D.M. 2016. Chapter 13 Simple Epithelial Keratins. In: *Methods in Enzymology volume 568* (edited by Omary BM and Liem RKH), pp.351-388. Elsevier.

Strelkov, S.V., Herrmann, H., Aebi, U. 2003. Molecular architecture of intermediate filaments. *Bioessays.* 25:243-251.

Szeverenyi, I., Cassidy, A.J., Chung, C.W., Lee, B.T., Common, J.E., Ogg, S.C., Chen, H., Sim, S.Y., Goh, W.L., Ng, K.W., et al. 2008. The Human Intermediate Filament Database: comprehensive information on a gene family involved in many human diseases. *Hum Mutat.* 29:351-60.

Tamura, Y., Harada, Y., Nishikiwa, S., Yamano, K., Kamiya, M., Shiota, T., Kuroda, T., Kuge, O., Sesaki, H., Imai, K., et al. 2013. Tam41 Is a CDP-Diacylglycerol Synthase Required for Cardiolipin Biosynthesis in Mitochondria. *Cell metabolism.* 17:709-718.

Tao, G.Z., Strnad, P., Zhou, Q., Kamal, A., Zhang, L., Madani, N.D., Kugathasan, S., Brant, S.R., Cho, J.H., Omary, M.B., Duerr, R.H. 2007. Analysis of Keratin Polypeptides 8 and 19 Variants in Inflammatory Bowel Disease. *Clinical Gastroenterology and Hepatology.* 5:857-864.

Tao, G., Looi, K.S., Toivola, D.M., Strnad, P., Zhou, Q., Liao, J., Wei, Y., Habtezion, A., Omary, M.B. 2009. Keratins modulate the shape and function of hepatocyte mitochondria: a mechanism for protection from apoptosis. *Journal of Cell Science.* 122:3851-3855.

Teshima, C.W., Dieleman, L.A., Meddings, J.B. 2012. Abnormal intestinal permeability in Crohn's disease pathogenesis. *Annals of the New York Academy Sciences.* 1258:159–165.

Thomsen, P., Roepstorff, K., Stahlhut, M., Deurs, B. 2001. Caveolae Are Highly Immobile Plasma Membrane Microdomains, Which Are not Involved in Constitutive Endocytic Trafficking. *Molecular Biology of the Cell.* 13:238-250.

Timme, T.L., Goltsov, A., Salahaldin, T., Li, L., Wang, J., Ren, C., Johnston, R.N., Thompson, T. 2000. Caveolin-1 is regulated by c-myc and suppresses c-myc-induced apoptosis. *Oncogene.* 19: 3256–3265.

Toivola, D.M., Krishnan, S., Binder, H.J., Singh, S.K., Omary, M.B. 2004. Keratins modulate colonocyte electrolyte transport via protein mistargeting. *The Journal of Cell Biology.* 164:911-921.

Toivola, D.M., Strnad, P., Habtezion, A., Omary, M.B. 2010. Intermediate filaments take the heat as stress proteins. *Trends Cell Biol.* 20:79-91.

Torgersen, M.L., Skretting, G., van Deurs, B., Sandvig, K. 2001. Internalization of cholera toxin by different endocytic mechanisms. *J. Cell. Sci.* 114:3737-47.

Treuting, P.M., and Dintzis, S.M. 2012. Chapter 12 - Lower Gastrointestinal Tract. In: *Comparative Anatomy and Histology*. pp. 177-192. Academic Press.

Treuting, P.M., Valasek, M.A., Dintzis, S.M. 2012. Chapter 11 - Upper Gastrointestinal Tract. In: *Comparative Anatomy and Histolog*y. pp. 155-175. Academic Press.

Tyurina, Y.T., Winnica, D.E., Kapralova, V.I., Kapralov, A.A., Tyurin, V.A., Kagan, V.E. 2013. LC/MS characterization of rotenone induced cardiolipin oxidation in human lymphocytes: Implications for mitochondrial dysfunction associated with Parkinson's disease. *Molecular Nutrition & Food Research.* 57:1410-1422.

Ullman, T., and Itzkowitz, S. 2011. Intestinal Inflammation and Cancer. *Gastroenterology*. 140:1807-1816.

van der Bliek, A.M., Sedensky, M.M., Morgan, P.G. 2017. Cell Biology of the Mitochondrion. *Genetics.* 207:843-871.

van der Have, M., Mangen, M.J., van der Valk, M.E., Smeets, H.M., van Bodegraven, A., Dijkstra, G., Fidder, H.H., de Jong, D.J., Pierik, M., Ponsioen, C.Y., et al. 2014. Effect of aging on healthcare costs of inflammatory bowel disease: a glimpse into the future. *Inflammatory Bowel Disease.* 10:637-645.

Vijayaraj, P., Kröger, C., Reuter, U., Windoffer, R., Leube, R.E., Magin, T.M. 2009. Keratins regulate protein biosynthesis through localization of GLUT1 and -3 upstream of AMP kinase and Raptor. *J. Cell Biol.* 187:175–184.

Wang, L., Srinivasan, S., Theiss, A.L., Merlin, D., Sitaraman, S.V. 2007. Interleukin-6 induces keratin expression in intestinal epithelial cells: potential role of keratin-8 in interleukin-6-induced barrier function alterations. *Journal of Biological Chemistry.* 282;11: 8219–8227.

Wang, X.M., Kim, H.P., Nakahira, K., Ryter, S.W., Choi, A.M. 2009. The heme oxygenase-1/carbon monoxide pathway suppresses TLR4 signaling by regulating the interaction of TLR4 with caveolin-1. *J. Immunol.* 182:3809-3818.

Watson, A., Chu, S., Sieck, L., Gerasimenko, O., Bullen, T., Campbell, F., McKenna, M., Rose, T., Montrose, M.H. 2005. Epithelial Barrier Function In Vivo Is Sustained Despite Gaps in Epithelial Layers. *Gastroenterology.* 129:902-912.

Watson, A.J.M., and Collins, P.D. 2011. Colon Cancer: A Civilization Disorder. *Dig. Dis.* 29:222–228.

Weiss, C.R., Guan, Q., Ma, Y., Qing, G., Bernstein, C.N., Warrington, R.J., Peng, Z. 2015. The potential protective role of caveolin-1 in intestinal inflammation in TNBS-induced murine colitis. *PLoS One.* 10:e0119004.

Wickstead, B., and Gull, K. 2011.The evolution of the cytoskeleton. *The Journal of Cell Biology.* 194:513-525.

Widlansky, M.E., Wang, J., Shenouda, S.M., Hagen, T.M., Smith, A.R., Kizhakekuttu, T.J., Kluge, M.A., Weihrauch, D., Gutterman, D.D., Vita, J.A. 2010. Altered mitochondrial membrane potential, mass, and morphology in the mononuclear cells of humans with type 2 diabetes. *Transl. Res.* 156:15-25.

Winter, L., Abrahamsberg, C., Wiche, G. 2008. Plectin isoform 1b mediates mitochondrion – intermediate filament network linkage and controls organelle shape. *The Journal of Cell Biology.* 181:903-911.

Xu, Y., Phoon, C.K.L., Berno, B., D´Souza, K., Hoedt, E., Zhang, G., Neubert, T.A., Epand, R.M., Ren, M., Schlame, M. 2016. Loss of protein association causes cardiolipin degradation in Barth syndrome. *Nature Chemical Biology.* 12:641-647.

Yan, Y., and Kang, B. 2012. The Role of Cardiolipin Remodeling in Mitochondrial Function and Human Diseases. *Journal of Molecular Biology Research.* 2;1: 1-11.

Yi, M., Weaver, D., Hajnóczky, G. 2004. Control of mitochondrial motility and distribution by the calcium signal: a homeostatic circuit. *J. Cell Biol.* 167:661-672.

Youle, R.J., and van der Bliek, A.M. 2012. Mitochondrial Fission, Fusion and Stress. *Science.* 337:1062-1065.

Yu, D.M., Jung, S.H., An, H.T., Lee, S., Hong, J, Park, J.S., Lee, H., Lee, H., Bahn, M.S., Lee, H.C., et al. 2017. Caveolin-1 deficiency induces premature senescence with mitochondrial dysfunction. *Aging Cell.* 16:773-784.

Zhou, W., Toivola, D.M., Feng, N., Greenberg, H.B., Franke, W.W., Omary, M.B. 2003. Keratin 20 helps maintain intermediate filament organization in intestinal epithelia. *Molecular Biology of the Cell.* 14:2959-71.

Zorova, L.D., Popkov, V.A., Plotnikov, E.Y., Silachev, D.N., Pevzner, I.B., Jankauskas, S.S., Babenko, V.A., Zorov, S.D., Balakireva, A.V., Juhaszova, M., et al. 2018, Mitochondrial membrane potential. *Anal. Biochem.* 552:50-59.

Zupancic, T., Stojan, J., Lane, E.B., Komel, R., Bedina-Zavec, A., Liovic, M. 2014. Intestinal cell barrier function in vitro is severely compromised by K8 and 18 mutations identified in patients with inflammatory bowel disease. *PLoS One.* 9: e99398.

APPENDIX

Appendix A. Plate reader optimization

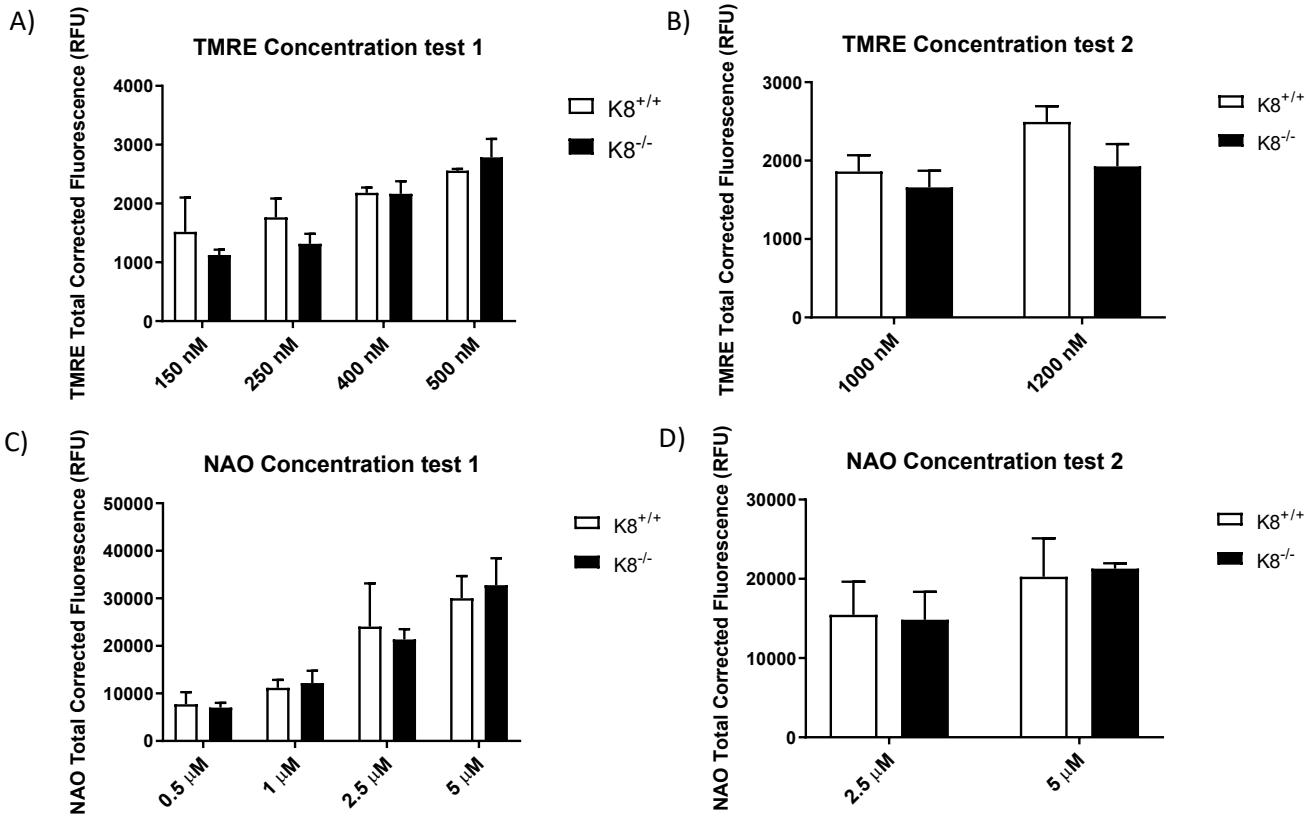

Appendix A figure 1. TMRE and NAO concentration test for mitochondrial membrane potential plate reader assay. TMRE concentrations between 150nM-1200 nM was tested in the MMP plate reader assays. A) Test of 150 nM-120 0nM TMRE B) Test of 1000 nM and 1200 nM TMRE. A) and B) are done on different plates and different times so TMRE RFU values of test 1 and test 2 are not directly comparable C) Test of 0.5 µM- 5 µM NAO. D) Test of 2.5 µM-5µM NAO. Each concentration is the average of 3 or 6 wells per genotype in a 24-well plate. White bar = CRISPR/Cas9 $K8^{+/+}$ Caco-2 cells. Black bar = CRISPR/Cas9 $K8^{-/-}$ Caco-2 cells. RFU = relative fluorescence units. Data is presented as mean plus/minus standard deviation.

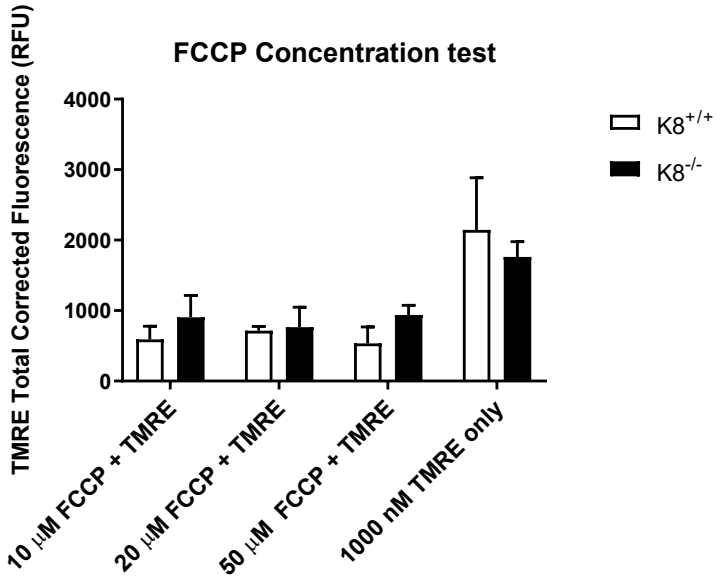

Appendix A figure 2. MMP plate reader assay: FCCP concentration test. Positive control FCCP concentration from 10 μM to 50 μM was tested with 96-well plate reader assay with 1000 nM TMRE staining and without FCCP. FCCP without TMRE was used as blank for FCCP + TMRE wells and blank wells containing only cells without any dye for TMRE only wells. Each FCCP concentration is the average of 4 wells per genotype from which the average of 4 blank wells has subtracted. TMRE is the average of 8 wells per genotype subtracted of 8 wells of blanks. White bar = CRISPR/Cas9 K8$^{+/+}$ Caco-2 cells. Black bar = CRISPR/Cas9 K8$^{-/-}$ Caco-2 cells. RFU = relative fluorescence units. Data is presented as mean plus/minus standard deviation.

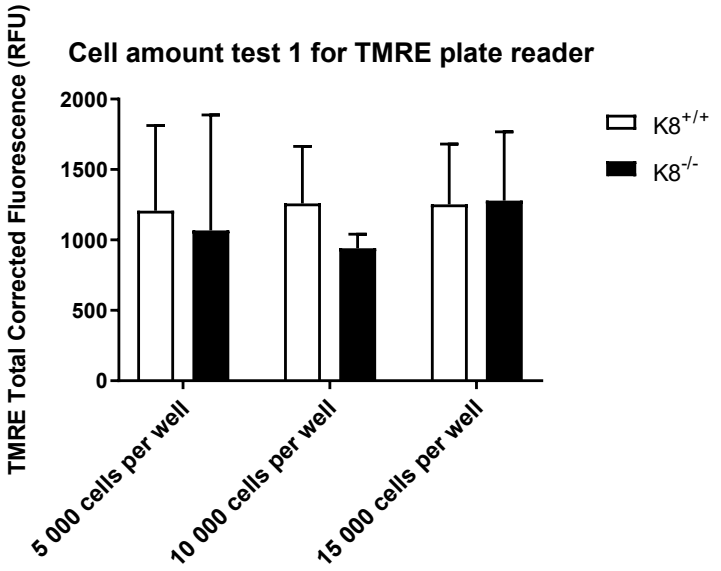

Appendix A figure 3. Cell amount test for a plate reader assay. The number of cells per well in a 96-well plate was calculated by the Countess device. Results are the average of 12 or 18 wells per genotype and cell number. The TMRE intensity levels between tested cell numbers do not have a major change, probably due to too little difference between cell numbers and too low number of cells plated. Cell number experiment were repeated several times for both TMRE and NAO dyes and with different number of cells (not shown). White bar = CRISPR/Cas9 K8$^{+/+}$ Caco-2 cells. Black bar = CRISPR/Cas9 K8$^{-/-}$ Caco-2 cells. RFU = relative fluorescence units. Data is presented as mean plus/minus standard deviation.

Appendix B. Plate reader normalization

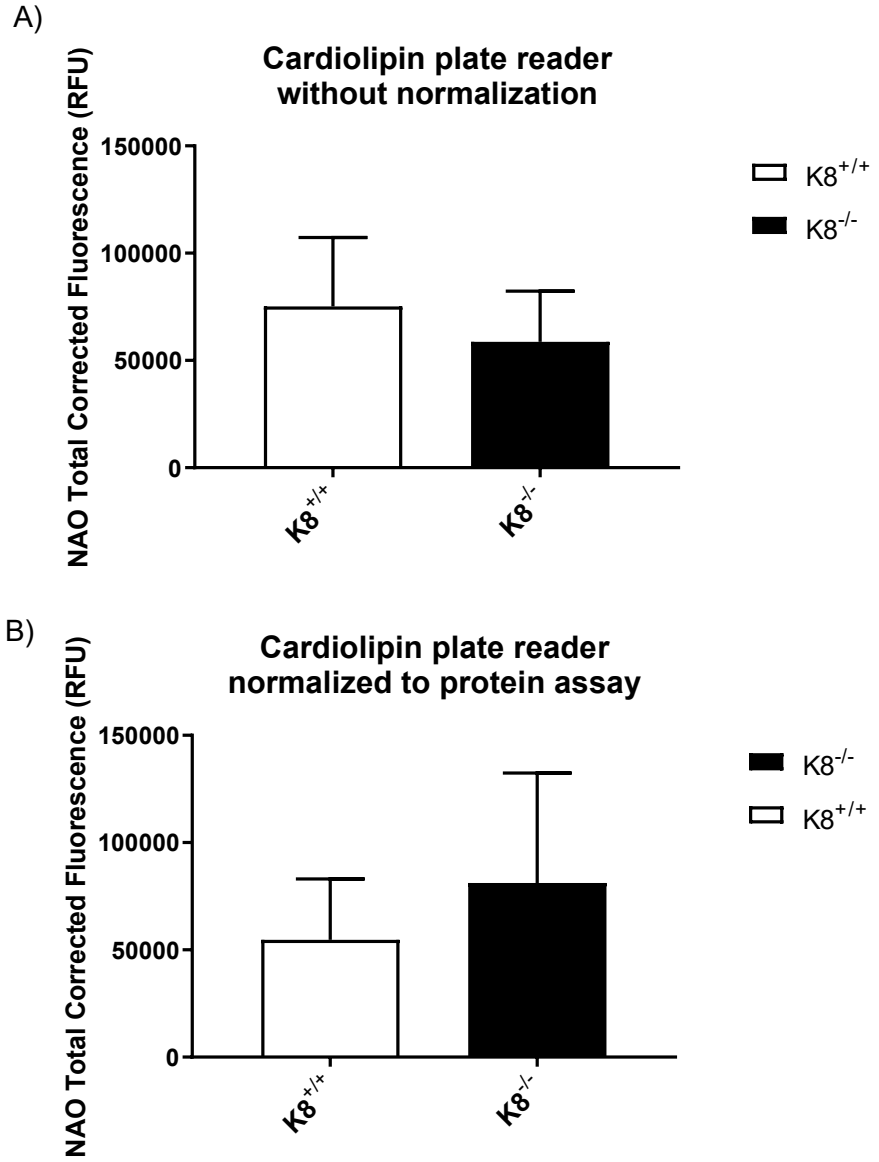

Appendix B figure 3. Plate reader normalization to protein content. Normalization of CL plate reader assay to protein assay was tested once. A) CL plate reader results without normalization. B) CL plate reader results with normalization to the total amount of protein. Results are the average of 24 well per genotype in 96-well plate from which the average of 8 blanks wells per genotype has been subtracted. White bar = CRISPR/Cas9 $K8^{+/+}$ Caco-2 cells. Black bar = CRISPR/Cas9 $K8^{-/-}$ Caco-2 cells. RFU = relative fluorescence units. Data is presented as mean plus/minus standard deviation.

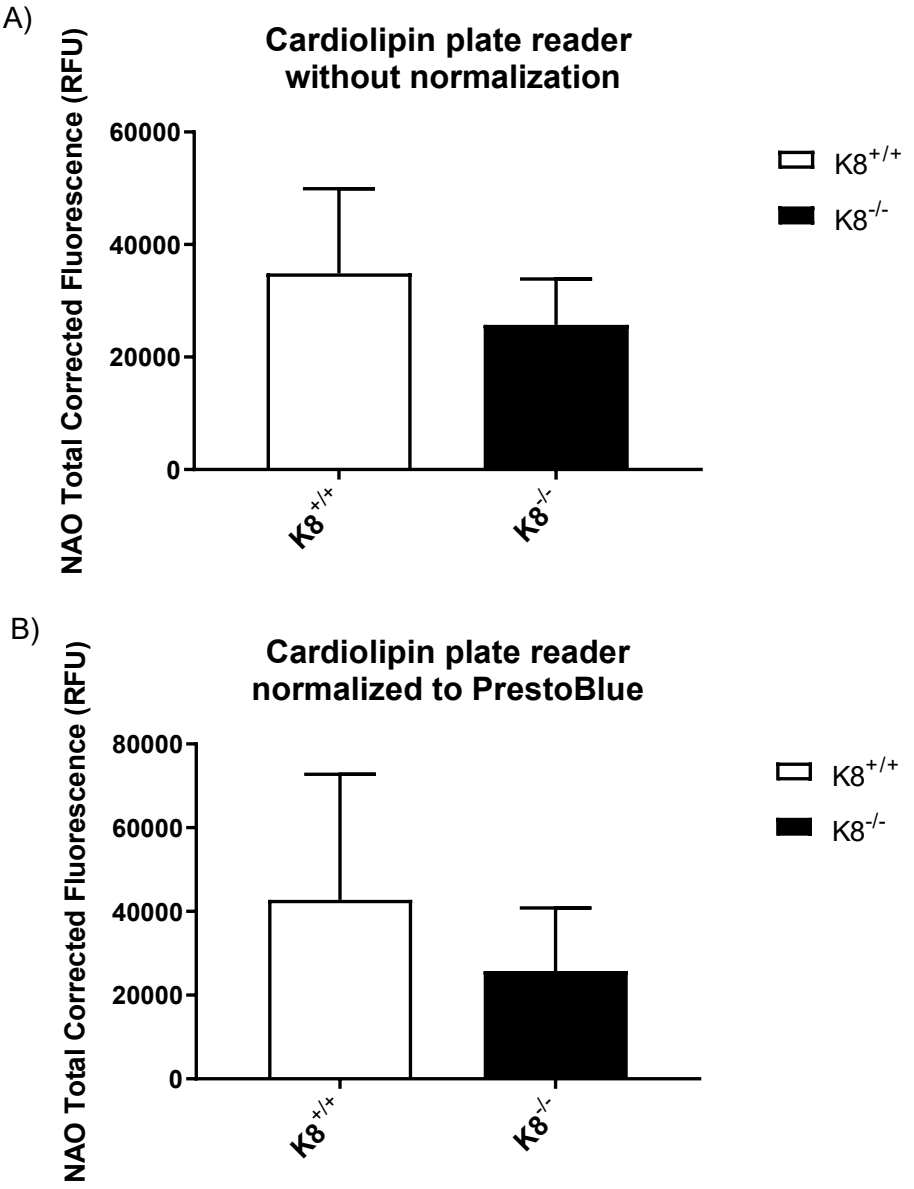

Appendix B figure 4. Normalization with PrestoBlue Cell Viability Reagent for plate reader assay. A) CL plate reader assay without normalization. B) CL plate reader assay normalized to cell number by using PrestoBlue. Results are the average of 16 wells per genotype on 96-well plate from which 8 blanks wells per genotype has been subtracted. White bar = CRISPR/Cas9 $K8^{+/+}$ Caco-2 cells. Black bar = CRISPR/Cas9 $K8^{-/-}$ Caco-2 cells. RFU = relative fluorescence units. Data is presented as mean plus/minus standard deviation.

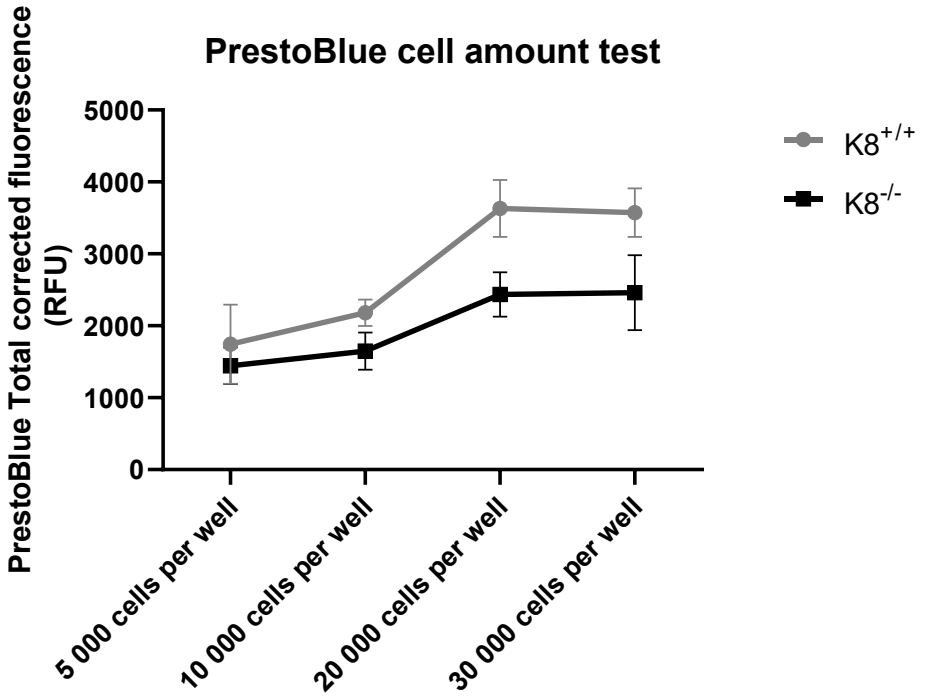

Appendix B figure 5. PrestoBlue Cell Viability Reagent plate reader assay with different cell numbers. 5 000 to 30 000 cells per well were stained with PrestoBlue and measured with microplate reader. Results are the average of 5 wells per genotype and number of cells on 96-well plate from which one blank well per genotype and the number of cells has been subtracted. Grey line = CRISPR/Cas9 $K8^{+/+}$ Caco-2 cells. Black line = CRISPR/Cas9 $K8^{-/-}$ Caco-2 cells. Data is presented as mean plus/minus standard deviation.

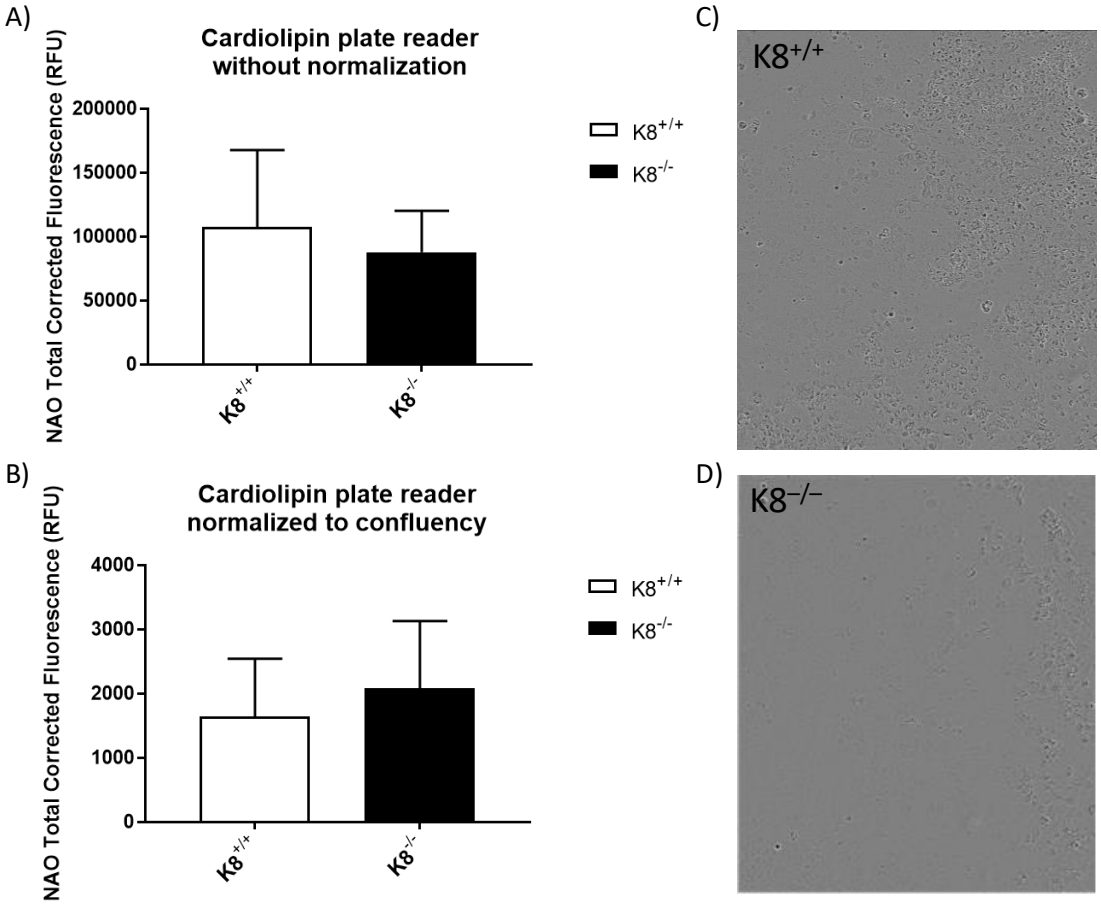

Appendix B figure 6. Plate reader normalization to confluency with Incucyte microscope. Incucyte S3 High Content microscopy was used to test plate reader normalization to cell confluency. A) CL plate reader assay without normalization. B) CL plate reader assay normalized to confluency. With Incucyte software (Sartorious, IncuCyte® S3 Software (v2018B)) threshold can be set to select cells from the images and based on threshold the program gives the confluency of the wells. After TMRE (not shown) or NAO plate reader assay cells get loose and got washed away. C) and D) Example images taken with Incucyte 10x objective showing the lost of cells after plate reader assay C) CRISPR/cas9 Caco-2 $K8^{+/+}$ cells D) CRISPR/cas9 Caco-2 $K8^{-/-}$. 2.5 µM of NAO was used. Results are the average of 40 wells per genotype in 96-well plate from which the average of 8 blanks wells per genotype has been subtracted. White bar = CRISPR/Cas9 $K8^{+/+}$ Caco-2 cells. Black bar = CRISPR/Cas9 $K8^{-/-}$ Caco-2 cells. RFU = relative fluorescence units. Data is presented as mean plus/minus standard deviation.

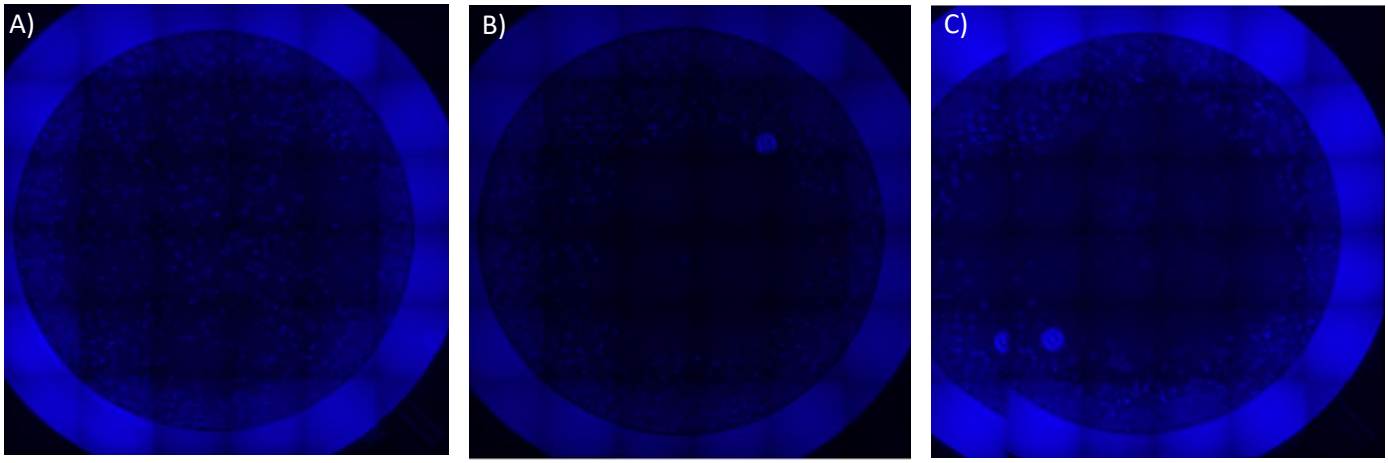

Appendix B figure 7. Plate reader assay normalization to a cell number with Hoechst staining and Eclipse Ti2-E microscopy example images. Hoechst is fluorescent stain for DNA for both fixed and live-cell imaging. After conducting plate reader analysis for TMRE or NAO, the plate was stained with Hoechst and imaged with Nikon eclipse microscope. A) CRISPR/Cas9 Caco-2 $K8^{+/+}$ cells, B) CRISPR/Cas9 Caco-2 $K8^{-/-}$ cells. C) Example of image which is wrongly constructed from the smaller tile images.

C. Live cell imaging optimization

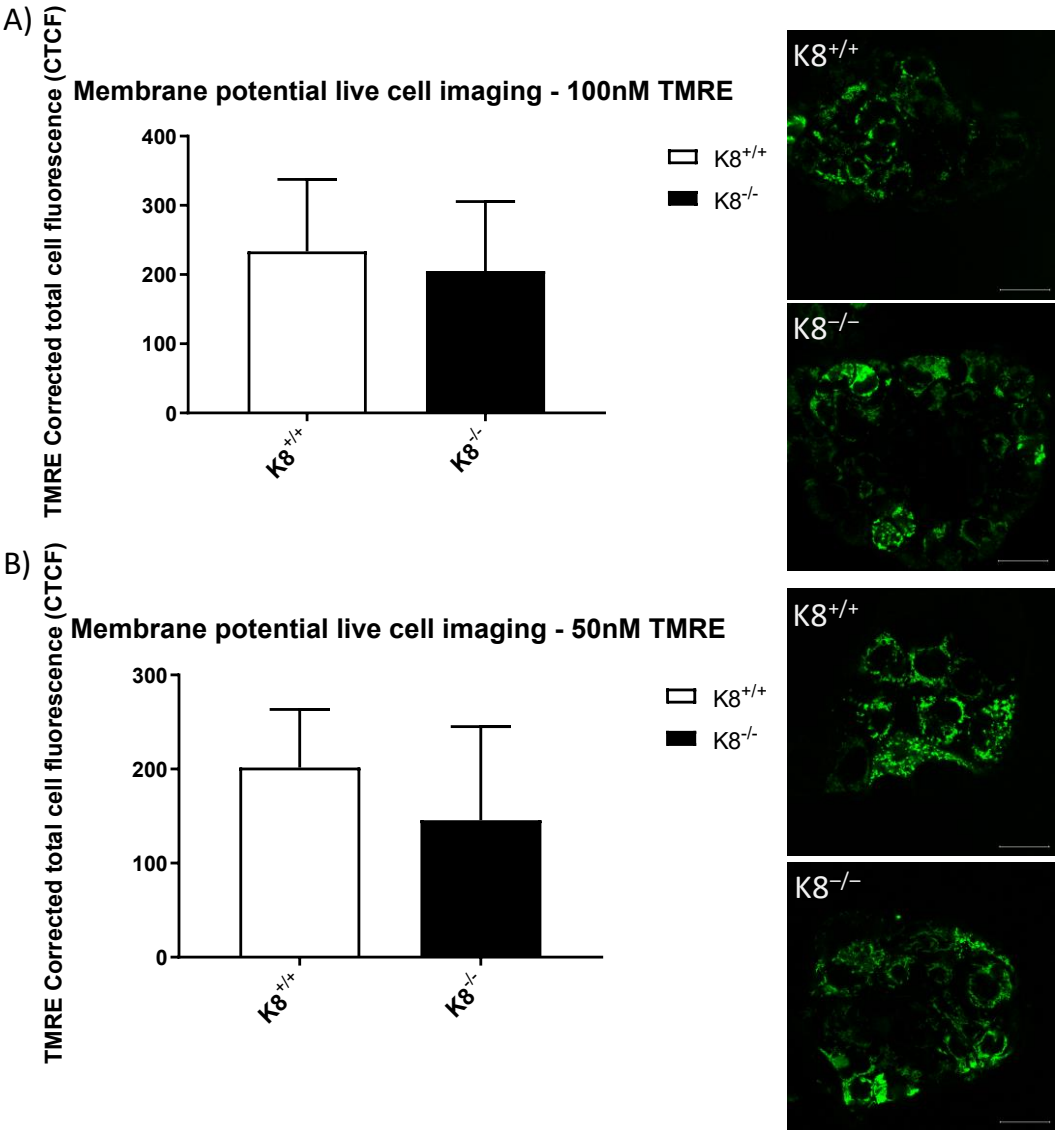

Appendix C figure 8. Mitochondrial membrane potential live cell imaging TMRE concentration test. CRISPR/cas9 Caco2 $K8^{+/+}$ and $K8^{-/-}$ cells were stained with TMRE and live cell imaging was done with confocal microscope. A) Quantification and example images with 100nM TMRE concentration, which was determined to result in too bright images B) Quantification and example images with TMRE concentration 50nM. Results are the average of 5 to 7 images per genotype with 10 mitochondrion per image from which the average of 3 blanks (areas without dye) has been subtracted. White bar = CRISPR/Cas9 $K8^{+/+}$ Caco-2 cells. Black bar = CRISPR/Cas9 $K8^{-/-}$ Caco-2 cells. RFU = relative fluorescence units. Data is presented as mean plus/minus standard deviation. Green color = mitochondria (TMRE). CTCF = corrected total cell fluorescence. Scale bar = 25 μm.

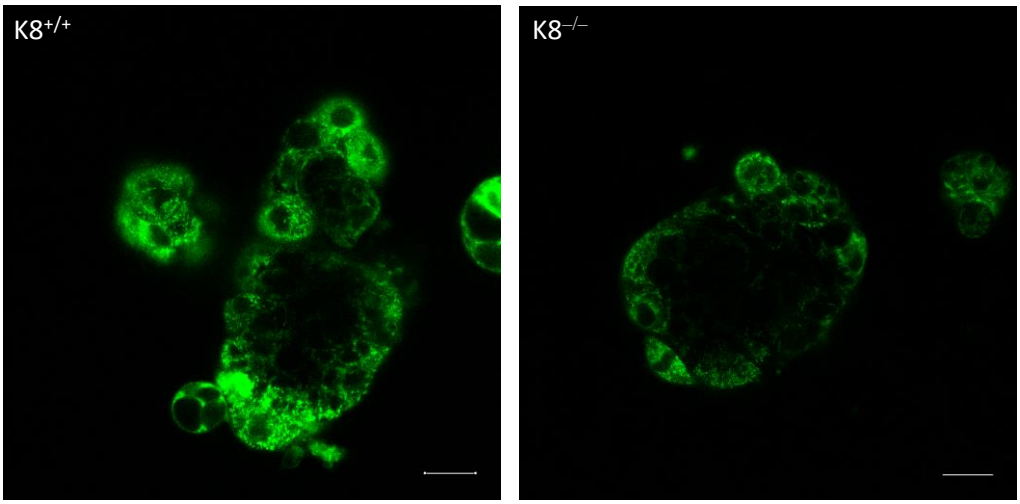

Appendix C figure 9. Cardiolipin live cell imaging. In CRISPR/Cas9 $K8^{+/+}$ and $K8^{-/-}$ Caco-2 cells cardiolipin was stained with 50 nM live cell dye NAO and imaged with confocal microscope. Green= cardiolipin (NAO). Scale bar = 25µm.